

Utah State University

DigitalCommons@USU

---

All Graduate Theses and Dissertations

Graduate Studies

---

5-1982

## On the Transport Equations for Anisotropic Plasmas

Abdallah R. Barakat

Follow this and additional works at: <https://digitalcommons.usu.edu/etd>



Part of the [Physics Commons](#)

---

### Recommended Citation

Barakat, Abdallah R., "On the Transport Equations for Anisotropic Plasmas" (1982). *All Graduate Theses and Dissertations*. 6854.

<https://digitalcommons.usu.edu/etd/6854>

This Dissertation is brought to you for free and open access by the Graduate Studies at DigitalCommons@USU. It has been accepted for inclusion in All Graduate Theses and Dissertations by an authorized administrator of DigitalCommons@USU. For more information, please contact [digitalcommons@usu.edu](mailto:digitalcommons@usu.edu).



ON THE TRANSPORT EQUATIONS  
FOR ANISOTROPIC PLASMAS

by

Abdallah R. Barakat

A dissertation submitted in partial fulfillment  
of the requirements for the degree

of

DOCTOR OF PHILOSOPHY

in

Physics

Approved:

UTAH STATE UNIVERSITY  
Logan, Utah

1982

## ACKNOWLEDGMENTS

A very special thanks is extended to Dr. Robert W. Schunk, who, through his patience and understanding, helped me to write and otherwise develop this program.

I express appreciation to NASA under contract NAGW-77 with Utah State University, for financial support.

I am very indebted to my wife, Wedad, for her help and encouragement throughout my thesis program.

Abdallah R. Barakat

## TABLE OF CONTENTS

	Page
ACKNOWLEDGMENTS . . . . .	ii
LIST OF TABLES . . . . .	v
LIST OF FIGURES . . . . .	vii
ABSTRACT . . . . .	x
 Chapter	
I. INTRODUCTION . . . . .	1
II. TRANSPORT EQUATIONS FOR MULTICOMPONENT ANISOTROPIC SPACE PLASMAS . . . . .	12
1. General transport equations . . . . .	12
2. The sixteen-moment approximation . . . . .	19
3. Collision terms . . . . .	22
4. Simplified sets of transport equations. . . . .	30
III. MOMENTUM AND ENERGY EXCHANGE TERMS FOR INTERPENETRATING BI-MAXWELLIAN GASES . . . . .	43
1. Theoretical formulation . . . . .	43
2. Collision terms . . . . .	45
3. Numerical results and approximate expressions . . . . .	52
IV. COMPARISON OF TRANSPORT EQUATIONS BASED ON MAXWELLIAN AND BI-MAXWELLIAN DISTRIBUTIONS FOR ANISOTROPIC PLASMAS . . . . .	73
1. Theoretical formulation . . . . .	73
2. Comparison of transport equations. . . . .	85
V. COMPARISON OF MAXWELLIAN AND BI-MAXWELLIAN EXPANSIONS WITH MONTE CARLO SIMULATION FOR ANISOTROPIC PLASMAS . . . . .	104
1. The Monte Carlo technique . . . . .	104
2. Velocity distributions for the polarization model . . . . .	109
3. Velocity distributions for the hard sphere model . . . . .	124
VI. SUMMARY AND CONCLUSION . . . . .	133



REFERENCES . . . . .	141
APPENDIX . . . . .	143
VITA . . . . .	155

## LIST OF TABLES

Table	Page
1. The numerical values of $\phi_{33}^{(3)}$ (Coulomb interaction and parallel relative drift) for different values of $\Delta/a_{\perp}$ and $T_{\parallel}/T_{\perp}$ . . . . .	56
2. The numerical values of $\Omega_1^{  }$ (3) (Coulomb interaction and parallel relative drift) for different values of $\Delta/a_{\perp}$ and $T_{\parallel}/T_{\perp}$ . . . . .	57
3. The numerical values of $\Omega_2^{  }$ (3) (Coulomb interaction and parallel relative drift) for different values of $\Delta/a_{\perp}$ and $T_{\parallel}/T_{\perp}$ . . . . .	58
4. The numerical values of $\phi_{11}^{(3)}$ (Coulomb interaction and perpendicular relative drift) for different values of $\Delta/a_{\perp}$ and $T_{\parallel}/T_{\perp}$ . ( $\phi_{11}=\phi_{22}$ ) . . . . .	59
5. The numerical values of $\Omega_1^{\perp}$ (3) (Coulomb interaction and perpendicular relative drift) for different values of $\Delta/a_{\perp}$ and $T_{\parallel}/T_{\perp}$ . . . . .	60
6. The numerical values of $\Omega_2^{\perp}$ (3) (Coulomb interaction and perpendicular relative drift) for different values of $\Delta/a_{\perp}$ and $T_{\parallel}/T_{\perp}$ . . . . .	61
7. The numerical values of $\phi_{33}^{(-1)}$ (hard sphere interaction and parallel relative drift) for different values of $\Delta/a_{\perp}$ and $T_{\parallel}/T_{\perp}$ . . . . .	64
8. The numerical values of $\Omega_1^{  }$ (-1) (hard sphere interaction and parallel relative drift) for different values of $\Delta/a_{\perp}$ and $T_{\parallel}/T_{\perp}$ . . . . .	65
9. The numerical values of $\Omega_2^{  }$ (-1) (hard sphere interaction and parallel relative drift) for different values of $\Delta/a_{\perp}$ and $T_{\parallel}/T_{\perp}$ . . . . .	66
10. The numerical values of $\phi_{11}^{(-1)}$ (hard sphere interaction and perpendicular relative drift) for different values of $\Delta/a_{\perp}$ and $T_{\parallel}/T_{\perp}$ . ( $\phi_{11}=\phi_{22}$ ) . . . . .	67
11. The numerical values of $\Omega_1^{\perp}$ (-1) (hard sphere interaction and perpendicular relative drift) for different values of $\Delta/a_{\perp}$ and $T_{\parallel}/T_{\perp}$ . . . . .	68
12. The numerical values of $\Omega_2^{\perp}$ (-1) (hard sphere interaction and perpendicular relative drift) for	

	different values of $\Delta/a_{\perp}$ and $T_{\parallel}/T_{\perp}$ . . . . .	69
13.	Optimum values of $\alpha$ 's and $\beta$ 's. . . . .	70
14.	Maximum percentage error of the approximate expressions given in equations (193)'-(200)' . . . . .	71
15.	The $I_{LM,N}$ for Coulomb and Hard sphere interactions . . . . .	72
16.	Ion temperature anisotropy ( $T_{i\parallel}/T_{i\perp}$ ) . . . . .	100

## LIST OF FIGURES

Figure		page
1.	Schematic illustration of a drifting bi-Maxwellian velocity distribution. . . . .	6
2.	Flow diagram showing the procedure for obtaining transport equations that are based on a bi-Maxwellian velocity distribution. . . . .	7
3.	Contours of the ion distribution function in the principal velocity plane parallel to the electric field for the Maxwellian-based expansions and for parallel electric and magnetic fields. . . . .	88
4.	Contours of the ion distribution function in the principal velocity plane parallel to the electric field for the bi-Maxwellian-based expansions and for parallel electric and magnetic fields . . . . .	89
5.	Comparison of the exact form with the 16-moment and the 20-moment expansions for the ion distribution function in the principal velocity plane parallel to the electric field for the case of parallel electric and magnetic fields. . . . .	90
6.	Contours of the exact ion distribution function in the principal velocity ( $\underline{E}-\underline{ExB}$ ) plane for the case of perpendicular electric and magnetic fields. . . . .	91
7.	Contours of the ion distribution function in the principal velocity ( $\underline{B}-\underline{ExB}$ ) plane for the exact form and the Maxwellian-based expansions and for perpendicular electric and magnetic fields. . . . .	92
8.	Contours of the ion distribution function in the principal velocity ( $\underline{B}-\underline{ExB}$ )-plane for the exact form and the bi-Maxwellian-based expansions and for perpendicular electric and magnetic fields . . . . .	93
9.	Comparison of the exact form with the 16-moment and the 20-moment expansions of the ion distribution function for the case of perpendicular electric and magnetic fields and for $D_{\perp} = 1.0$ and $\alpha = 0.1$ . . . . .	94
10.	Comparison of the exact form with the 16-moment and the 20-moment expansions of the ion distribution function for the case of perpendicular electric and magnetic fields and for $D_{\perp} = 1.0$ and $\alpha = 1.0$ . . . . .	95

11. Comparison of the exact form with the 16-moment and the 20-moment expansions of the ion distribution function for the case of perpendicular electric and magnetic fields and for  $D_{\perp} = 3.0$  and  $\alpha = 1.0$  . . . 96
12. Comparison of the exact form with the 16-moment and the 20-moment expansions of the ion distribution function for the case of perpendicular electric and magnetic fields and for  $D_{\perp} = 3.0$  and  $\alpha = 0.1$  . . . 97
13. Comparison of the MCS with the 16-moment and 20-moment expansions of  $f_i$  in the principal velocity plane parallel to the electric field for the polarization collision model, equal ion and neutral masses, and parallel electric and magnetic fields . . . . . 111
14. Contours of  $f_i$  obtained from the MCS in the principal velocity ( $\underline{E} - \underline{E} \times \underline{B}$ ) plane for the polarization collision model, equal ion and neutral masses, and perpendicular electric and magnetic fields. . . . . 112
15. Comparison of the MCS with the 16-moment and 20-moment expansions of  $f_i$  for the polarization collision model, equal ion and neutral masses, perpendicular electric and magnetic fields,  $D_{\perp} = 3$ , and  $\alpha = 0.1$ . . . . . 113
16. Comparison of the MCS with the 16-moment and 20-moment expansions of  $f_i$  for the polarization collision model, equal ion and neutral masses, perpendicular electric and magnetic fields,  $D_{\perp} = 1$ , and  $\alpha = 0.1$ . . . . . 114
17. Comparison of the MCS with the 16-moment and 20-moment expansions of  $f_i$  for the polarization collision model, equal ion and neutral masses, perpendicular electric and magnetic fields,  $D_{\perp} = 3$ , and  $\alpha = 1$ . . . . . 115
18. Comparison of the MCS with the 16-moment and 20-moment expansions of  $f_i$  for the polarization collision model, equal ion and neutral masses, perpendicular electric and magnetic fields,  $D_{\perp} = 1$ , and  $\alpha = 1$ . . . . . 116
19. Comparison of the MCS with the 16-moment and 20-moment expressions of  $f_i$  in the principal velocity plane parallel to the electric field for

- the hard-sphere collision model, equal ion and neutral masses, and parallel electric and magnetic fields. . . . . 125
20. Contours of  $f_1$  obtained from the MCS in the principal ( $\underline{E}_1 - \underline{E} \times \underline{B}$ ) plane for the hard-sphere collision model, equal ion and neutral masses, and perpendicular electric and magnetic fields. . . . . 126
21. Comparison of the MCS with the 16-moment and 20-moment expansions of  $f_1$  for the hard-sphere collision model, equal ion and neutral masses, perpendicular electric and magnetic fields,  $D_{\perp}=3$ , and  $\alpha=0.1$ . . . . . 127
22. Comparison of the MCS with the 16-moment and 20-moment expansions of  $f_1$  for the hard-sphere collision model, equal ion and neutral masses, perpendicular electric and magnetic fields,  $D_{\perp}=1$ , and  $\alpha=0.1$ . . . . . 128
23. Comparison of the MCS with the 16-moment and 20-moment expansions of  $f_1$  for the hard-sphere collision model, equal ion and neutral masses, perpendicular electric and magnetic fields,  $D_{\perp}=3$ , and  $\alpha=1$ . . . . . 129
24. Comparison of the MCS with the 16-moment and 20-moment expansions of  $f_1$  for the hard-sphere collision model, equal ion and neutral masses, perpendicular electric and magnetic fields,  $D_{\perp}=1$ , and  $\alpha=1$ . . . . . 130

## ABSTRACT

On the Transport Equations  
for Anisotropic Plasmas

by

Abdallah R. Barakat, Doctor of Philosophy

Utah State University, 1982

Major Professor: Dr. R.W. Schunk  
Department: Physics

First, I attempt to present a unified approach to the study of transport phenomena in multicomponent anisotropic space plasmas. In the limit of small temperature anisotropies this system of generalized transport equations reduces to Grad's 13-moment system of transport equations. In the collisionless limit, the generalized transport equations account for collisionless heat flow, collisionless viscosity, and large temperature anisotropies. Also, I show that with the appropriate assumptions, the system of generalized transport equations reduces to all of the other major systems of transport equations for anisotropic plasmas that have been derived to date.

Next, for application to aeronomy and space physics problems involving strongly magnetized plasma flows, I derive momentum and energy exchange collision terms for interpenetrating bi-Maxwellian gases. Collision terms are derived for Coulomb, Maxwell molecule, and constant collision cross section interaction potentials. The collision terms are

valid for arbitrary flow velocity differences and temperature differences between the interacting gases as well as for arbitrary temperature anisotropies. The collision terms have to be evaluated numerically and the appropriate coefficients are presented in tables. However, the collision terms are also fitted with simplified expressions, the accuracy of which depends on both the interaction potential and the temperature anisotropy. In addition, I derive the closed set of transport equations that are associated with the momentum and energy collision terms.

Finally, I study the extent to which Maxwellian and bi-Maxwellian series expansions can describe plasma flows characterized by non-Maxwellian velocity distributions, with emphasis given to modeling the anisotropic character of the distribution function. The problem considered is the steady state flow of a weakly-ionized plasma subjected to homogeneous electric and magnetic fields, and different collision models are used. In the case of relaxation collision model, a closed form expression is found for the ion velocity distribution function, while for more rigorous models (polarization and hard sphere) I have to use the Monte Carlo simulation. These provided a basis for determining the adequacy of a given series expansion. I find that, in general, the bi-Maxwellian-based expansions for the velocity distribution function is better suited to describing anisotropic plasmas than the Maxwellian-based expansions.

(166 pages)



## CHAPTER I

### INTRODUCTION

A wide variety of plasma flow conditions can be found in all areas of aeronomy and space plasma physics. For example, gentle near-equilibrium flows occur in corotating planetary ionospheres and in the lower solar corona, while highly non-equilibrium flow conditions exist in the solar and terrestrial polar winds, in planetary magnetospheres, and in the terrestrial F-region at high latitudes, where convection electric fields drive the charged particles through the neutral atmosphere at speeds approaching a few kilometers per second. In general, the plasma flows encountered are multispecies flows that may be characterized by large temperature differences between the interacting species or by anisotropic temperature distributions for the individual species. The plasma flows may contain transitions from collision dominated to collisionless regimes, from subsonic to supersonic flow, or from one major ion species to another. In addition, the flowing plasma may encounter a changing magnetic field topology or it may be subjected to anomalous resistivity, electrostatic shocks, double layers, or magnetic merging processes.

Many of the highly nonequilibrium flows found in the solar terrestrial environment are characterized by appreciable temperature anisotropies, i.e., unequal species temperatures parallel and perpendicular to a magnetic field, with the degree of the anisotropy given by the parallel to perpendicular temperature ratio. For solar wind protons the measured temperature anisotropy typically varies between a

factor of 2 and 4 at the orbit of the Earth (cf. Brandt 1970, Hundhausen 1972), while in the terrestrial polar wind initial theoretical calculations indicate that the temperature anisotropy is about a factor of 10 for  $O^+$  and about a factor of 20 for  $H^+$  at a distance of eight Earth radii (Holzer et al. 1971). In the Earth's dayside magnetosheath and in the high-latitude F-region, the temperature anisotropies are smaller, with the parallel-to-perpendicular ion temperature ratio varying from 1 to 1/2 in both regions (cf. Crooker et al. 1979, St.-Maurice and Schunk 1979).

It should be noted that appreciable temperature anisotropies occur in a plasma at all levels of ionization. The temperature anisotropy in the solar wind develops in a region of the flow where only Coulomb collisions are important, i.e., the flow is effectively fully-ionized. On the other hand, in the terrestrial polar wind the  $H^+$  temperature anisotropy develops in a region of the flow where Coulomb collisions and nonresonant ion-neutral interactions occur, i.e., the flow is partially-ionized. Finally, we note that the temperature anisotropy in the high-latitude F-layer occurs in a plasma that is weakly-ionized and arises primarily as a result of the nature of the  $O^+ - O$  resonant charge exchange process.

Understanding the behavior of both near-equilibrium and far-from-equilibrium plasma flows is crucial to our understanding of the coupling, through mass, momentum, and energy transfer, between the different regions within the solar terrestrial environment. In general, the quantitative study of such flows is begun through the use of

conservation equations which describe the spatial and temporal evolution of the concentration, bulk flow velocity, and temperature of the plasma. To date, a variety of conservation equations have been used, including the Euler, Navier-Stokes, and Chew-Goldberger-Low equations. In addition, transport equations have been adopted from the classical work of Chapman and Enskog.

Most of the conservation equations available for use in aeronomy and space physics are based on an isotropic Maxwellian velocity distribution function. Basically, the conservation equations are obtained by taking velocity moments of Boltzmann's equation. Although such a procedure may seem to be relatively straightforward, difficulties arise because the equation governing the moment of order  $r$  contains the moment of order  $r+1$ . Consequently, it is necessary to make an assumption about the form of the velocity distribution function,  $f$ , in order to truncate the set of transport equations. Typically, the velocity distribution function is expanded in an orthogonal series about a Maxwellian weight factor and then the series is truncated at some level. By taking velocity moments of the resulting approximate expression for  $f$ , higher-order moments can be expressed in terms of lower-order moments, and these expressions can be used to close the system of transport equations (see, for example, Tanenbaum 1967, Burgers 1969, Schunk 1977). Although various levels of approximation can be considered, the 13-moment approximation attracted most of the attention. At this level of approximation, stress and heat flow are put on an equal footing with density, drift

velocity, and temperature, and therefore, these moments are described by transport equations just as the density, drift velocity and temperature moments are described by continuity, momentum, and energy equations, respectively.

The 13-moment system of transport equations is fairly general and can be used to describe a wide range of plasma flows. In the collision-dominated limit, the 13-moment system of equations reduces to the Euler, Navier-Stokes, and Burnett equations depending on whether terms proportional to the zeroth, first, or second power of the collisional mean-free-path are retained. At the Navier-Stokes approximation, transport processes such as ordinary diffusion, thermal diffusion, thermal conduction, diffusion-thermal heat flow, thermoelectric heat flow, and viscosity are included at a level of approximation that corresponds to either the first or second approximation of Chapman and Cowling (1970), depending on the particular transport coefficient. In the collisionless limit, the 13-moment system of equations reduces to the Chew-Goldberger-Low (CGL) and extended CGL equations depending on whether terms proportional to the zeroth or first power of the Larmor radius are retained. The 13-moment system of transport equations also accounts for collisionless heat flow, collisionless viscosity, and temperature anisotropies.

With regard to anisotropic plasmas, the 13-moment transport equations have limited applicability because they cannot be used to describe plasma flows that are characterized by large temperature

anisotropies. In the 13-moment formulation, the temperature anisotropy enters through the stress and heat flow terms, which act to modify the zeroth-order isotropic Maxwellian distribution, and the restriction to a small temperature anisotropy results from the fact that only small deviations from the Maxwellian are allowed, i.e., small stress and heat flow terms.

The flow of an anisotropic plasma is better described by transport equations that are based on a two-temperature or bi-Maxwellian velocity distribution function, which is shown schematically in Figure 1. The procedure for obtaining these transport equations is similar to that of the 13-moment expansion except that the transport equations are closed by expanding the velocity distribution function in an orthogonal series about an anisotropic bi-Maxwellian weight factor instead of an isotropic Maxwellian. This change produces transport equations that can describe highly anisotropic plasma flows.

Although a significant effort has been devoted to developing transport equations that are based on an isotropic Maxwellian distribution function (see, for example, Tanenbaum 1967, Burgers 1969), in comparison much less effort has been directed toward developing transport equations that are based on a bi-Maxwellian distribution function. Chew et al. (1956) were the first to derive transport equations based on a bi-Maxwellian distribution function for application to collisionless anisotropic plasmas. In this now famous study, corrections to the zeroth-order bi-Maxwellian distribution function

Figure 1. Schematic illustration of a drifting bi-Maxwellian velocity distribution. The solid lines represent contours of constant  $f$  in the  $v_x$ - $v_z$  plane, with the peak of the distribution centered at the drift velocity point. For the case shown, the temperature along the  $v_z$ -axis is greater than the temperature perpendicular to this axis.

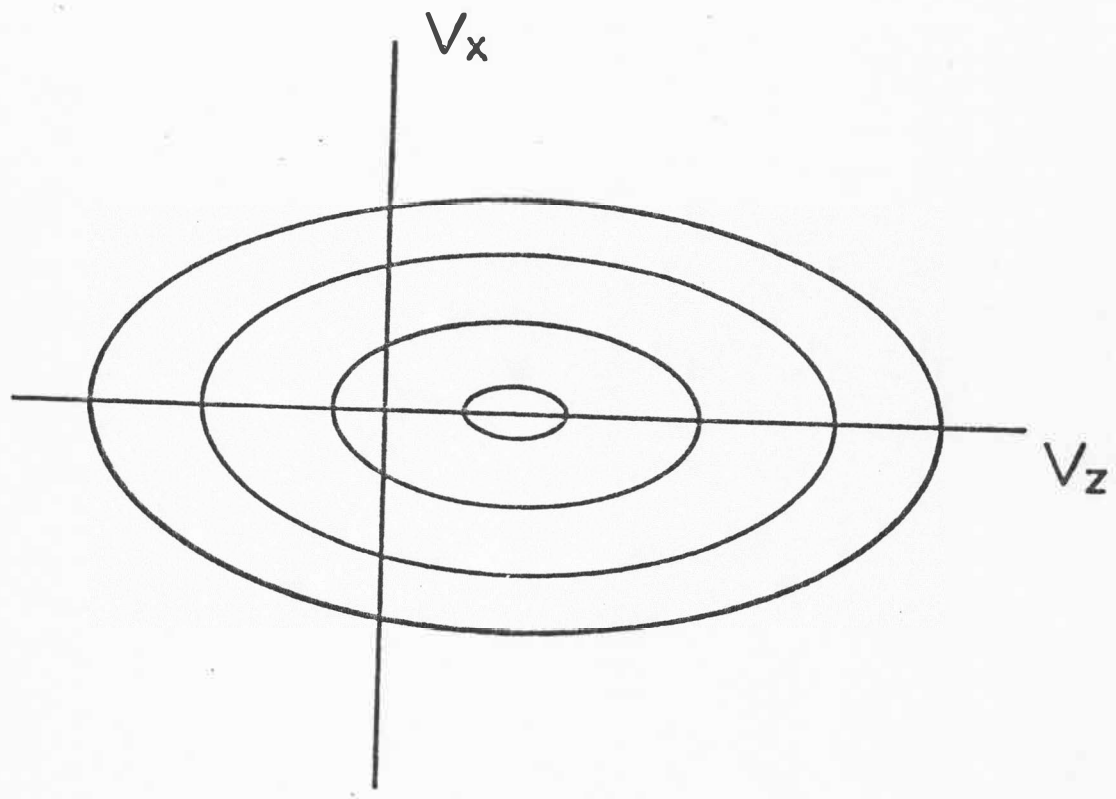
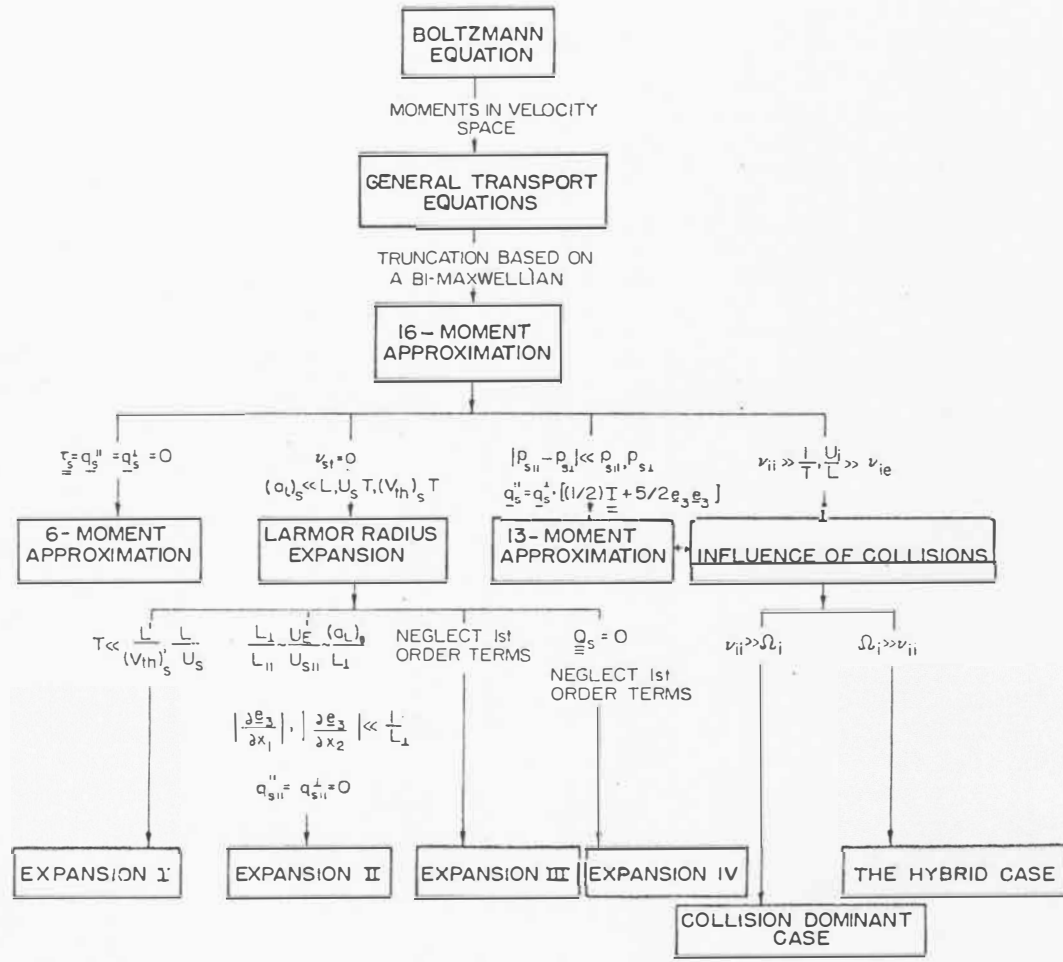


Figure 2. Flow diagram showing the procedure for obtaining transport equations that are based on a bi-Maxwellian velocity distribution. Also shown are the assumptions needed to arrive at various sets of simplified transport equations.





due to heat flow were neglected and the resulting transport equations for the species temperatures parallel and perpendicular to the magnetic field were termed 'double-adiabatic' energy equations. Since this initial study, several authors (Kennel and Green 1966, MacMahon 1965, Frieman et al. 1966, Bowers and Hains 1968, Oraevskii et al. 1968) have extended the work of Chew et al. (1956) by deriving transport equations for a collisionless anisotropic plasma including transport phenomena such as collisionless 'viscosity' and heat flow.

All of the studies cited above were concerned with collisionless anisotropic plasmas. However, Chodura and Pohl (1971) derived transport equations for an anisotropic plasma that were based on a bi-Maxwellian species distribution function and that included Coulomb collisions between the interacting species. This study was extended by Demars and Schunk (1979), who derived collision terms for an anisotropic plasma of arbitrary degree of ionization. Specifically, Demars and Schunk (1979) derived collision terms for a resonant charge exchange interaction between an ion and its parent neutral and for an arbitrary inverse-power interaction potential, which includes Coulomb, nonresonant ion-neutral (Maxwell molecule), and constant collision cross section (hard sphere) interactions as special cases.

In chapter (II), I try to present a unified approach to the study of transport phenomena in multicomponent anisotropic space plasmas. In particular, a system of generalized transport equations is presented that can be applied to a highly anisotropic plasma of arbitrary degree of ionization. This system of generalized transport equations

is shown to reduce to the 13-moment system of transport equations in the limit of small temperature anisotropies. Also, the system of generalized transport equations is shown to contain all of the other major systems of transport equations for anisotropic plasmas that have been derived to date.

The collision terms derived by Chodura and Pohl (1971) and by Demars and Schunk (1979) are valid for arbitrary temperature differences between the interacting gases and arbitrary temperature anisotropies, but are restricted to small relative drifts between the interacting gases. In chapter (III), I remove the latter restriction and calculate momentum and energy exchange collision terms for interpenetrating bi-Maxwellian gases that are valid for arbitrary drift velocity differences and temperature differences between the interacting gases as well as for arbitrary temperature anisotropies. I also derive the closed set of transport equations that are associated with the momentum and energy collision terms.

In chapter (IV) I study the extent to which transport equations based on both Maxwellian and bi-Maxwellian series expansions can describe plasma flows characterized by non-Maxwellian velocity distributions, with emphasis given to modelling the anisotropic character of the distribution function. For the Maxwellian expansion, I consider the 5-, 13-, and 20-moment approximations of Grad (1958). For the bi-Maxwellian expansion, I consider the 6- and 16-moment approximations (cf. Chodura and Pohl 1971, Demars and Schunk 1979). To determine the adequacy of a given series expansion, I select a simple plasma

flow problem which possesses an analytic solution so that the distribution functions obtained from the different series expansions can be compared with the exact, closed-form solution.

This simple plasma flow problem is the steady state flow of a homogeneous, weakly-ionized plasma subjected to homogeneous electric and magnetic fields. By modelling the ion-neutral collision process with a simple relaxation model, it is possible to obtain an exact, closed-form solution for the ion velocity distribution function. A range of non-Maxwellian ion velocity distributions is generated by varying the magnitude and direction of the electric field and by varying the ion collision-to-cyclotron frequency ratio. Although this plasma flow model is relevant to both the terrestrial (St-Maurice and Schunk 1979) and Venusian (Schunk and St-Maurice 1981) ionospheres, in this study it is only used to generate non-Maxwellian ion velocity distributions to test the adequacy of the different series expansions. The main result I obtain is that the Maxwellian-based 20-moment approximation is a reasonable approximation for temperature anisotropies up to  $T_{\parallel} / T_{\perp} \sim 2-3$ , while the bi-Maxwellian-based 16-moment approximation can describe temperature anisotropies as large as  $T_{\parallel} / T_{\perp} \sim 20$ .

Although the results of chapter (IV) are obtained for a homogeneous plasma and a simple collision model, they should be useful in providing clues as to the extent to which a given series expansion can account for the anisotropic character of a plasma. However, a more realistic collision model will produce a smaller temperature aniso-

tropy than the simple collision model for given electric and magnetic fields, and it is not clear to what extent this will affect the results. Therefore, in chapter (V) I use more rigorous collision models and compare Maxwellian and bi-Maxwellian expansions with Monte Carlo simulations in order to determine the adequacy of a given series expansion. Also, it should be noted that Monte Carlo simulations with crossed electric and magnetic fields have not been presented before.

In this work I do not discuss plasma instabilities and wave-particle interactions. Although these processes undoubtedly affect certain transport properties in, for example, the aurora and the solar wind, they are difficult to include mathematically in a rigorous way. The difficulty with wave-particle interactions is that accurate expressions for the "collision" cross sections are not available. However, from classical collision theory we know that accurate collision cross sections are needed to correctly describe transport processes such as thermal diffusion and thermoelectric transport. For example, thermal diffusion does not occur for elastic ion-neutral interactions, but is important for Coulomb interactions. A further difficulty with wave-particle interactions is the inability to obtain reliable approximations for the species velocity distribution functions when these interactions are included. This, in turn, makes it difficult to close the general system of transport equations.

## CHAPTER II

TRANSPORT EQUATIONS FOR MULTICOMPONENT  
ANISOTROPIC SPACE PLASMAS

In this chapter I present a unified approach to the study of transport phenomena in multicomponent anisotropic space plasmas. In particular, a system of generalized transport equations is presented that can be applied to a highly anisotropic plasma of arbitrary degree of ionization. This system of generalized transport equations is shown to reduce to the 13-moment system of transport equations in the limit of small temperature anisotropies. Also, the system of generalized transport equations is shown to contain all of the other major systems of transport equations for anisotropic plasmas that have been derived to date.

## 1. General transport equations

In dealing with gas mixtures it is convenient to describe each species in the mixture by a separate velocity distribution function,  $f_s(\underline{r}, \underline{v}_s, t)$ . The distribution function is defined such that  $f_s(\underline{r}, \underline{v}_s, t) d\underline{r}d\underline{v}_s$  represents the number of particles of species  $s$  which at time  $t$  have positions between  $\underline{r}$  and  $\underline{r}+d\underline{r}$  and velocities between  $\underline{v}_s$  and  $\underline{v}_s+d\underline{v}_s$ . Alternatively,  $f_s$  can be viewed as a probability density in the  $\underline{r}, \underline{v}_s$  phase space. The evolution in time of the species distribution function is determined by the net effect of collisions and the flow in phase space of particles under the influence of external forces. The mathematical description of this evolution is given by the well known

Boltzmann equation

$$\frac{\partial f_s}{\partial t} + \underline{v}_s \cdot \underline{\nabla} f_s + \frac{e_s}{m_s} (\underline{E} + \frac{1}{c} \underline{v}_s \times \underline{B}) \cdot \underline{\nabla}_v f_s = \frac{\delta f_s}{\delta t} \quad (1)$$

where  $e_s$  and  $m_s$  are the charge and mass of species  $s$ ,  $\underline{E}$  is the electric field,  $\underline{B}$  is the magnetic field,  $c$  is the speed of light,  $\frac{\partial}{\partial t}$  is the time derivative,  $\underline{\nabla}$  is coordinate space gradient, and  $\underline{\nabla}_v$  is the velocity space gradient.

The quantity  $\frac{\delta f_s}{\delta t}$  in Boltzmann's equation represents the rate of change of  $f_s$  in a given region of phase space as a result of collisions. For collisions governed by inverse power potentials and for resonant charge exchange collisions, the appropriate expression for  $\frac{\delta f_s}{\delta t}$  is the Boltzmann collision integral which is given by

$$\frac{\delta f_s}{\delta t} = \sum_t \int d\underline{v}_t \, d\Omega \, g_{st} \, \sigma_{st}(g_{st}, \chi) [f'_s f'_t - f_s f_t] \quad (2)$$

where  $d\underline{v}_t$  is the velocity-space volume element of species  $t$ ,  $g_{st}$  is the relative velocity of the colliding particles  $s$  and  $t$ ,  $\sigma_{st}(g_{st}, \chi)$  is the differential scattering cross-section,  $d\Omega$  is the element of solid angle in the  $s$  particle reference frame,  $\chi$  is the scattering angle, and the primes denote quantities evaluated after a collision.

Although it would be nice to know the individual velocity distribution functions of the different species, the mathematical difficulties associated with obtaining closed-form solutions to Boltzmann's equation precludes this approach for most flow situations. As a consequence, one is generally restricted to obtaining information on a limited number of low-order velocity moments of the species distribution function.

Burgers (1969, p. 14) proposed that the transport properties of a

given species can be defined with respect to the average drift velocity of that species. In terms of the species average drift velocity  $\underline{u}_s$ , the random or thermal velocity is defined as

$$\underline{c}_s = \underline{v}_s - \underline{u}_s \quad (3)$$

and the physically significant moments of the species distribution function are given by

$$\underline{u}_s = \langle \underline{v}_s \rangle \quad \text{species drift velocity} \quad (4)$$

$$T_{s\parallel} = \frac{m_s}{k} \langle c_{s\parallel}^2 \rangle \quad \text{parallel temperature} \quad (5)$$

$$T_{s\perp} = \frac{m_s}{2k} \langle c_{s\perp}^2 \rangle \quad \text{perpendicular temperature} \quad (6)$$

$$\underline{q}_{s\parallel} = n_s m_s \langle c_{s\parallel}^2 \underline{c}_s \rangle \quad \text{heat flow vector for parallel energy} \quad (7)$$

$$\underline{q}_{s\perp} = \frac{1}{2} n_s m_s \langle c_{s\perp}^2 \underline{c}_s \rangle \quad \text{heat flow vector for perpendicular energy} \quad (8)$$

$$\underline{P}_s = n_s m_s \langle \underline{c}_s \underline{c}_s \rangle \quad \text{pressure tensor} \quad (9)$$

$$\underline{r}_s = \underline{P}_s - p_s \underline{1} - (p_{s\parallel} - p_{s\perp}) \underline{e}_3 \underline{e}_3 \quad \text{stress tensor} \quad (10)$$

$$\underline{\mu}_{s\parallel} = n_s m_s \langle c_{s\parallel}^2 \underline{c}_s \underline{c}_s \rangle \quad \text{higher order pressure tensor related to parallel energy} \quad (11)$$

$$\underline{\mu}_{s\perp} = n_s m_s \langle c_{s\perp}^2 \underline{c}_s \underline{c}_s \rangle \quad \text{higher order pressure tensor related to perpendicular energy} \quad (12)$$

$$\underline{Q}_s = n_s m_s \langle \underline{c}_s \underline{c}_s \underline{c}_s \rangle \quad \text{heat flow tensor} \quad (13)$$

$$\underline{R}_s = n_s m_s \langle \underline{c}_s \underline{c}_s \underline{c}_s \underline{c}_s \rangle \quad \text{higher order pressure tensor} \quad (14)$$

where  $p_{s\parallel} = n_s k T_{s\parallel}$ ,  $p_{s\perp} = n_s k T_{s\perp}$ ,  $n_s$  is the number density of species  $s$ ,  $k$  is Boltzmann's constant,  $\underline{1} = \underline{e}_1 \underline{e}_1 + \underline{e}_2 \underline{e}_2 + \underline{e}_3 \underline{e}_3$  is the unit dyadic,  $(\underline{e}_1, \underline{e}_2, \underline{e}_3)$  is an orthogonal set of unit vectors with  $\underline{e}_3$  aligned along the direction of the magnetic field, and the angle brackets denote the average



$$\langle \underline{A} \rangle = \frac{1}{n_s} \int d\underline{v}_s f_s \underline{A} \quad (15)$$

The symbols  $\parallel$  and  $\perp$  are used to denote components of vectors parallel and perpendicular to the magnetic field, respectively, as well as to identify quantities related to parallel and perpendicular thermal energy. In general subscripts are used, but for quantities such as  $\underline{q}_s^{\parallel}$ ,  $\underline{q}_s^{\perp}$ ,  $\underline{\mu}_s^{\parallel}$ , and  $\underline{\mu}_s^{\perp}$  superscripts are used to relate them to the parallel and perpendicular thermal energies, while subscripts are used to define components parallel and perpendicular to the magnetic field.

The quantities  $p_{s\parallel}$ ,  $p_{s\perp}$ ,  $\underline{q}_s^{\parallel}$ ,  $\underline{q}_s^{\perp}$ ,  $\underline{\mu}_s^{\parallel}$  and  $\underline{\mu}_s^{\perp}$  can be expressed as contracted forms of the higher order tensors  $\underline{P}_s$ ,  $\underline{Q}_s$  and  $\underline{R}_s$  as follows

$$p_{s\parallel} = \underline{P}_s : \underline{e}_3 \underline{e}_3 \quad (16)$$

$$p_{s\perp} = (1/2) \underline{P}_s : (\underline{I} - \underline{e}_3 \underline{e}_3) \quad (17)$$

$$\underline{q}_s^{\parallel} = \underline{Q}_s : \underline{e}_3 \underline{e}_3 \quad (18)$$

$$\underline{q}_s^{\perp} = (1/2) \underline{Q}_s : (\underline{I} - \underline{e}_3 \underline{e}_3) \quad (19)$$

$$\underline{\mu}_s^{\parallel} = \underline{R}_s : \underline{e}_3 \underline{e}_3 \quad (20)$$

$$\underline{\mu}_s^{\perp} = \underline{R}_s : (\underline{I} - \underline{e}_3 \underline{e}_3) \quad (21)$$

The starting point for the derivation of transport equations for gas mixtures is Boltzmann's equation (1). The transport equations are obtained by multiplying Boltzmann's equations with an appropriate function of velocity, and then integrating over velocity space. The resulting transport equations describe the spatial and temporal behavior of the physically significant moments of the distribution function such as species concentration, drift velocity, parallel and perpendicular temperature, stress tensor, and parallel and perpendicular heat flow.

If we multiply equation (1) by  $m_s$ ,  $m_s c_{s\perp}^2$ ,  $m_s c_{s\parallel}^2$ ,  $m_s c_{s\perp}^2/2$ ,  $m_s c_{s\perp} c_{s\perp}$ ,  $m_s c_{s\parallel}^2$  and  $m_s c_{s\perp} c_{s\perp}/2$  and integrate over velocity space we obtain the

continuity, momentum, parallel energy, perpendicular energy, pressure tensor, parallel heat flow, and perpendicular heat flow equations, respectively, for species  $s$ . The stress tensor equation is obtained by subtracting  $\underline{e}_3 \underline{e}_3$  times the parallel energy equation and  $(\underline{I} - \underline{e}_3 \underline{e}_3)$  times the perpendicular energy equation from the pressure tensor equation. The resulting system of transport equations is given by

Continuity

$$\frac{\partial \rho_s}{\partial t} + \underline{\nabla} \cdot (\rho_s \underline{u}_s) = 0 \quad (22)$$

Momentum

$$\begin{aligned} \rho_s \frac{D_s \underline{u}_s}{Dt} + \underline{\nabla}_\perp p_{s\perp} + \underline{\nabla}_\parallel p_{s\parallel} + \underline{\nabla} \cdot \underline{\tau}'_s - n_s e_s (\underline{E} + \frac{1}{c} \underline{u}_s \times \underline{B}) \\ + (P_{s\parallel\parallel} - P_{s\perp\perp}) \underline{\nabla} \cdot (\underline{e}_3 \underline{e}_3) = \frac{\delta M_s}{\delta t} \end{aligned} \quad (23)$$

Parallel energy

$$\begin{aligned} \frac{D_s p_{s\parallel\parallel}}{Dt} + p_{s\parallel\parallel} (\underline{\nabla} \cdot \underline{u}_s + 2 \underline{\nabla}_\parallel \cdot \underline{u}_s) + 2 \underline{e}_3 \underline{e}_3 : [\underline{\tau}'_s \cdot \underline{\nabla} \underline{u}_s] + \underline{\nabla} \cdot \underline{q}_s^\parallel \\ - \underline{\tau}'_s : \frac{D_s}{Dt} (\underline{e}_3 \underline{e}_3) - \underline{Q}_s : \underline{\nabla} (\underline{e}_3 \underline{e}_3) = \frac{\delta E_{s\parallel\parallel}}{\delta t} \end{aligned} \quad (24)$$

Perpendicular energy

$$\begin{aligned} \frac{D_s p_{s\perp\perp}}{Dt} + p_{s\perp\perp} (\underline{\nabla} \cdot \underline{u}_s + \underline{\nabla}_\perp \cdot \underline{u}_s) + (\underline{I} - \underline{e}_3 \underline{e}_3) : [\underline{\tau}'_s \cdot \underline{\nabla} \underline{u}_s] + \underline{\nabla} \cdot \underline{q}_s^\perp \\ + \frac{1}{2} \underline{\tau}'_s : \frac{D_s}{Dt} (\underline{e}_3 \underline{e}_3) + \frac{1}{2} \underline{Q}_s : \underline{\nabla} (\underline{e}_3 \underline{e}_3) = \frac{\delta E_{s\perp\perp}}{\delta t} \end{aligned} \quad (25)$$

Stress tensor

$$\begin{aligned} \frac{D_s \underline{\tau}'_s}{Dt} + p_{s\parallel\parallel} [\underline{\nabla}_\parallel \underline{u}_s + (\underline{\nabla}_\parallel \underline{u}_s)^T - 2 \underline{e}_3 \underline{e}_3 \underline{\nabla}_\parallel \cdot \underline{u}_s] + p_{s\perp\perp} [\underline{\nabla}_\perp \underline{u}_s + (\underline{\nabla}_\perp \underline{u}_s)^T \\ - (\underline{I} - \underline{e}_3 \underline{e}_3) \underline{\nabla}_\perp \cdot \underline{u}_s] + \underline{\tau}'_s (\underline{\nabla} \cdot \underline{u}_s) + \underline{\tau}'_s \cdot \underline{\nabla} \underline{u}_s + (\underline{\tau}'_s \cdot \underline{\nabla} \underline{u}_s)^T - 2 \underline{e}_3 \underline{e}_3 \underline{e}_3 \underline{e}_3 : [\underline{\tau}'_s \cdot \underline{\nabla} \underline{u}_s] \\ - (\underline{I} - \underline{e}_3 \underline{e}_3) (\underline{I} - \underline{e}_3 \underline{e}_3) : [\underline{\tau}'_s \cdot \underline{\nabla} \underline{u}_s] + \underline{\nabla} \cdot \underline{Q}_s - \underline{e}_3 \underline{e}_3 \underline{\nabla} \cdot \underline{q}_s^\parallel - (\underline{I} - \underline{e}_3 \underline{e}_3) \underline{\nabla} \cdot \underline{q}_s^\perp \end{aligned}$$

$$\begin{aligned}
& + \underline{\Omega}_s \times \underline{\tau}'_s - \underline{\tau}'_s \times \underline{\Omega}_s + (\rho_{s\parallel} - \rho_{s\perp}) \frac{D_s}{Dt} (\underline{e}_3 \underline{e}_3) - \frac{1}{2} (\underline{I} - 3 \underline{e}_3 \underline{e}_3) \\
& \times [\underline{\tau}'_s : \frac{D_s}{Dt} (\underline{e}_3 \underline{e}_3) + \underline{Q}_s : \underline{\nabla} (\underline{e}_3 \underline{e}_3)] = \frac{\delta \underline{\tau}'_s}{\delta t}
\end{aligned} \quad (26)$$

Parallel heat flow

$$\begin{aligned}
& \frac{D_s q_s^{\parallel}}{Dt} + 2 [\underline{Q}_s \cdot \underline{\nabla} \underline{u}_s] : \underline{e}_3 \underline{e}_3 + \underline{q}_s^{\parallel} \underline{\nabla} \cdot \underline{u}_s + \underline{q}_s^{\parallel} \cdot \underline{\nabla} \underline{u}_s + \underline{\nabla} \cdot \underline{u}_s^{\parallel} \\
& + \left[ \frac{D_s \underline{u}_s}{Dt} - \frac{e_s}{m_s} (\underline{E} + \frac{1}{c} \underline{u}_s \times \underline{B}) \right] \cdot \left[ \rho_{s\parallel} \underline{I} + 2 \underline{e}_3 \underline{e}_3 \cdot (\rho_{s\parallel} \underline{I} + \underline{\tau}'_s) \right] \\
& + \underline{\Omega}_s \times \underline{q}_s^{\parallel} - \underline{Q}_s : \frac{D_s}{Dt} (\underline{e}_3 \underline{e}_3) - \underline{R}_s : \underline{\nabla} (\underline{e}_3 \underline{e}_3) = \frac{\delta q_s^{\parallel}}{\delta t}
\end{aligned} \quad (27)$$

Perpendicular heat flow

$$\begin{aligned}
& \frac{D_s q_s^{\perp}}{Dt} + [\underline{Q}_s \cdot \underline{\nabla} \underline{u}_s] : (\underline{I} - \underline{e}_3 \underline{e}_3) + \underline{q}_s^{\perp} \underline{\nabla} \cdot \underline{u}_s + \underline{q}_s^{\perp} \cdot \underline{\nabla} \underline{u}_s + \frac{1}{2} \underline{\nabla} \cdot \underline{u}_s^{\perp} \\
& + \left[ \frac{D_s \underline{u}_s}{Dt} - \frac{e_s}{m_s} (\underline{E} + \frac{1}{c} \underline{u}_s \times \underline{B}) \right] \cdot \left[ \rho_{s\perp} \underline{I} + (\underline{I} - \underline{e}_3 \underline{e}_3) \cdot (\rho_{s\perp} \underline{I} + \underline{\tau}'_s) \right] \\
& + \underline{\Omega}_s \times \underline{q}_s^{\perp} + \frac{1}{2} \underline{Q}_s : \frac{D_s}{Dt} (\underline{e}_3 \underline{e}_3) + \frac{1}{2} \underline{R}_s : \underline{\nabla} (\underline{e}_3 \underline{e}_3) = \frac{\delta q_s^{\perp}}{\delta t}
\end{aligned} \quad (28)$$

where  $\frac{D_s}{Dt} = \frac{\partial}{\partial t} + \underline{u}_s \cdot \underline{\nabla}$  is the convective derivative,  $\rho_s = n_s m_s$  is the mass density,  $\underline{\Omega}_s = \frac{e_s}{m_s c} \underline{B}$  is the cyclotron frequency, and the single, double, and triple dot products are defined, for example, as

$$\begin{aligned}
\underline{q} \cdot \underline{\nabla} &= \sum_{\alpha} q_{\alpha} \frac{\partial}{\partial x_{\alpha}}, & \underline{\tau}' : \underline{\nabla} \underline{u} &= \sum_{\alpha, \beta} \tau'_{\alpha\beta} (\underline{\nabla} \underline{u})_{\beta\alpha}, \\
\underline{Q} : \underline{\nabla} \underline{e}_3 \underline{e}_3 &= \sum_{\alpha, \beta, \gamma} Q_{\alpha\beta\gamma} (\underline{\nabla} \underline{e}_3 \underline{e}_3)_{\gamma\beta\alpha}
\end{aligned}$$

and where  $\alpha$ ,  $\beta$  and  $\gamma$  are coordinate indices (cf. Chapman and Cowling 1970). The parallel and perpendicular components of a vector  $\underline{A}$  are defined by  $\underline{A}_{\parallel} = \underline{e}_3 \underline{e}_3 \cdot \underline{A}$  and  $\underline{A}_{\perp} = (\underline{I} - \underline{e}_3 \underline{e}_3) \cdot \underline{A}$ , respectively. A superscript T on a tensor means the elements of the tensor should be transposed.

The quantities on the right-hand sides of equations (23) - (28) correspond to the velocity moments of the Boltzmann collision integral (2) and describe, respectively, the rate of change of momentum, parallel and perpendicular energy, stress, and parallel and perpendicular heat flow as a result of collisions; these quantities will be discussed in detail in section (3).

2. The sixteen-moment approximation

The system of transport equations given in section (1) does not constitute a closed set, since the equation governing the moment of order  $l$  contains the moment of order  $l + 1$ . In order to close the system of transport equations, it is necessary to adopt an approximate expression for the species distribution function. My approximation expression is based on a bi-Maxwellian or two-temperature species distribution function and takes the form

$$f_s = f_s^{(b)} [1 + \phi_s] \quad (29)$$

where the zeroth-order bi-Maxwellian distribution is given by

$$f_s^{(b)} = n_s (2\pi)^{-3/2} \beta_{s\perp} (\beta_{s\parallel})^{1/2} \exp\left(-\frac{1}{2} \beta_{s\perp} c_{s\perp}^2 - \frac{1}{2} \beta_{s\parallel} c_{s\parallel}^2\right) \quad (30)$$

and where

$$\begin{aligned} \phi_s = & \frac{\beta_{s\perp}}{2\rho_s} [\beta_{s\perp} (c_{s1}^2 - c_{s2}^2) (\tau_s' : e_1 e_1) + 2 \beta_{s\perp} (\tau_s' : e_1 e_2) c_{s1} c_{s2} \\ & + 2 \beta_{s\parallel} \tau_s' : c_{s\perp} c_{s\parallel}] - \frac{\beta_{s\perp}^2}{\rho_s} \left(1 - \frac{\beta_{s\perp} c_{s\perp}^2}{4}\right) \frac{q_s \cdot c_{s\perp}}{q_s \cdot c_{s\perp}} \\ & - \frac{\beta_{s\perp} \beta_{s\parallel}}{\rho_s} \left(1 - \frac{\beta_{s\perp} c_{s\perp}^2}{2}\right) \frac{q_s \cdot c_{s\parallel}}{q_s \cdot c_{s\parallel}} - \frac{\beta_{s\parallel}^2}{2\rho_s} \left(1 - \frac{\beta_{s\parallel} c_{s\parallel}^2}{3}\right) \frac{q_s \cdot c_s}{q_s \cdot c_s} \\ & - \frac{\beta_{s\perp} \beta_{s\parallel}}{2\rho_s} \left(1 - \beta_{s\parallel} c_{s\parallel}^2\right) \frac{q_s \cdot c_{s\perp}}{q_s \cdot c_{s\perp}} \end{aligned} \quad (31)$$

In equations (30) and (31),  $\beta_{s\parallel} = m_s / (k T_{s\parallel})$  and  $\beta_{s\perp} = m_s / (k T_{s\perp})$ .

By taking the appropriate velocity moments of (29), it is easy to verify that this distribution function correctly accounts for the density, drift velocity, parallel and perpendicular temperatures, stress tensor, and parallel and perpendicular heat flow moments. By taking the higher-order velocity moments of equation (29) it is possible to express these moments in terms of the 16 lower-order moments

$$\begin{aligned}
\underline{Q}_s &= \underline{q}_s^{||} \underline{e}_3 \underline{e}_3 + \underline{e}_3 \underline{q}_s^{||} \underline{e}_3 + \underline{e}_3 \underline{e}_3 \underline{q}_s^{||} - 2 \underline{q}_s^{||} \underline{e}_3 \underline{e}_3 \\
&+ \frac{1}{2} [\underline{q}_s^{\perp} (\underline{I} - \underline{e}_3 \underline{e}_3) + \underline{e}_1 \underline{q}_s^{\perp} \underline{e}_1 + \underline{e}_2 \underline{q}_s^{\perp} \underline{e}_2 + (\underline{I} - \underline{e}_3 \underline{e}_3) \underline{q}_s^{\perp}] \\
&+ \frac{1}{2} [\underline{q}_s^{\perp} (\underline{I} - \underline{e}_3 \underline{e}_3) + \underline{e}_1 \underline{q}_s^{\perp} \underline{e}_1 + \underline{e}_2 \underline{q}_s^{\perp} \underline{e}_2 + (\underline{I} - \underline{e}_3 \underline{e}_3) \underline{q}_s^{\perp}] \quad (32)
\end{aligned}$$

$$\begin{aligned}
(\underline{R}_s)_{\alpha\beta\gamma\delta} &= \frac{1}{\rho_s} \left[ (\underline{P}_s)_{\alpha\beta} (\underline{P}_s)_{\gamma\delta} + (\underline{P}_s)_{\alpha\gamma} (\underline{P}_s)_{\beta\delta} + (\underline{P}_s)_{\alpha\delta} (\underline{P}_s)_{\beta\gamma} \right. \\
&\left. - (\underline{\tau}'_s)_{\alpha\beta} (\underline{\tau}'_s)_{\gamma\delta} - (\underline{\tau}'_s)_{\alpha\gamma} (\underline{\tau}'_s)_{\beta\delta} - (\underline{\tau}'_s)_{\alpha\delta} (\underline{\tau}'_s)_{\beta\gamma} \right] \quad (33)
\end{aligned}$$

$$\underline{u}_s^{||} = \frac{p_{s||}}{\rho_s} [3p_{s||} \underline{e}_3 \underline{e}_3 + p_{s\perp} (\underline{I} - \underline{e}_3 \underline{e}_3) + \underline{\tau}'_s + 2\underline{\tau}'_s \cdot \underline{e}_3 \underline{e}_3 + 2\underline{e}_3 \underline{e}_3 \cdot \underline{\tau}'_s] \quad (34)$$

$$\underline{u}_s^{\perp} = \frac{p_{s\perp}}{\rho_s} [2p_{s||} \underline{e}_3 \underline{e}_3 + 4p_{s\perp} (\underline{I} - \underline{e}_3 \underline{e}_3) + 6\underline{\tau}'_s - 2\underline{\tau}'_s \cdot \underline{e}_3 \underline{e}_3 - 2\underline{e}_3 \underline{e}_3 \cdot \underline{\tau}'_s] \quad (35)$$

where we have temporarily introduced index notation into (33). From equations (32)-(35) we can readily obtain the terms needed to close the system of moment equations.

$$\begin{aligned}
\underline{\nabla} \cdot \underline{Q}_s &= \underline{\nabla}_{||} \underline{q}_s^{||} + (\underline{\nabla}_{||} \underline{q}_s^{||})^T + \underline{e}_3 \underline{e}_3 \underline{\nabla} \cdot (\underline{q}_s^{||} - 2\underline{q}_s^{||}) + \frac{1}{2} [\underline{\nabla}_{\perp} (\underline{q}_s^{\perp} + \underline{q}_s^{\perp}) \\
&+ (\underline{\nabla}_{\perp} (\underline{q}_s^{\perp} + \underline{q}_s^{\perp}))^T + (\underline{I} - \underline{e}_3 \underline{e}_3) \underline{\nabla} \cdot (\underline{q}_s^{\perp} + \underline{q}_s^{\perp})] + (\underline{q}_s^{||} - \frac{1}{2} \underline{q}_s^{\perp} - \frac{1}{2} \underline{q}_s^{\perp}) \underline{\nabla} \cdot (\underline{e}_3 \underline{e}_3) \\
&+ \underline{\nabla} \cdot (\underline{e}_3 \underline{e}_3) (\underline{q}_s^{||} - \frac{1}{2} \underline{q}_s^{\perp} - \frac{1}{2} \underline{q}_s^{\perp}) + (\underline{q}_s^{||} - 2\underline{q}_s^{||} - \frac{1}{2} \underline{q}_s^{\perp} - \frac{1}{2} \underline{q}_s^{\perp}) \cdot \underline{\nabla} \underline{e}_3 \underline{e}_3 \quad (36)
\end{aligned}$$

$$[\underline{Q}_s \cdot \underline{\nabla} \underline{u}_s] : \underline{e}_3 \underline{e}_3 = \underline{e}_3 \underline{e}_3 \underline{q}_s^{||} : \underline{\nabla} \underline{u}_s + \underline{q}_s^{\perp} \underline{\nabla}_{||} \cdot \underline{u}_s + (\underline{\nabla}_{\perp} \underline{u}_s) \cdot \underline{q}_s^{\perp} \quad (37)$$

$$\begin{aligned}
[\underline{Q}_s \cdot \underline{\nabla} \underline{u}_s] : (\underline{I} - \underline{e}_3 \underline{e}_3) &= (\underline{\nabla}_{||} \underline{u}_s) \cdot \underline{q}_s^{\perp} + \frac{1}{2} \left[ (\underline{\nabla}_{\perp} \underline{u}_s) \cdot \underline{q}_s^{\perp} + (\underline{q}_s^{\perp} + \underline{q}_s^{\perp}) (\underline{\nabla}_{\perp} \cdot \underline{u}_s) \right. \\
&\left. + (\underline{I} - \underline{e}_3 \underline{e}_3) (\underline{q}_s^{\perp} + \underline{q}_s^{\perp}) : \underline{\nabla} \underline{u}_s \right] \quad (38)
\end{aligned}$$

$$\underline{Q}_s : \frac{D_s}{Dt} (\underline{e}_3 \underline{e}_3) = 2 \left[ \underline{e}_3 \underline{q}_s^{||} \cdot \frac{D_s \underline{e}_3}{Dt} + \underline{e}_3 \cdot \underline{q}_s^{\perp} \frac{D_s \underline{e}_3}{Dt} \right] \quad (39)$$

$$\underline{Q}_s : \underline{\nabla} (\underline{e}_3 \underline{e}_3) = 2 [\underline{q}_s^{||} \underline{e}_3 : \underline{\nabla} \underline{e}_3 + (\underline{q}_s^{\perp} \cdot \underline{e}_3) (\underline{\nabla} \cdot \underline{e}_3)] \quad (40)$$

$$\begin{aligned} \underline{\nabla} \cdot \underline{\mu}_{\perp}^{\parallel} &= \underline{\nabla}_{\perp} \cdot \left( \frac{p_{s\parallel} p_{s\perp}}{\rho_s} \right) + 3 \underline{\nabla}_{\parallel} \left( \frac{p_{s\parallel}^2}{\rho_s} \right) + (1 + 2 \underline{e}_3 \underline{e}_3) \underline{\nabla} : \left( \frac{p_{s\parallel}}{\rho_s} \underline{\tau}'_s \right) + 2 \underline{\nabla} \cdot \left( \frac{p_{s\parallel}}{\rho_s} \underline{\tau}'_s \right) \\ &+ \frac{p_{s\parallel} (3 p_{s\parallel} - p_{s\perp})}{\rho_s} \underline{\nabla} \cdot \underline{e}_3 \underline{e}_3 + 2 \frac{p_{s\parallel}}{\rho_s} (\underline{\tau}'_s : \underline{\nabla} \underline{e}_3 \underline{e}_3 + \underline{\tau}'_s \underline{\nabla} : \underline{e}_3 \underline{e}_3) \end{aligned} \quad (41)$$

$$\begin{aligned} \underline{\nabla} \cdot \underline{\mu}_{\perp}^{\perp} &= 4 \underline{\nabla}_{\perp} \cdot \left( \frac{p_{s\perp}^2}{\rho_s} \right) + 2 \underline{\nabla}_{\parallel} \left( \frac{p_{s\parallel} p_{s\perp}}{\rho_s} \right) + 2 (3 \underline{1} - \underline{e}_3 \underline{e}_3) \underline{\nabla} : \left( \frac{p_{s\perp}}{\rho_s} \underline{\tau}'_s \right) - 2 \underline{\nabla} \cdot \left( \frac{p_{s\perp}}{\rho_s} \underline{\tau}'_s \right) \\ &+ \frac{2 p_{s\perp} (p_{s\parallel} - 2 p_{s\perp})}{\rho_s} \underline{\nabla} \cdot \underline{e}_3 \underline{e}_3 - 2 \frac{p_{s\perp}}{\rho_s} (\underline{\tau}'_s : \underline{\nabla} \underline{e}_3 \underline{e}_3 + \underline{\tau}'_s \underline{\nabla} : \underline{e}_3 \underline{e}_3) \end{aligned} \quad (42)$$

$$\begin{aligned} \underline{R}_s : \underline{\nabla} (\underline{e}_3 \underline{e}_3) &= \frac{2}{\rho_s} \left[ \underline{P}_s : (\underline{\nabla} \underline{e}_3) \underline{e}_3 \cdot \underline{P}_s + \underline{P}_s \cdot (\underline{\nabla} \underline{e}_3) \underline{e}_3 : \underline{P}_s + \underline{P}_s : \underline{e}_3 (\underline{\nabla} \underline{e}_3) \cdot \underline{P}_s \right. \\ &\left. - \underline{\tau}'_s : (\underline{\nabla} \underline{e}_3) \underline{e}_3 \cdot \underline{\tau}'_s + \underline{\tau}'_s \cdot (\underline{\nabla} \underline{e}_3) \underline{e}_3 : \underline{\tau}'_s - \underline{\tau}'_s : \underline{e}_3 (\underline{\nabla} \underline{e}_3) \cdot \underline{\tau}'_s \right] \end{aligned} \quad (43)$$

Equations (22) - (28) and the closing terms given by equations (36) - (43) constitute, together with Maxwell's equations, a set of closed transport equations that can be applied to a wide range of plasma flow conditions. These generalized transport equations can describe subsonic and supersonic flows, collision-dominated and collisionless flows, plasma flows in rapidly changing magnetic field configurations, multi-component plasma flows with large temperature differences between the interacting species, and plasma flows that contain anisotropic temperature distributions. In addition, these generalized transport equations can describe certain aspects of electrostatic shocks, double layers, and magnetic merging processes.

### 3. Collision terms

Unfortunately, at present there are no general expressions for the collision terms for the 16-moment approximation; namely, collision terms that are valid for arbitrary collision cross section, arbitrary relative drift between different species, arbitrary parallel-to-perpendicular temperature ratio, and arbitrary difference between species temperatures. In this section I present collision terms appropriate for some special cases.

#### 3.1. Maxwell molecule interactions

For the special case of Maxwell molecule interaction, where the interaction force varies inversely as the fifth power of the particle separation, collision terms can be derived without assuming a specific form for the species distribution functions. The collision terms in dyadic notation are given by (Demars and Schunk 1979)

$$\frac{\delta M_s}{\delta t} = - \sum_t \rho_s^v \nu_{st} (\underline{u}_s - \underline{u}_t) \quad (44)$$

$$\begin{aligned} \frac{\delta E_{s\parallel}}{\delta t} = & - \sum_t \frac{\rho_s^v \nu_{st}}{(m_s + m_t)} \left\{ 2k(T_{s\parallel} - T_{t\parallel}) - 2m_t (\underline{u}_s - \underline{u}_t)_\parallel^2 \right. \\ & \left. + \frac{m_t}{2} \frac{A_2(5)}{A_1(5)} \left[ 2k(\sigma_\parallel - \sigma_\perp) - (\underline{u}_s - \underline{u}_t)^2 + 3(\underline{u}_s - \underline{u}_t)_\parallel^2 \right] \right\} \quad (45) \end{aligned}$$

$$\begin{aligned} \frac{\delta E_{s\perp}}{\delta t} = & - \sum_t \frac{\rho_s^v \nu_{st}}{(m_s + m_t)} \left\{ 2k(T_{s\perp} - T_{t\perp}) - m_t (\underline{u}_s - \underline{u}_t)_\perp^2 \right. \\ & \left. + \frac{m_t}{4} \frac{A_2(5)}{A_1(5)} \left[ 2k(\sigma_\perp - \sigma_\parallel) - 2(\underline{u}_s - \underline{u}_t)^2 + 3(\underline{u}_s - \underline{u}_t)_\perp^2 \right] \right\} \quad (46) \end{aligned}$$



$$\frac{\delta \tau'_s}{\delta t} = - \sum_t \frac{2m_s v_{st}}{m_s + m_t} \left\{ \tau'_s \left[ 1 + \frac{3}{4} \frac{m_t}{m_s} \frac{A_2(5)}{A_1(5)} \right] - \frac{n_s}{n_t} \tau'_t \left[ 1 - \frac{3}{4} \frac{A_2(5)}{A_1(5)} \right] \right. \\ \left. - n_s m_t \left[ 1 - \frac{3}{4} \frac{A_2(5)}{A_1(5)} \right] \left[ (\underline{u}_s - \underline{u}_t) (\underline{u}_s - \underline{u}_t) \right. \right. \\ \left. \left. - (\underline{u}_s - \underline{u}_t)_{\parallel} \underline{e}_3 \underline{e}_3 - \frac{1}{2} (\underline{u}_s - \underline{u}_t)_{\perp}^2 (\underline{I} - \underline{e}_3 \underline{e}_3) \right] \right\} \quad (47)$$

$$\frac{\delta q_s^{\parallel}}{\delta t} = - \sum_t v_{st} \left\{ H_{st}^{(7)} \underline{q}_s^{\parallel} - 2H_{st}^{(3)} \frac{\rho_s}{\rho_t} \underline{q}_t^{\parallel} + H_{st}^{(1)} \underline{q}_s^{\perp} - H_{st}^{(2)} \frac{\rho_s}{\rho_t} \underline{q}_t^{\perp} \right. \\ \left. + 2 \left[ H_{st}^{(1)} \underline{q}_s - H_{st}^{(2)} \frac{\rho_s}{\rho_t} \underline{q}_t \right] \cdot \underline{e}_3 \underline{e}_3 \right. \\ \left. + (\underline{u}_s - \underline{u}_t) \cdot \left[ H_{st}^{(1)} \underline{p}_s + H_{st}^{(2)} \frac{\rho_s}{\rho_t} \underline{p}_t \right] \cdot (\underline{I} + 2\underline{e}_3 \underline{e}_3) \right. \\ \left. + (\underline{u}_s - \underline{u}_t)_{\parallel} \cdot \left[ H_{st}^{(6)} \underline{p}_s + H_{st}^{(4)} \frac{\rho_s}{\rho_t} \underline{p}_t \right] \right. \\ \left. + (\underline{u}_s - \underline{u}_t) \left[ H_{st}^{(8)} p_{s\parallel} + 2H_{st}^{(3)} \frac{\rho_s}{\rho_t} p_{t\parallel} + H_{st}^{(2)} p_{s\perp} + H_{st}^{(2)} \frac{\rho_s}{\rho_t} p_{t\perp} \right. \right. \\ \left. \left. + \frac{1}{2} H_{st}^{(2)} \rho_s (\underline{u}_s - \underline{u}_t)^2 + \frac{1}{2} H_{st}^{(4)} \rho_s (\underline{u}_s - \underline{u}_t)_{\parallel}^2 \right] \right. \\ \left. + H_{st}^{(2)} (\underline{u}_s - \underline{u}_t)_{\parallel} \left[ 3p_s + 3 \frac{\rho_s}{\rho_t} p_t + \rho_s (\underline{u}_s - \underline{u}_t)^2 \right] \right\} \quad (48)$$

$$\frac{\delta q_s^{\perp}}{\delta t} = - \sum_t \frac{v_{st}}{2} \left\{ H_{st}^{(1)} \underline{q}_s^{\parallel} - H_{st}^{(2)} \frac{\rho_s}{\rho_t} \underline{q}_t^{\parallel} + H_{st}^{(9)} \underline{q}_s^{\perp} - H_{st}^{(5)} \frac{\rho_s}{\rho_t} \underline{q}_t^{\perp} \right. \\ \left. + 2 \left[ H_{st}^{(1)} \underline{q}_s - H_{st}^{(2)} \frac{\rho_s}{\rho_t} \underline{q}_t \right] \cdot (\underline{I} - \underline{e}_3 \underline{e}_3) \right. \\ \left. + 2(\underline{u}_s - \underline{u}_t) \cdot \left[ H_{st}^{(1)} \underline{p}_s + H_{st}^{(2)} \frac{\rho_s}{\rho_t} \underline{p}_t \right] \cdot (2\underline{I} - \underline{e}_3 \underline{e}_3) \right. \\ \left. + (\underline{u}_s - \underline{u}_t)_{\perp} \cdot \left[ H_{st}^{(6)} \underline{p}_s + H_{st}^{(4)} \frac{\rho_s}{\rho_t} \underline{p}_t \right] \right\}$$

$$\begin{aligned}
& + (\underline{u}_s - \underline{u}_t) \left[ H_{st}^{(2)} p_{s\parallel} + H_{st}^{(2)} \frac{\rho_s}{\rho_t} p_{t\parallel} + H_{st}^{(10)} p_{s\perp} + H_{st}^{(5)} \frac{\rho_s}{\rho_t} p_{t\perp} \right. \\
& \left. + H_{st}^{(2)} \rho_s (\underline{u}_s - \underline{u}_t)^2 + \frac{1}{2} H_{st}^{(4)} \rho_s (\underline{u}_s - \underline{u}_t)_{\perp}^2 \right] \\
& \left. + H_{st}^{(2)} (\underline{u}_s - \underline{u}_t)_{\perp} \left[ 3 p_s + 3 \frac{\rho_s}{\rho_t} p_t + \rho_s (\underline{u}_s - \underline{u}_t)^2 \right] \right\} \quad (49)
\end{aligned}$$

where

$$\sigma_{\parallel} = \frac{T_{s\parallel}}{m_s} + \frac{T_{t\parallel}}{m_t} \quad (50)$$

$$\sigma_{\perp} = \frac{T_{s\perp}}{m_s} + \frac{T_{t\perp}}{m_t} \quad (51)$$

$$p_s = \frac{1}{3} (p_{s\parallel} + 2p_{s\perp}) \quad (52)$$

$$\underline{q}_s = \frac{1}{2} (\underline{q}_{s\parallel} + 2\underline{q}_{s\perp}) \quad (53)$$

and where  $A_1(5)$ ,  $A_2(5)$  and  $v_{st}$  are defined by equations (63) and (64). The quantities  $H_{st}^{(1)}$  to  $H_{st}^{(10)}$  become pure numbers once the identity of the colliding particles is specified; they are given by Demars and Schunk (1979) and are not repeated here.

Equations (44) - (49) show some important features of the collision terms. The rate of change of momentum due to collisions is proportional to the relative drift velocity of the interacting species. The rate of change of parallel energy due to collision is proportional to the difference between the parallel temperatures, the square of the relative drift velocity of the interacting species as well as the difference between parallel and perpendicular temperatures for the same species. The collision term  $\delta E_{s\perp}/\delta t$  has similar form as  $\delta E_{s\parallel}/\delta t$  but it depends on the difference between the perpendicular temperatures rather than the parallel ones and the term due to the anisotropy ( $\sigma_{\parallel} - \sigma_{\perp}$ ) has an opposite

sign because it represents the energy transfer between the parallel and perpendicular directions.

### 3.2. General inverse-power interactions

For interparticle forces other than the inverse fifth-power force discussed above, it is necessary to assume an approximate expression for the distribution function in order to be able to evaluate collision terms. Adopting the 16-moment approximation given by equation (29), Demars and Schunk (1979) derived expressions for the collision terms which are valid for a general inverse-power force, an arbitrary difference between species temperatures and an arbitrary difference between parallel and perpendicular temperatures for the same species. However, they assumed small relative drift velocity, small stress tensor, and small heat flow and kept only linear terms in these quantities. These are known as "quasilinear collision terms" and given by

$$\begin{aligned}
 \frac{\delta M_s}{\delta t} = & - \sum_t \frac{3}{4} \frac{v_{st}}{\pi k \Gamma(\frac{5-n}{2})} \left\{ 2k\rho_s \left[ I_{200} (\underline{u}_s - \underline{u}_t)_\perp + \frac{\sigma_\perp}{\sigma_\parallel} I_{002} (\underline{u}_s - \underline{u}_t)_\parallel \right] \right. \\
 & + \frac{2}{\sigma_\perp} \left[ (2I_{220} - I_{200}) \left( \underline{q}_{s\perp}^\perp - \frac{\rho_s}{\rho_t} \underline{q}_{t\perp}^\perp \right) \right. \\
 & \left. \left. + \frac{\sigma_\perp}{\sigma_\parallel} (2I_{202} - I_{002}) \left( \underline{q}_{s\parallel}^\perp - \frac{\rho_s}{\rho_t} \underline{q}_{t\parallel}^\perp \right) \right] \right\} \\
 & + \frac{1}{\sigma_\parallel} \left[ \left( 2 \frac{\sigma_\perp}{\sigma_\parallel} I_{202} - I_{200} \right) \left( \underline{q}_{s\perp}^\parallel - \frac{\rho_s}{\rho_t} \underline{q}_{t\perp}^\parallel \right) \right. \\
 & \left. \left. + \frac{\sigma_\perp}{\sigma_\parallel} \left( \frac{2}{3} \frac{\sigma_\perp}{\sigma_\parallel} I_{004} - I_{002} \right) \left( \underline{q}_{s\parallel}^\parallel - \frac{\rho_s}{\rho_t} \underline{q}_{t\parallel}^\parallel \right) \right] \right\} \quad (54)
 \end{aligned}$$

$$\frac{\delta E_{s\parallel}}{\delta t} = - \sum_t \frac{3}{2} \frac{\rho_s v_{st}^k}{\pi \Gamma(\frac{5-n}{2}) (m_s + m_t)} \left\{ 2 \frac{\sigma_{\perp}}{\sigma_{\parallel}} (T_{s\parallel} - T_{t\parallel}) I_{002} + m_t \frac{A_2(a)}{A_1(a)} \sigma_{\perp} (I_{002} - I_{200}) \right\} \quad (55)$$

$$\frac{\delta E_{s\perp}}{\delta t} = - \sum_t \frac{3}{4} \frac{\rho_s v_{st}^k}{\pi \Gamma(\frac{5-n}{2}) (m_s + m_t)} \left\{ 4 (T_{s\perp} - T_{t\perp}) I_{200} + m_t \frac{A_2(a)}{A_1(a)} \sigma_{\perp} (I_{200} - I_{002}) \right\} \quad (56)$$

$$\begin{aligned} \frac{\delta \tau'_s}{\delta t} = & - \sum_t \frac{3}{2} \frac{v_{st}}{\pi \Gamma(\frac{5-n}{2})} \left\{ \left[ (\tau'_{s11} (e_{-1}e_{-1} - e_{-2}e_{-2}) + (\tau'_{s12} (e_{-1}e_{-2} + e_{-2}e_{-1}))) \right] \right. \\ & \times \left( \frac{4}{m_o \sigma_{\perp}} (T_{s\perp} - T_{t\perp}) I_{220} + \frac{2}{\sigma_{\perp}} \frac{T_{t\perp}}{m_t} I_{200} + 3 \frac{m_t}{m_o} \frac{A_2(a)}{A_1(a)} I_{220} \right) \\ & + \frac{\rho_s}{\rho_t} \left[ (\tau'_{t11} (e_{-1}e_{-1} - e_{-2}e_{-2}) + (\tau'_{t12} (e_{-1}e_{-2} + e_{-2}e_{-1}))) \right] \\ & \times \left( \frac{4}{m_o \sigma_{\perp}} (T_{s\perp} - T_{t\perp}) I_{220} - \frac{2}{\sigma_{\perp}} \frac{T_{s\perp}}{m_s} I_{200} + 3 \frac{m_t}{m_o} \frac{A_2(a)}{A_1(a)} I_{220} \right) \\ & + \frac{1}{\sigma_{\parallel}} \left[ (\tau'_{s13} (e_{-1}e_{-3} + e_{-3}e_{-1}) + (\tau'_{s23} (e_{-2}e_{-3} + e_{-3}e_{-2}))) \right] \\ & \times \left( \frac{2}{m_o} I_{202} \left[ (T_{s\perp} - T_{t\perp}) + \frac{\sigma_{\perp}}{\sigma_{\parallel}} (T_{s\parallel} - T_{t\parallel}) \right] \right. \\ & \left. + \frac{T_{t\parallel}}{m_t} I_{200} + \frac{T_{t\perp}}{m_t} I_{002} + 3 \frac{m_t}{m_o} \frac{A_2(a)}{A_1(a)} \sigma_{\perp} I_{202} \right) \end{aligned}$$

$$\begin{aligned}
& + \frac{\rho_s}{\rho_t} \frac{1}{\sigma_{\parallel}} \left[ (\tau'_t)_{13} (e_{-1}e_{-3} + e_{-3}e_{-1}) + (\tau'_t)_{23} (e_{-2}e_{-3} + e_{-3}e_{-2}) \right] \\
& \times \left( \frac{2}{m_o} I_{202} \left[ (T_{s\perp} - T_{t\perp}) + \frac{\sigma_{\perp}}{\sigma_{\parallel}} (T_{s\parallel} - T_{t\parallel}) \right] - \frac{T_{s\parallel}}{m_s} I_{200} \right. \\
& \left. - \frac{T_{s\perp}}{m_s} I_{002} + 3 \frac{m_t}{m_o} \frac{A_2(a)}{A_1(a)} \sigma_{\perp} I_{202} \right) \} \quad (57)
\end{aligned}$$

$$\begin{aligned}
\frac{\delta q_{\parallel}}{\delta t} = & - \sum_t \frac{3}{2} \frac{v_{st}}{\pi \Gamma(\frac{5-n}{2})} \left\{ k \rho_s \left[ \sigma_{\parallel} R_{st}^{(1)} (u_s - u_t)_{\perp} + \sigma_{\perp} R_{st}^{(2)} (u_s - u_t)_{\parallel} \right] \right. \\
& + R_{st}^{(3)} q_{s\perp} + \frac{\sigma_{\perp}}{\sigma_{\parallel}} R_{st}^{(4)} q_{s\parallel} - \frac{\rho_s}{\rho_t} \left[ R_{st}^{(5)} q_{t\perp} + \frac{\sigma_{\perp}}{\sigma_{\parallel}} R_{st}^{(6)} q_{t\parallel} \right] \\
& \left. + R_{st}^{(7)} q_{s\parallel} + \frac{\sigma_{\perp}}{\sigma_{\parallel}} R_{st}^{(8)} q_{s\perp} - \frac{\rho_s}{\rho_t} \left[ R_{st}^{(9)} q_{t\perp} + \frac{\sigma_{\perp}}{\sigma_{\parallel}} R_{st}^{(10)} q_{t\parallel} \right] \right\} \quad (58)
\end{aligned}$$

$$\begin{aligned}
\frac{\delta q_{\perp}}{\delta t} = & - \sum_t \frac{3}{2} \frac{v_{st}}{\pi \Gamma(\frac{5-n}{2})} \left\{ k \rho_s \left[ \sigma_{\parallel} S_{st}^{(1)} (u_s - u_t)_{\perp} + \sigma_{\perp} S_{st}^{(2)} (u_s - u_t)_{\parallel} \right] \right. \\
& + S_{st}^{(3)} q_{s\perp} + \frac{\sigma_{\perp}}{\sigma_{\parallel}} S_{st}^{(4)} q_{s\parallel} - \frac{\rho_s}{\rho_t} \left[ S_{st}^{(5)} q_{t\perp} + \frac{\sigma_{\perp}}{\sigma_{\parallel}} S_{st}^{(6)} q_{t\parallel} \right] \\
& \left. + S_{st}^{(7)} q_{s\parallel} + \frac{\sigma_{\perp}}{\sigma_{\parallel}} S_{st}^{(8)} q_{s\perp} - \frac{\rho_s}{\rho_t} \left[ S_{st}^{(9)} q_{t\perp} + \frac{\sigma_{\perp}}{\sigma_{\parallel}} S_{st}^{(10)} q_{t\parallel} \right] \right\} \quad (59)
\end{aligned}$$

where  $\Gamma(x)$  is a gamma function,  $a$  is the power of the particle separation ( $r$ ) in the interaction force law

$$\text{Force} = \frac{K_{st}}{r^a} \quad (60)$$

and where  $n$  is related to  $a$  by the equation

$$n = \frac{4}{a-1} - 1 \quad (61)$$

$\sigma_{\parallel}$  and  $\sigma_{\perp}$  are given by equations (50) and (51) and the quantities  $m_0$ ,  $v_{st}$ ,  $A_l(a)$  and  $I_{LMN}$  are defined as

$$m_0 = m_s + m_t \quad (62)$$

$$v_{st} = \frac{8\sqrt{\pi}}{3} (2k)^{-n/2} A_l(a) \Gamma\left(\frac{5-n}{2}\right) \frac{n_t m_t}{m_s + m_t} \left(\frac{K_{st}}{\mu_{st}}\right)^{(n+1)/2} \sigma_{\parallel}^{-1/2} \sigma_{\perp}^{-(n-1)/2} \quad (63)$$

$$A_l(a) = \int_0^{\infty} (1 - \cos^l \chi) v_0 dv_0 \quad (64)$$

$$I_{LMN} = \int_{-\infty}^{\infty} dx_1 \int_{-\infty}^{\infty} dx_2 \int_{-\infty}^{\infty} dx_3 \exp[-(x_1^2 + x_2^2 + \frac{\sigma_{\perp}}{\sigma_{\parallel}} x_3^2)] \frac{x_1^L x_2^M x_3^N}{(x_1^2 + x_2^2 + x_3^2)^{n/2}} \quad (65)$$

where  $K_{st}$  is constant,  $\chi$  is the scattering angle,  $v_0$  is the nondimensional impact parameter (cf. Chapman and Cowling 1970), and  $\mu_{st}$  is the reduced mass

$$\mu_{st} = \frac{m_s m_t}{m_s + m_t} \quad (66)$$

The values of the R's and S's are given by Demars and Schunk. They also give the values of the I's for general  $n$  and for Maxwell molecule interactions ( $a=5$ ,  $n=0$ ), hard sphere interactions ( $a=\infty$ ,  $n=-1$ ), while the case of Coulomb interactions ( $a=2$ ,  $n=3$ ) is given by Chodura and Poil (1971). These values will not be repeated here.

For the special case of Maxwell molecule interactions ( $a=5$ ) equations (54) - (59) agree with the general Maxwell molecule collision terms (44) - (49) up to the linear terms in the drift velocity, stress, and heat flow.

### 3.3. Resonant charge exchange interactions

The Quasilinear collision terms for resonant charge exchange interactions were derived by Demars and Schunk (1979). They are similar in form to the collision terms for the general inverse power interactions given in the previous subsection and they will not be repeated here.

#### 4. Simplified sets of transport equations

Several sets of simplified transport equations for anisotropic plasmas have been derived during the last two decades. In this section I show how all of the important sets of simplified transport equations can be obtained from the generalized transport equations given in section (2). First, I show that the generalized transport equations reduce to Grad's 13-moment transport equations in the limit of small temperature anisotropies. Next, I present a set of simplified transport equations that is based on a finite Larmor radius expansion of the generalized transport equations. Within the finite Larmor radius approximation, previous authors have made several additional assumptions, and the resulting transport equations are derived and discussed. I also study the effect of collisions on the transport equations for an anisotropic plasma, and present a set of simplified transport equations for a hybrid case where the collisional mean-free-path is the small parameter in the magnetic field direction, while perpendicular to the magnetic field the Larmor radius is the small parameter.

It should be noted that many plasma flows may be adequately modelled with a set of simplified transport equations. Therefore, in what follows I outline the derivation of the sets of simplified transport equations so that the intrinsic limitations of a given set will be more apparent.

##### 4.1. 13-moment approximation

To recover Grad's 13-moment system of transport equations from the set of generalized transport equations given in section (2), we must



assume that the species temperature (or pressure) anisotropy is small and we must take account of the fact that the heat flow vectors for parallel and perpendicular thermal energy become linearly dependent in the 13-moment approximation,

$$|p_{s\parallel} - p_{s\perp}| \ll p_{s\parallel}, p_{s\perp} \quad (67)$$

$$\underline{q}_s^{\parallel} = \frac{2}{5} (\underline{I} + 2\underline{e}_3\underline{e}_3) \cdot \underline{q}_s \quad (68)$$

$$\underline{q}_s^{\perp} = \frac{2}{5} (2\underline{I} - \underline{e}_3\underline{e}_3) \cdot \underline{q}_s \quad (69)$$

Substituting equations (68) and (69) into the 16-moment distribution function given by equations (29)-(31), expanding the distribution function using the inequality (67), and retaining only linear terms in  $\underline{\tau}'_s$ ,  $\underline{q}_s$  and  $(p_{s\parallel} - p_{s\perp})$  we recover the 13-moment approximation for the species distribution function, which is given by

$$f_s = f_s^{(M)} [1 + \phi_s] \quad (70)$$

where

$$f_s^{(M)} = n_s \left( \frac{m_s}{2\pi k T_s} \right)^{3/2} \exp \left[ - \frac{m_s c_s^2}{2k T_s} \right] \quad (71)$$

$$\phi_s = \frac{m_s}{2k T_s p_s} \underline{\tau}'_s : \underline{c}_s \underline{c}_s - \left( 1 - \frac{m_s c_s^2}{5k T_s} \right) \frac{m_s}{k T_s p_s} \underline{q}_s \cdot \underline{c}_s \quad (72)$$

and where  $T_s = 1/3 (T_{s\parallel} + 2T_{s\perp})$ ,  $p_s = n_s k T_s$  and

$$\underline{\tau}'_s = \underline{\tau}_s - 1/3 (p_{s\parallel} - p_{s\perp}) (\underline{I} - 3\underline{e}_3\underline{e}_3) \quad (73)$$

and the prime is used to distinguish between the stress tensor corresponding to the 16-moment approximation ( $\underline{\tau}'_s$ ) and that corresponding to the 13-moment approximation ( $\underline{\tau}_s$ ).

As expected, by using the same set of assumptions together with the 16-moment transport equations (22) - (28), (36) - (43), we can recover

the 13-moment transport equations given by

$$\frac{\partial \rho_s}{\partial t} + \nabla \cdot (\rho_s \underline{u}_s) = 0 \quad (74)$$

$$\rho_s \frac{D_s \underline{u}_s}{Dt} + \nabla p_s + \nabla \cdot \underline{\tau}_s - n_s e_s (\underline{E} + \frac{1}{c} \underline{u}_s \times \underline{B}) = \frac{\delta M_s}{\delta t} \quad (75)$$

$$\frac{D_s}{Dt} \left( \frac{3}{2} p_s \right) + \frac{5}{2} p_s (\nabla \cdot \underline{u}_s) + \nabla \cdot \underline{q}_s + \underline{\tau}_s : \nabla \underline{u}_s = \frac{\delta E_s}{\delta t} \quad (76)$$

$$\begin{aligned} \frac{D_s \underline{\tau}_s}{Dt} + p_s [\nabla \underline{u}_s + (\nabla \underline{u}_s)^T - \frac{2}{3} (\nabla \cdot \underline{u}_s) \underline{I}] + \underline{\tau}_s (\nabla \cdot \underline{u}_s) + [\underline{\tau}_s \cdot \nabla \underline{u}_s \\ + (\underline{\tau}_s \cdot \nabla \underline{u}_s)^T - \frac{2}{3} (\underline{\tau}_s : \nabla \underline{u}_s) \underline{I}] + \frac{2}{5} [\nabla \underline{q}_s + (\nabla \underline{q}_s)^T - \frac{2}{3} (\nabla \cdot \underline{q}_s) \underline{I}] \\ + [\underline{\Omega}_s \times \underline{\tau}_s - \underline{\tau}_s \times \underline{\Omega}_s] = \frac{\delta \underline{\tau}_s}{\delta t} \end{aligned} \quad (77)$$

$$\begin{aligned} \frac{D_s \underline{q}_s}{Dt} + \frac{5}{2} \nabla \cdot \left( \frac{p_s}{\rho_s} \right) + \frac{7}{2} \nabla \cdot \left( \frac{p_s}{\rho_s} \underline{\tau}_s \right) + \frac{7}{5} \underline{q}_s \cdot \nabla \underline{u}_s + \frac{7}{5} \underline{q}_s (\nabla \cdot \underline{u}_s) \\ + \frac{2}{5} (\nabla \underline{u}_s) \cdot \underline{q}_s + \left[ \frac{D_s \underline{u}_s}{Dt} - \frac{e_s}{n_s} (\underline{E} + \frac{1}{c} \underline{u}_s \times \underline{B}) \right] \cdot \left[ \frac{5}{2} p_s \underline{I} + \underline{\tau}_s \right] \\ + \underline{\Omega}_s \times \underline{q}_s = \frac{\delta \underline{q}_s}{\delta t} \end{aligned} \quad (78)$$

where the collision terms  $\frac{\delta M_s}{\delta t}$ ,  $\frac{\delta E_s}{\delta t}$ ,  $\frac{\delta \underline{\tau}_s}{\delta t}$  and  $\frac{\delta \underline{q}_s}{\delta t}$  are given by Schunk (1977).

Since Grad's 13-moment transport equations correspond to a special case of the more general 16-moment transport equations, the latter equations are capable of describing all of the transport effects that the 13-moment equations can, as outlined in the introduction.

#### 4.2. Larmor radius expansion

In this subsection I consider a collisionless plasma immersed in a

magnetic field which is strong enough to make the Larmor radius  $(a_L)_s$  much smaller than the other characteristic lengths of the problem, namely  $(a_L)_s \ll L, u_s T, (v_{th})_s T$  where  $L$  and  $T$  are the scale length and scale time respectively and  $u_s$  and  $(v_{th})_s$  are the coherent and thermal speeds respectively. With this assumption the transport equations simplify radically and we get a closed set of equations which consists of Maxwell equations in addition to the following set of transport equations

$$\frac{\partial \rho_s}{\partial t} + \nabla \cdot (\rho_s \underline{u}_s) = 0 \quad (79)$$

$$\rho_s \frac{D_s u_{s||}}{Dt} + \underline{e}_3 \cdot \nabla p_{s||} + \underline{e}_3 \cdot \nabla \left[ \tau_s - n_s \frac{e_3}{s} E_{||} - \underline{u}_s \cdot \frac{D_s \underline{e}_3}{Dt} \right] + (p_{s||} - p_{s\perp}) \nabla \cdot \underline{e}_3 = 0 \quad (80)$$

$$\frac{D_s p_{s||}}{Dt} + p_{s||} (\nabla \cdot \underline{u}_s + 2 \nabla_{||} \cdot \underline{u}_s) + 2 [\tau_s \cdot \nabla \underline{u}_s - (\nabla \underline{u}_s) \cdot \tau_s] : \underline{e}_3 \underline{e}_3 + \nabla \cdot \underline{q}_{s||}^{||} - 2 \underline{q}_{s\perp}^{||} : \nabla \underline{e}_3 - 2 q_{s||}^{\perp} \nabla \cdot \underline{e}_3 = 0 \quad (81)$$

$$\frac{D_s p_{s\perp}}{Dt} + p_{s\perp} (\nabla \cdot \underline{u}_s + \nabla_{\perp} \cdot \underline{u}_s) + \tau_s \cdot \nabla \underline{u}_s - [\tau_s \cdot \nabla \underline{u}_s - (\nabla \underline{u}_s) \cdot \tau_s] : \underline{e}_3 \underline{e}_3 + \nabla \cdot \underline{q}_{s\perp}^{\perp} + \underline{q}_{s\perp}^{||} : \nabla \underline{e}_3 + q_{s||}^{\perp} \nabla \cdot \underline{e}_3 = 0 \quad (82)$$

$$\frac{D_s q_{s||}^{||}}{Dt} + \frac{p_s}{\rho_s} \left[ \underline{e}_3 \cdot \nabla \left( \frac{p_{s||}}{\rho_s} \right) + 2 \nabla \cdot \left( \frac{\underline{e}_3 \underline{e}_3 \cdot \underline{p}_s}{\rho_s} \right) \cdot \underline{e}_3 \right] + \left[ 3 \underline{e}_3 \underline{q}_{s||}^{||} - 3 \underline{q}_{s\perp}^{||} \underline{e}_3 + q_{s||}^{\perp} \underline{I} \right] : \nabla \underline{u}_s - \frac{2}{\rho_s} [p_{s||} \underline{p}_s + 2 \underline{p}_s \cdot \underline{e}_3 \underline{e}_3 \cdot \underline{p}_s] : \nabla \underline{e}_3 = 0 \quad (83)$$

$$\frac{D_s q_{s\perp}^{\perp}}{Dt} + \frac{p_s}{\rho_s} \left[ \underline{e}_3 \cdot \nabla \left( \frac{p_{s\perp}}{\rho_s} \right) + \nabla \cdot \left( \frac{(\underline{I} - \underline{e}_3 \underline{e}_3) \cdot \underline{p}_s}{\rho_s} \right) \cdot \underline{e}_3 \right] + [2 q_{s||}^{\perp} \underline{I} + 2 \underline{q}_{s\perp}^{||} \underline{e}_3$$

$$-\underline{q}_{s\perp}^{\perp} e_3 + e_3 \cdot \underline{q}_{s\perp}^{\perp} ] : \underline{\nabla} u_s + \frac{1}{\rho_s} [p_{s\parallel} p_s + 2p_s \cdot e_3 e_3 \cdot p_s] : \underline{\nabla} e_3 = 0 \quad (84)$$

$$\underline{u}_{s\perp} = \underline{u}_E + \frac{1}{\Omega_s} e_3 \times \left\{ u_{s\parallel} \frac{D_s e_3}{Dt} + \frac{D_s u_E}{Dt} + \frac{1}{\rho_s} [\underline{\nabla}_{\perp} p_{s\perp} + (p_{s\parallel} - p_{s\perp}) e_3 \cdot \underline{\nabla} e_3] \right\} \quad (85)$$

$$(\underline{\tau}'_s)_{11} = -(\underline{\tau}'_s)_{22} = \frac{-1}{2\Omega_s} (e_1 e_2 + e_2 e_1) : [p_{s\perp} \underline{\nabla} u_s + \underline{q}_{s\parallel}^{\perp} \underline{\nabla} e_3] \quad (86)$$

$$(\underline{\tau}'_s)_{12} = \frac{1}{2\Omega_s} (e_1 e_1 - e_2 e_2) : [p_{s\perp} \underline{\nabla} u_s + \underline{q}_{s\parallel}^{\perp} \underline{\nabla} e_3] \quad (87)$$

$$(\underline{\tau}'_s)_{23} = \frac{1}{\Omega_s} \left\{ [(2p_{s\parallel} - p_{s\perp}) e_1 e_3 + p_{s\perp} e_3 e_1] : \underline{\nabla} u_s + e_1 \cdot \underline{\nabla} \underline{q}_{s\parallel}^{\perp} + e_1 (\underline{q}_{s\parallel}^{\parallel} - 2\underline{q}_{s\parallel}^{\perp}) : \underline{\nabla} e_3 \right\} \quad (88)$$

$$(\underline{\tau}'_s)_{31} = \frac{-1}{\Omega_s} \left\{ [(2p_{s\parallel} - p_{s\perp}) e_2 e_3 + p_{s\perp} e_3 e_2] : \underline{\nabla} u_s + e_2 \cdot \underline{\nabla} \underline{q}_{s\parallel}^{\perp} + e_2 (\underline{q}_{s\parallel}^{\parallel} - 2\underline{q}_{s\parallel}^{\perp}) : \underline{\nabla} e_3 \right\} \quad (89)$$

$$\underline{q}_{s1}^{\parallel} = \frac{-1}{\Omega_s} \left\{ p_{s\perp} \frac{\partial}{\partial x_2} \left( \frac{p_{s\parallel}}{\rho_s} \right) + [2e_2 (\underline{q}_{s\parallel}^{\parallel} - \underline{q}_{s\parallel}^{\perp}) + 2\underline{q}_{s\parallel}^{\perp} e_2] : \underline{\nabla} u_s + 2 \frac{p_s}{\rho_s} (p_{s\parallel} - p_{s\perp}) e_2 e_3 : \underline{\nabla} e_3 \right\} \quad (90)$$

$$\underline{q}_{s2}^{\parallel} = \frac{1}{\Omega_s} \left\{ p_{s\perp} \frac{\partial}{\partial x_1} \left( \frac{p_{s\parallel}}{\rho_s} \right) + [2e_1 (\underline{q}_{s\parallel}^{\parallel} - \underline{q}_{s\parallel}^{\perp}) + 2\underline{q}_{s\parallel}^{\perp} e_1] : \underline{\nabla} u_s + 2 \frac{p_{s\parallel}}{\rho_s} (p_{s\parallel} - p_{s\perp}) e_1 e_3 : \underline{\nabla} e_3 \right\} \quad (91)$$

$$\underline{q}_{s1}^{\perp} = \frac{-1}{\Omega_s} \left\{ 2p_{s\perp} \frac{\partial}{\partial x_2} \left( \frac{p_{s\perp}}{\rho_s} \right) + 4e_2 \underline{q}_{s\parallel}^{\perp} : \underline{\nabla} u_s \right\} \quad (92)$$

$$q_{s2}^{\perp} = \frac{1}{\omega_s} \left\{ 2p_{s\perp} \frac{\partial}{\partial x_{\perp}} \left( \frac{p_{s\perp}}{\rho_s} \right) + 4 \frac{e_{\perp} q_{s\parallel}^{\perp}}{\omega_s} : \nabla u_s \right\} \quad (93)$$

where  $\underline{u}_E = c \frac{E \times B}{B^2}$  is the  $\underline{E} \times \underline{B}$  drift velocity, and I used the relation

$$\frac{D e_3}{Dt} = (\underline{1} - e_3 e_3) e_3 : \nabla u_s \quad (94)$$

which is correct to the zeroth order, to get the above equations in that form.

These equations are accurate up to first order terms. Although I treated  $q_{s\parallel}^{\parallel}$  and  $q_{s\parallel}^{\perp}$  as zeroth order terms, in practice they ought to be small enough so that they do not invalidate the more general 16-moment approximation.

Equations (78) - (82) and (85) - (93) are similar to those derived by MacMahon (1965) when a bi-Maxwellian zeroth order distribution function is adopted to evaluate his expressions. However, there is a factor 2 error in his equations for  $q_{s1}^{\perp}$  and  $q_{s2}^{\perp}$ .

In the following paragraphs, some special cases will be studied. For each case a set of assumptions will be needed in addition to the general ones (collisionless plasma and small Larmor radius) stated in the beginning of this subsection. These assumptions will be stated and the above equations will be expanded accordingly.

Expansion I. The extra assumption needed for this cases is that

$$T \ll \frac{L}{(v_{th})_s}, \frac{L}{u_s} \quad (95)$$

That is to say, the periodic time of oscillations is much less than all characteristic times, except for the gyration period ( $2\pi/\Omega_s$ ).

The simplified closed set of equations is Maxwell equations,

equations (79) - (82), (85) and

$$\frac{D_s q_{s||}^{||}}{Dt} + 3p_{s||} \frac{\partial}{\partial x_3} \left( \frac{p_{s||}}{\rho_s} \right) = 0 \quad (96)$$

$$\frac{D_s q_{s||}^{\perp}}{Dt} + p_{s||} \frac{\partial}{\partial x_3} \left( \frac{p_{s\perp}}{\rho_s} \right) + \frac{p_{s\perp}}{\rho_s} (p_{s||} - p_{s\perp}) \nabla \cdot \underline{e}_3 = 0 \quad (97)$$

$$(\tau_s^{\perp})_{11} = -(\tau_s^{\perp})_{22} = \frac{-p_{s\perp}}{2\Omega_s} (\underline{e}_1 \underline{e}_2 + \underline{e}_2 \underline{e}_1) : \nabla \underline{u}_s \quad (98)$$

$$(\tau_s^{\perp})_{12} = \frac{p_{s\perp}}{2\Omega_s} (\underline{e}_1 \underline{e}_1 - \underline{e}_2 \underline{e}_2) : \nabla \underline{u}_s \quad (99)$$

$$(\tau_s^{\perp})_{23} = \frac{1}{\Omega_s} [(2p_{s||} - p_{s\perp}) \underline{e}_1 \underline{e}_3 + p_{s\perp} \underline{e}_3 \underline{e}_1] : \nabla \underline{u}_s \quad (100)$$

$$(\tau_s^{\perp})_{31} = \frac{-1}{\Omega_s} [(2p_{s||} - p_{s\perp}) \underline{e}_2 \underline{e}_3 + p_{s\perp} \underline{e}_3 \underline{e}_2] : \nabla \underline{u}_s \quad (101)$$

$$q_{s1}^{||} = \frac{-1}{\Omega_s} \left[ p_{s\perp} \frac{\partial}{\partial x_2} \left( \frac{p_{s||}}{\rho_s} \right) + 2 \frac{p_{s||}}{\rho_s} (p_{s||} - p_{s\perp}) \underline{e}_2 \underline{e}_3 : \nabla \underline{e}_3 \right] \quad (102)$$

$$q_{s2}^{||} = \frac{1}{\Omega_s} \left[ p_{s\perp} \frac{\partial}{\partial x_1} \left( \frac{p_{s||}}{\rho_s} \right) + 2 \frac{p_{s||}}{\rho_s} (p_{s||} - p_{s\perp}) \underline{e}_1 \underline{e}_3 : \nabla \underline{e}_3 \right] \quad (103)$$

$$q_{s1}^{\perp} = \frac{-1}{\Omega_s} \left[ 2p_{s\perp} \frac{\partial}{\partial x_2} \left( \frac{p_{s\perp}}{\rho_s} \right) \right] \quad (104)$$

$$q_{s2}^{\perp} = \frac{1}{\Omega_s} \left[ 2p_{s\perp} \frac{\partial}{\partial x_1} \left( \frac{p_{s\perp}}{\rho_s} \right) \right] \quad (105)$$

In the above equations (96) - (105) I retained only the greatest non zero term in the small quantities  $q_s^{||}$ ,  $q_s^{\perp}$  and  $\tau_s^{\perp}$ . These equations are consistent with those found by Oraevskii, Chodura and Feneberg (1968). However, the latter had a missing  $\rho_s$  in the equations for ( $q_{s||}^{||}$  and  $q_{s||}^{\perp}$ ) and an opposite sign for  $\tau_s^{\perp}$ .

Expansion II. The extra set of assumptions needed in this case is

$$(i) \quad L_{\perp} \ll \epsilon L_{||} \quad (106)$$

$$(ii) \quad u_E \equiv \frac{E_{\perp}}{B} \approx \epsilon u_{s\parallel} \quad (107)$$

$$(iii) \quad \left| \frac{\partial}{\partial x_1} e_3 \right|, \left| \frac{\partial}{\partial x_2} e_3 \right| \ll \frac{1}{L_{\perp}} \quad (108)$$

$$(iv) \quad q_{s\parallel}^{\parallel} = q_{s\parallel}^{\perp} = 0 \quad (109)$$

where  $\epsilon = \frac{(a_{L_s})}{L_{\perp}}$  is the smallness parameter, and  $L_{\parallel}$  and  $L_{\perp}$  are the parallel and perpendicular scale lengths, respectively.

The proper closed set of equations is Maxwell equations, equations (79) - (82), (85), (109) and

$$(\tau_s')_{11} = (\tau_s')_{22} = (\tau_s')_{12} = 0 \quad (110)$$

$$(\tau_s')_{23} = \frac{p_{s\perp}}{\Omega_s} \frac{\partial u_{s3}}{\partial x_1} \quad (111)$$

$$(\tau_s')_{31} = -\frac{p_{s\perp}}{\Omega_s} \frac{\partial u_{s3}}{\partial x_2} \quad (112)$$

$$q_{s1}^{\parallel} = \frac{-p_{s\perp}}{\Omega_s} \frac{\partial}{\partial x_2} \left( \frac{p_{s\parallel}}{\rho_s} \right) \quad (113)$$

$$q_{s2}^{\parallel} = \frac{p_{s\perp}}{\Omega_s} \frac{\partial}{\partial x_1} \left( \frac{p_{s\parallel}}{\rho_s} \right) \quad (114)$$

$$q_{s1}^{\perp} = \frac{-2p_{s\perp}}{\Omega_s} \frac{\partial}{\partial x_2} \left( \frac{p_{s\perp}}{\rho_s} \right) \quad (115)$$

$$q_{s2}^{\perp} = \frac{2p_{s\perp}}{\Omega_s} \frac{\partial}{\partial x_1} \left( \frac{p_{s\perp}}{\rho_s} \right) \quad (116)$$

Equations (110) - (116) are consistent with the relations derived by Srivastava and Bhatnagar (1975). However, they used a different set of coordinates whose  $x_3$  axis makes a small angle ( $\theta \ll 1$ ) with the magnetic field. The assumption of zero parallel components of the heat flow vectors restricts, to a large extent, the usefulness of these equations in practical problems.

Expansion III. If we keep only zeroth order terms, in addition to the small Larmor radius and collisionless plasma assumptions, equations (24) and (25) reduce to

$$\frac{D_s}{Dt} \left( \frac{p_{s\perp} B^2}{\rho_s} \right) = - \frac{B^2}{\rho_s} \underline{e}_3 \underline{e}_3 : (\nabla \cdot \underline{Q}_s) \quad (117)$$

$$\frac{D_s}{Dt} \left( \frac{p_{s\perp}}{\rho_s B} \right) = - \frac{1}{2\rho_s B} (\underline{I} - \underline{e}_3 \underline{e}_3) : (\nabla \cdot \underline{Q}_s) \quad (118)$$

which are similar to the results given by Chapman and Cowling (1970).

Moreover, if we apply the same assumptions to the closed 16-moment transport equations, they may be reduced to

$$\frac{D_s}{Dt} \left( \frac{p_{s\parallel} B^2}{\rho_s} \right) = - \frac{B^2}{\rho_s} \underline{e}_3 \cdot \left[ B \nabla \left( \frac{q_{s\parallel}^{\parallel}}{B} \right) + 2 \frac{q_{s\parallel}^{\perp}}{B} \nabla B \right] \quad (119)$$

$$\frac{D_s}{Dt} \left( \frac{p_{s\perp}}{\rho_s B} \right) = - \frac{B}{\rho_s} \underline{e}_3 \cdot \nabla \left( \frac{q_{s\parallel}^{\perp}}{B^2} \right) \quad (120)$$

$$\frac{D_s}{Dt} \left( \frac{q_{s\parallel}^{\parallel} B^3}{\rho_s} \right) = - \frac{3 p_{s\parallel} B^3}{\rho_s} \underline{e}_3 \cdot \nabla \left( \frac{p_{s\parallel}}{\rho_s} \right) \quad (121)$$

$$\frac{D_s}{Dt} \left( \frac{q_{s\parallel}^{\perp}}{\rho_s^2} \right) = - \frac{p_{s\parallel}}{\rho_s^2} \underline{e}_3 \cdot \left[ \nabla \left( \frac{p_{s\perp}}{\rho_s} \right) + \frac{p_{s\perp} (p_{s\perp} - p_{s\parallel})}{\rho_s p_{s\parallel}} \frac{\nabla B}{B} \right] \quad (122)$$

Equations (119) - (122), in addition to Maxwell's equations, the continuity equation (79), and

$$\frac{D_s u_{s\parallel}}{Dt} + \frac{\partial p_{s\parallel}}{\partial x_3} - n_s e_s E_{\parallel} - \frac{u_s}{c} \cdot \frac{D_s \underline{e}_3}{Dt} + (p_{s\parallel} - p_{s\perp}) \frac{\nabla \cdot \underline{e}_3}{B} = 0 \quad (123)$$

$$\underline{u}_{s\perp} = c \frac{\underline{E} \times \underline{B}}{B^2} \quad (124)$$

are similar to the equations given by Whang (1971), except for an algebraic error in his calculations.

Expansion IV. If, in addition to the small Larmor radius and collisionless plasma assumptions, we neglect the heat flow tensor, we get the following relations, which are accurate to the zeroth order,



$$\frac{D_S}{Dt} \left( \frac{p_{S||} B^2}{\rho_S^3} \right) = 0 \quad (125)$$

$$\frac{D_S}{Dt} \left( \frac{p_{S\perp}}{\rho_S B} \right) = 0 \quad (126)$$

These are the 'double adiabatic' energy equations of Chew, Goldberger and Low (1956). In this case the proper closed set of equations consists of Maxwell's equations in addition to equations (79), and (123) - (126).

#### 4.3. Influence of collisions

To study the effect of collisions I consider the transport equations for ions in a binary ion-electron plasma in which ion-ion collisions dominate the collision terms. Specifically, I assume that the ion-ion collision frequency is much greater than all characteristic frequencies other than the gyration frequency (i.e.  $\nu_{ii} \gg 1/T$ ,  $u_i/L \ll \nu_{ie}$ ).

According to these assumptions, it is possible to prove that the relations (67) - (69) are satisfied for ions. Therefore, the transport equations reduce to the 13-moment approximation mentioned earlier. Keeping only the greatest non-zero terms in the first order quantities ( $\underline{\tau}_S$ ,  $\underline{q}_S$ ) we get the following set of transport equations for the ions

$$\frac{\partial \rho_i}{\partial t} + \nabla \cdot (\rho_i \underline{u}_i) = 0 \quad (127)$$

$$\rho_i \frac{D_i \underline{u}_i}{Dt} + \nabla p_i + \nabla \cdot \underline{\tau}_i - n_i e_i (\underline{E} + \frac{1}{c} \underline{u}_i \times \underline{B}) = 0 \quad (128)$$

$$\frac{D_i}{Dt} (p_i) + \frac{5}{3} p_i (\nabla \cdot \underline{u}_i) + \frac{2}{3} \nabla \cdot \underline{q}_i + \frac{2}{3} \underline{\tau}_i : \nabla \underline{u}_i = 0 \quad (129)$$

$$(\underline{\tau}_i)_{11} = -\frac{1}{2} \frac{\Omega_i W_{12} + 0.3 \nu_{ii} (W_{11} - W_{22})}{\Omega_i^2 + (0.6 \nu_{ii})^2} + \frac{5W_{33}}{12\nu_{ii}} \quad (130)$$

$$(\tau_i)_{22} = + \frac{1}{2} \frac{\Omega_i W_{12} + 0.3 v_{ii} (W_{11} - W_{22})}{\Omega_i^2 + (0.6 v_{ii})^2} + \frac{5W_{33}}{12v_{ii}} \quad (131)$$

$$(\tau_i)_{33} = \frac{-5W_{33}}{6v_{ii}} \quad (132)$$

$$(\tau_i)_{12} = \frac{1}{4} \frac{\Omega_i (W_{11} - W_{22}) - 1.2 v_{ii} W_{12}}{\Omega_i^2 + (0.6 v_{ii})^2} \quad (133)$$

$$(\tau_i)_{23} = \frac{\Omega_i W_{13} - 1.2 v_{ii} W_{23}}{\Omega_i^2 + (1.2 v_{ii})^2} \quad (134)$$

$$(\tau_i)_{31} = - \frac{\Omega_i W_{23} + 1.2 v_{ii} W_{13}}{\Omega_i^2 + (1.2 v_{ii})^2} \quad (135)$$

$$q_i = - \frac{25 p_i \nabla_{\perp} (p_i / \rho_i)}{8 v_{ii}} + \frac{p_i [2.5 \Omega_i \times \nabla_{\perp} (p_i / \rho_i) - 2 v_{ii} \nabla_{\perp} (p_i / \rho_i)]}{\Omega_i^2 + (0.8 v_{ii})^2} \quad (136)$$

where the subscript  $i$  indicates quantities related to ions and where

$$W_{\alpha\beta} = p_i \left[ \nabla_{\perp} \underline{u}_i + (\nabla_{\perp} \underline{u}_i)^T - \frac{2}{3} \nabla_{\perp} \cdot \underline{u}_i \underline{I} \right]_{\alpha\beta} \quad (137)$$

In the subsections that follow I consider the special cases when  $v_{ii}$  is much less and much greater than  $\Omega_i$ .

Collision dominant case. In addition to the assumptions needed for the general case discussed above ( $v_{ii} \gg 1/T$ ,  $u_i/L \gg v_{ie}$ ), we need to assume that the ion-ion collision frequency is much greater than the ion gyro-frequency ( $v_{ii} \gg \Omega_i$ ). In this case equations (130) - (136) reduce to

$$\tau_i = - \frac{5 p_i}{6 v_{ii}} \left[ \nabla_{\perp} \underline{u}_i + (\nabla_{\perp} \underline{u}_i)^T - \frac{2}{3} \nabla_{\perp} \cdot \underline{u}_i \underline{I} \right] \quad (138)$$

$$q_i = - \frac{25}{8 v_{ii}} p_i \nabla_{\perp} (p_i / \rho_i) \quad (139)$$

As expected, the influence of the magnetic field disappears because rapid collisions prevent the ions from gyrating. These results correspond to the Navier-Stokes equations (Schunk 1977) and to what

Chapman and Cowling call the "first approximation" to the transport equations.

The hybrid case. Assuming that  $\Omega_i \gg v_{ii}$  in addition to the general assumptions ( $v_{ii} \gg 1/T$ ,  $u_i/L \gg v_{ie}$ ), leads to the following simplification of equations (130) - (136)

$$(\underline{\tau}_i)_{11} = (\underline{\tau}_i)_{22} = -\frac{1}{2} (\underline{\tau}_i)_{33} = \frac{5}{12v_{ii}} W_{33} \quad (140)$$

$$(\underline{\tau}_i)_{12} = \frac{1}{4\Omega_i} (W_{11} - W_{22}) \quad (141)$$

$$(\underline{\tau}_i)_{23} = \frac{W_{13}}{\Omega_i} \quad (142)$$

$$(\underline{\tau}_i)_{31} = -\frac{W_{23}}{\Omega_i} \quad (143)$$

$$\underline{q}_i = -\frac{25}{8v_{ii}} p_i \nabla_{\parallel} \left( \frac{p_i}{\rho_i} \right) + \frac{5}{2\Omega_i^2} p_i \Omega_i \times \nabla \left( \frac{p_i}{\rho_i} \right) \quad (144)$$

where  $W_{\alpha\beta}$  was defined by equation (137).

The off-diagonal terms of  $\underline{\tau}_i$ , as well as the transverse component of the heat flow vector, are inhibited by the strong magnetic field. On the other hand, the diagonal terms of  $\underline{\tau}_i$  and the longitudinal component of  $\underline{q}_i$  are controlled by collisions, since the former corresponds to the pressure anisotropy, which is opposed by collisions while the longitudinal component of  $\underline{q}_i$  cannot be inhibited by the magnetic field because it cannot exert a force parallel to itself.

These results are similar to those derived by Mikhailovskii and Tsypin (1971). However, the extra terms appearing in their work are due to two reasons. First, they used an expansion which is quantitatively more accurate than the 13-moment expansion. This difference amounts to about a 20% correction and can be compensated for by modifying the

numerical value of  $v_{ii}$ . Second, they kept higher-order terms in  $\underline{q}_i$  and  $\underline{\tau}_i$ . These terms may be restored by keeping terms of the order of  $\frac{v_i}{\Omega_i}$ ,  $\frac{v_i^2}{\Omega_i^2}$  compared to 1 and by keeping terms proportional to  $\underline{\tau}_i$  and  $\underline{q}_i$ .

## CHAPTER III

MOMENTUM AND ENERGY EXCHANGE COLLISION TERMS  
FOR INTERPENETRATING BI-MAXWELLIAN GASES

Here I follow steps similar to those of sections (1) and (2) in chapter (I). However, in this chapter the magnetic field  $\underline{B}$  is independent of time and co-ordinates. Also, in order to close the set of transport equations, I adopt the bi-Maxwellian distribution function given by equation (30).

The collision terms derived by Chodura and Pohl (1971) and by Demars and Schunk (1979) are valid for arbitrary temperature differences between the interacting gases and arbitrary temperature anisotropies, but are restricted to small relative drifts between the interacting gases. In this chapter I remove the latter restriction and calculate momentum and energy exchange collision terms for interpenetrating bi-Maxwellian gases that are valid for arbitrary drift velocity differences and temperature differences between the interacting gases as well as for arbitrary temperature anisotropies. I also derive the closed set of transport equations that are associated with the momentum and energy collision terms.

## 1. Theoretical formulation

If we multiply equation (1) by  $m_s$ ,  $m_{s-s} c_{s-s}$ ,  $m_s c_{s||}^2$ , and  $m_s c_{s\perp}^2/2$  and integrate over velocity space, taking into account that the velocity distribution function takes the bi-Maxwellian form given in equation (30), we obtain the continuity, momentum, parallel energy and

perpendicular energy equations, respectively, for species  $s$ . The resulting closed system of transport equations is given by

Continuity

$$\frac{\partial \rho_s}{\partial t} + \nabla \cdot (\rho_s \underline{u}_s) = 0 \quad (145)$$

Momentum

$$\rho_s \frac{D \underline{u}_s}{Dt} + \nabla_{\perp} p_{s\perp} + \nabla_{\parallel} p_{s\parallel} - \rho_s \underline{G} - n_s e_s (\underline{E} + \frac{1}{c} \underline{u}_s \times \underline{B}) = \frac{\delta \underline{M}_s}{\delta t} \quad (146)$$

Parallel energy

$$\frac{D p_{s\parallel}}{Dt} + p_{s\parallel} (\nabla \cdot \underline{u}_s + 2 \nabla_{\parallel} \cdot \underline{u}_s) = \frac{\delta E_{s\parallel}}{\delta t} \quad (147)$$

Perpendicular energy

$$\frac{D p_{s\perp}}{Dt} + p_{s\perp} (\nabla \cdot \underline{u}_s + \nabla_{\perp} \cdot \underline{u}_s) = \frac{\delta E_{s\perp}}{\delta t} \quad (148)$$

The quantities on the right-hand sides of equations (146) - (148) correspond to the velocity moments of the Boltzmann collision integral (2) and describe, respectively, the rate of change of momentum, parallel energy, and perpendicular energy. These quantities will be evaluated in Sections (2) and (3).

## 2. Collision terms

In this section I will present collision terms for the general inverse-power interaction and verify that the answer is consistent with the literature in some limiting cases.

Following the steps mentioned in section (1), the collision terms take the form:

$$\frac{\delta M_s}{\delta t} = \sum_t \int d\underline{c}_s \int d\underline{c}_t \int d\Omega g \sigma_{st}(g, \chi) f_s f_t m_s (\underline{c}'_s - \underline{c}_s) \quad (149)$$

$$\frac{\delta E_s}{\delta t} = \sum_t \int d\underline{c}_s \int d\underline{c}_t \int d\Omega g \sigma_{st}(g, \chi) f_s f_t m_s (c_{s\parallel}'^2 - c_{s\parallel}^2) \quad (150)$$

$$\frac{\delta E_{s\perp}}{\delta t} = \sum_t \int d\underline{c}_s \int d\underline{c}_t \int d\Omega g \sigma_{st}(g, \chi) f_s f_t \frac{m_s}{2} (c_{s\perp}'^2 - c_{s\perp}^2) \quad (151)$$

where  $\underline{c}'_s$  is the random velocity after scattering. Expressions (149) - (151) are valid for a general distribution function and a general differential scattering cross-section.

If we choose the distribution function to have the bi-Maxwellian form given in equation (30) and assume a general inverse-power interaction (equation (60)) the collision terms reduce to

$$\frac{\delta M_s}{\delta t} = - \sum_t \frac{\mu_{st} n_s n_t}{\pi^{3/2}} \int d\underline{x} \underline{g} g Q_{st}^{(1)}(g) e^{-(\underline{x}-\underline{\epsilon})^2} \quad (152)$$

$$\frac{\delta E_s}{\delta t} = - \sum_t \frac{\mu_{st} n_s n_t}{\pi^{3/2}} \int d\underline{x} g Q_{st}^{(1)}(g) e^{-(\underline{x}-\underline{\epsilon})^2} \underline{g} \cdot \left[ 2\underline{y}_{\parallel} + \frac{A_2(a)}{A_1(a)} \frac{\mu_{st}}{m_s} \right. \\ \left. \cdot \left( a_{\parallel} \frac{x_{\parallel}}{2} - \frac{a_{\perp}}{2} \frac{x_{\perp}}{2} \right) \right] \quad (153)$$

$$\frac{\delta E_{s\perp}}{\delta t} = - \sum_t \frac{\mu_{st} n_s n_t}{\pi^{3/2}} \int d\underline{x} g Q_{st}^{(1)}(g) e^{-(\underline{x}-\underline{\epsilon})^2} \underline{g} \cdot \left[ \frac{y_{\perp}}{2} - \frac{A_2(a)}{A_1(a)} \frac{\mu_{st}}{2m_s} \right]$$

$$\left[ (a_{\parallel} x_{\parallel} - \frac{a_{\perp}}{2} x_{\perp}) \right] \quad (154)$$

where

$$a_{s\parallel} = (2kT_{s\parallel}/m_s)^{1/2} \quad (155)$$

$$a_{s\perp} = (2kT_{s\perp}/m_s)^{1/2} \quad (156)$$

$$a_{\parallel} = (a_{s\parallel}^2 + a_{t\parallel}^2)^{1/2} \quad (157)$$

$$a_{\perp} = (a_{s\perp}^2 + a_{t\perp}^2)^{1/2} \quad (158)$$

$$T_{\parallel} = \mu_{st} a_{\parallel}^2 / 2k \quad (159)$$

$$T_{\perp} = \mu_{st} a_{\perp}^2 / 2k \quad (160)$$

$$\underline{\Delta} = \underline{u}_s - \underline{u}_t \quad (161)$$

$$\underline{x} = \underline{g}_{\parallel} / a_{\parallel} + \underline{g}_{\perp} / a_{\perp} \quad (162)$$

$$\underline{\varepsilon} = \underline{\Delta}_{\parallel} / a_{\parallel} + \underline{\Delta}_{\perp} / a_{\perp} \quad (163)$$

$$\underline{y}_{\parallel} = \frac{2k(T_{s\parallel} - T_{t\parallel})}{a_{\parallel}(m_s + m_t)} (\underline{x}_{\parallel} - \underline{\varepsilon}_{\parallel}) - \frac{m_t}{m_s + m_t} a_{\parallel} \underline{\varepsilon}_{\parallel} \quad (164)$$

$$\underline{y}_{\perp} = \frac{2k(T_{s\perp} - T_{t\perp})}{a_{\perp}(m_s + m_t)} (\underline{x}_{\perp} - \underline{\varepsilon}_{\perp}) - \frac{m_t}{m_s + m_t} a_{\perp} \underline{\varepsilon}_{\perp} \quad (165)$$



$$Q_{st}^{(l)} = 2\pi A_l (a) \left( \frac{K_{st}}{\mu_{st} g^2} \right)^{2/(a-1)} \quad (166)$$

The above collision terms can be expressed in the following convenient forms

$$\frac{\delta M_s}{\delta t} = - \sum_t n_s m_s v_{st} \underline{\phi} \cdot \underline{\Delta} \quad (167)$$

$$\begin{aligned} \frac{\delta E_{s||}}{\delta t} = \sum_t \frac{n_s m_s v_{st}}{m_s + m_t} & \left[ 3k(T_{t||} - T_{s||}) \psi_{||} + 2m_t \underline{\Delta}_{||} \cdot \underline{\phi} \cdot \underline{\Delta} + \frac{A_2(a)}{A_1(a)} \frac{m_t}{2} \right. \\ & \left. \cdot [a_{\perp}^2 \Omega_2(n) - 2a_{||}^2 \Omega_1(n)] \right] \quad (168) \end{aligned}$$

$$\begin{aligned} \frac{\delta E_{s\perp}}{\delta t} = \sum_t \frac{n_s m_s v_{st}}{m_s + m_t} & \left[ 3k(T_{t\perp} - T_{s\perp}) \psi_{\perp} + m_t \underline{\Delta}_{\perp} \cdot \underline{\phi} \cdot \underline{\Delta} - \frac{A_2(a)}{A_1(a)} \frac{m_t}{4} \right. \\ & \left. \cdot [a_{\perp}^2 \Omega_2(n) - 2a_{||}^2 \Omega_1(n)] \right] \quad (169) \end{aligned}$$

where

$$\underline{\phi} \cdot \underline{\Delta} = a_{\perp} \Lambda(n) \quad (170)$$

$$\psi_{||} = \frac{4}{3} \left[ \Omega_1(n) - \epsilon_{||} \cdot \underline{\phi} \cdot \frac{\underline{\Delta}}{a_{||}} \right] \quad (171)$$

$$\psi_{\perp} = \frac{2}{3} \left[ \Omega_2(n) - \epsilon_{\perp} \cdot \underline{\phi} \cdot \frac{\underline{\Delta}}{a_{\perp}} \right] \quad (172)$$

$$v_{st} = \frac{8\sqrt{\pi}\Gamma\left(\frac{5-n}{2}\right)}{3} A_1 (a) \frac{m_t n_t}{m_s + m_t} \frac{a_{\perp}^{1-n} \left(\frac{K_{st}}{\mu_{st}}\right)^{(n+1)/2}}{a_{\parallel}} \quad (173)$$

and

$$\underline{\Lambda}(n) = \frac{3a_{\parallel}}{4\pi\Gamma\left(\frac{5-n}{2}\right)a_{\perp}} \int d\underline{x} e^{-(\underline{x}-\underline{\epsilon})^2} \left(\frac{g}{a_{\perp}}\right)^{-n} \frac{g}{a_{\perp}} \quad (174)$$

$$\underline{\Omega}_1(n) = \frac{3a_{\parallel}}{4\pi\Gamma\left(\frac{5-n}{2}\right)a_{\perp}} \int d\underline{x} e^{-(\underline{x}-\underline{\epsilon})^2} \left(\frac{g}{a_{\perp}}\right)^{-n} \frac{g_{\parallel}^2}{a_{\parallel}^2} \quad (175)$$

$$\underline{\Omega}_2(n) = \frac{3a_{\parallel}}{4\pi\Gamma\left(\frac{5-n}{2}\right)a_{\perp}} \int d\underline{x} e^{-(\underline{x}-\underline{\epsilon})^2} \left(\frac{g}{a_{\perp}}\right)^{-n} \frac{g_{\perp}^2}{a_{\perp}^2} \quad (176)$$

Only the limiting forms of the tensor  $\underline{\phi}$  are needed and these are given below for a Cartesian coordinate system  $(x_1, x_2, x_3)$  with the magnetic field parallel to the  $x_3$ -axis.

### 2.1. Limiting forms

If the relative drift is much smaller than the average thermal speed (i.e.)  $|\underline{\epsilon}| \ll 1$  the quantities given above reduces to

$$\underline{\Lambda}(n) = \frac{3}{2\pi\Gamma\left(\frac{5-n}{2}\right)} \left[ \frac{a_{\perp}}{2} I_{00,2} \underline{\Delta}_{\parallel} + \frac{1}{a_{\perp}} I_{20,0} \underline{\Delta}_{\perp} \right] \quad (177)$$

$$\underline{\Omega}_1(n) = \frac{3}{4\pi\Gamma\left(\frac{5-n}{2}\right)} \frac{a_{\perp}^2}{a_{\parallel}^2} I_{00,2} \quad (178)$$

$$\Omega_2(n) = \frac{3}{2\pi\Gamma\left(\frac{5-n}{2}\right)} I_{20,0} \quad (179)$$

From which

$$\underline{\Phi} = \frac{3}{2\pi\Gamma\left(\frac{5-n}{2}\right)} \begin{pmatrix} I_{20,0} & 0 & 0 \\ 0 & I_{20,0} & 0 \\ 0 & 0 & \frac{a_{\perp}^2}{a_{\parallel}^2} I_{00,2} \end{pmatrix} \quad (180)$$

$$\Psi_{\parallel} = \frac{1}{\pi\Gamma\left(\frac{5-n}{2}\right)} \frac{a_{\perp}^2}{a_{\parallel}^2} I_{00,2} \quad (181)$$

$$\Psi_{\perp} = \frac{1}{\pi\Gamma\left(\frac{5-n}{2}\right)} I_{20,0} \quad (182)$$

Substituting the expressions given in equations (178) - (182) into equations (167)-(169) the collision terms reduce to a form consistent with the expressions derived by Demars and Schunk (1979).

Considering the opposite case when the relative drift is much greater than the average thermal speed ( $|\epsilon| \gg 1$ ) we find that

$$\underline{\Delta}(n) = \frac{3\sqrt{\pi}}{4\Gamma\left(\frac{5-n}{2}\right)} \frac{a_{\parallel}}{a_{\perp}^{2-n}} \Delta^{-n} \underline{\Delta} \quad (183)$$

$$\Omega_1(n) = \frac{3\sqrt{\pi}}{4\Gamma\left(\frac{5-n}{2}\right)} \frac{1}{a_{\parallel} a_{\perp}^{1-n}} \Delta^{-n} \Delta_{\parallel}^2 \quad (184)$$

$$\Omega_2(n) = \frac{3\sqrt{\pi}}{4\Gamma\left(\frac{5-n}{2}\right)} \frac{a_{\parallel}}{a_{\perp}^{3-n}} \Delta^{-n} \Delta_{\perp}^2 \quad (185)$$

$$\Psi_{\parallel} \approx \Psi_{\perp} \approx 0 \quad (186)$$

$$\Phi = \frac{3\sqrt{\pi}}{4\Gamma\left(\frac{5-n}{2}\right)} \frac{a_{\parallel}}{a_{\perp}^{1-n}} \Delta^{-n} \underline{\underline{1}} \quad (187)$$

where  $\underline{\underline{1}}$  is a unit dyadic and  $\Delta$  is the magnitude of the vector  $\underline{\underline{\Delta}}$ .

In the limit when  $a_{\parallel}/a_{\perp} \rightarrow 1$  (isotropic temperatures) the collision terms reduce to forms which agree with the results given by Burgers (1969) and Schunk (1977).

## 2.2. Maxwell molecule interaction

For the special case of Maxwell molecule interactions, where the interaction force varies inversely as the fifth power of the particle separation ( $n=0$ ), the integrations in equations (174)-(176) can be reduced to a closed form,

$$\underline{\underline{\Delta}}(0) = \frac{a_{\parallel}}{a_{\perp}^2} \underline{\underline{\Delta}} \quad (188)$$

$$\Omega_1(0) = \frac{a_{\parallel}}{a_{\perp}} \left( \frac{1}{2} + \frac{\Delta_{\parallel}^2}{a_{\parallel}^2} \right) \quad (189)$$

$$\Omega_2(0) = \frac{a_{\parallel}}{a_{\perp}} \left( 1 + \frac{\Delta_{\perp}^2}{2 a_{\perp}^2} \right) \quad (190)$$

Consequently,

$$\underline{\phi} = \frac{a_{\parallel}}{a_{\perp}} \underline{1} \quad (191)$$

$$\psi_{\parallel} = \psi_{\perp} = \frac{2}{3} \frac{a_{\parallel}}{a_{\perp}} \quad (192)$$

These results agree with Demars and Schunk (1979).

Although these Maxwell molecule results were derived for the special case of a bi-Maxwellian distribution function, they are valid for arbitrary distribution functions.

### 3. Numerical results and approximate expressions

The momentum, parallel energy, and perpendicular energy collision terms, which depend on the quantities  $\underline{\Delta}$ ,  $\Omega_1$ ,  $\Omega_2$ ,  $\underline{\phi}$ ,  $\psi_{||}$ , and  $\psi_{\perp}$ , must be evaluated numerically for non-Maxwell molecule interactions. In order to limit the number of tables needed to present the numerical results, I restricted my calculations to the situations where the relative drift is either parallel or perpendicular to the magnetic field, which are the two most common cases in aeronomy and space physics.

In the case of parallel drift ( $\underline{\Delta} = \underline{\Delta}_{||}$ ), the appropriate expressions can be reduced to

$$\phi_{33}^{(n)} = \frac{3}{4\Gamma\left(\frac{5-n}{2}\right)} \frac{a_{||}}{\Delta_{||}} \int_{-\infty}^{\infty} d\xi \xi e^{-(\xi - \Delta_{||}/a_{||})^2} \cdot \exp\left(\frac{a_{||}^2}{a_{\perp}^2} \xi^2\right) \Gamma\left(1 - \frac{n}{2}, \frac{a_{||}^2}{a_{\perp}^2} \xi^2\right) \quad (193)$$

$$\phi_{13}^{(n)} = \phi_{23}^{(n)} = 0 \quad (194)$$

$$\Omega_1^{||} (n) = \frac{3}{4\Gamma\left(\frac{5-n}{2}\right)} \frac{a_{||}}{a_{\perp}} \int_{-\infty}^{\infty} d\xi \xi^2 e^{-(\xi - \Delta_{||}/a_{||})^2} \cdot \exp\left(\frac{a_{||}^2}{a_{\perp}^2} \xi^2\right) \Gamma\left(1 - \frac{n}{2}, \frac{a_{||}^2}{a_{\perp}^2} \xi^2\right) \quad (195)$$

$$\Omega_{2\parallel}^{||}(n) = \frac{3}{4\Gamma\left(\frac{5-n}{2}\right)} \frac{a_{\parallel}}{a_{\perp}} \int_{-\infty}^{\infty} d\xi e^{-(\xi - \Delta_{\parallel}/a_{\parallel})^2}$$

$$\cdot \left\{ \left[ 1 - \frac{n}{2} - \frac{a_{\parallel}^2}{a_{\perp}^2} \xi^2 \right] \exp\left(\frac{a_{\parallel}^2}{a_{\perp}^2} \xi^2\right) \Gamma\left(1 - \frac{n}{2}, \frac{a_{\parallel}^2}{a_{\perp}^2} \xi^2\right) + \left(\frac{a_{\parallel}^2}{a_{\perp}^2} \xi^2\right)^{(1-n/2)} \right\} \quad (196)$$

For the other special case, when the relative drift is perpendicular to the magnetic field ( $\underline{\Delta} = \underline{\Delta}_{\perp}$ ), the appropriate expressions reduce to

$$\phi_{11}(n) = \phi_{22}(n) = \frac{3\sqrt{\pi}}{2\Gamma\left(\frac{5-n}{2}\right)} \frac{a_{\parallel}^{(3-n)/2}}{a_{\perp}^{(1-n)/2} \Delta_{\perp}} \int_0^{\infty} d\xi \xi^{(3-n)/2} e^{-(\xi - \Delta_{\perp}/a_{\perp})^2}$$

$$\cdot \left[ e^{-2\Delta_{\perp}\xi/a_{\perp}} I_1(2\Delta_{\perp}\xi/a_{\perp}) \right] \left[ e^{(a_{\perp}^2 \xi^2 / 2a_{\parallel}^2)} W_{\frac{1-n}{4}, \frac{1-n}{4}} \left( \frac{a_{\perp}^2}{a_{\parallel}^2} \xi^2 \right) \right] \quad (197)$$

$$\phi_{31}(n) = \phi_{21}(n) = \phi_{32}(n) = \phi_{12}(n) = 0 \quad (198)$$

$$\Omega_{1\perp}^{\perp}(n) = \frac{3\sqrt{\pi}}{2\Gamma\left(\frac{5-n}{2}\right)} \left( \frac{a_{\parallel}}{a_{\perp}} \right)^{(1-n)/2} \int_0^{\infty} d\xi \xi^{(3-n)/2} e^{-(\xi - \Delta_{\perp}/a_{\perp})^2}$$

$$\cdot \left[ e^{-2\Delta_{\perp}\xi/a_{\perp}} I_0(2\Delta_{\perp}\xi/a_{\perp}) \right] \left[ e^{(a_{\perp}^2 \xi^2 / 2a_{\parallel}^2)} W_{\frac{-1-n}{4}, \frac{3-n}{4}} \left( \frac{a_{\perp}^2}{a_{\parallel}^2} \xi^2 \right) \right] \quad (199)$$

$$\Omega_{\perp}^{(n)} = \frac{3\sqrt{\pi}}{2\Gamma\left(\frac{5-n}{2}\right)} \left(\frac{a_{\parallel}}{a_{\perp}}\right)^{(3-n)/2} \int_0^{\infty} d\xi \xi^{(5-n)/2} e^{-(\xi - \Delta_{\perp}/a_{\perp})^2}$$

$$\cdot \left[ e^{-2\Delta_{\perp}\xi/a_{\perp}} I_0(2\Delta_{\perp}\xi/a_{\perp}) \right] \left[ e^{(a_{\perp}^2 \xi^2 / 2a_{\parallel}^2)} W_{\frac{1-n}{4}, \frac{1-n}{4}} \left( \frac{a_{\perp}^2}{a_{\parallel}^2} \xi^2 \right) \right] \quad (200)$$

In the above equations (193) - (200) the superscripts  $\parallel$  and  $\perp$  on the  $\Omega$ 's are used to denote the two cases when the relative drift is either parallel or perpendicular to the magnetic field, respectively.  $\Gamma(\alpha, x)$  is the incomplete gamma function,  $W_{\mu, \lambda}(x)$  is the Whittaker function, and  $I_m(x)$  is the Bessel function of the first kind of order  $m$ . They are defined in Gradshteyn and Ryzhik (1973).

These integrals still cannot be reduced to closed forms. However, an approximation could be found by combining the asymptotes at small and large relative drifts. These approximate expressions for nonzero quantities are given by

$$\Phi_{33}^{(n)} = \frac{3}{4\Gamma\left(\frac{5-n}{2}\right)} \left[ \left( \frac{2a_{\perp}^2}{\pi a_{\parallel}^2} I_{00,2} \right)^{\alpha_1(n)} + \left( \sqrt{\pi} \frac{a_{\parallel}}{a_{\perp}^{1-n}} \Delta_{\parallel}^{-n} \right)^{\alpha_1(n)} \right]^{1/\alpha_1(n)} \quad (193)'$$

$$\Omega_{\parallel}^{(n)} = \frac{3}{4\Gamma\left(\frac{5-n}{2}\right)} \left[ \left( \frac{1a_{\perp}^2}{\pi a_{\parallel}^2} I_{00,2} \right)^{\alpha_2(n)} + \left( \sqrt{\pi} \frac{1}{a_{\parallel} a_{\perp}^{1-n}} \Delta_{\parallel}^{2-n} \right)^{\alpha_2(n)} \right]^{1/\alpha_2(n)} \quad (195)'$$



$$\Omega_2^{||}(n) = \frac{3}{4\Gamma\left(\frac{5-n}{2}\right)} \left[ \left( \frac{2}{\pi} I_{20,0} \right)^{\alpha_3(n)} + \left( \sqrt{\pi} \frac{a_{||}}{a_{\perp}^{1-n}} \Delta_{\perp}^{-n} \right)^{\alpha_3(n)} \right]^{1/\alpha_3(n)} \quad (196)'$$

$$\Phi_{11}(n) = \Phi_{22}(n) = \frac{3}{4\Gamma\left(\frac{5-n}{2}\right)} \left[ \left( \frac{2}{\pi} I_{20,0} \right)^{\beta_1(n)} + \left( \sqrt{\pi} \frac{a_{||}}{a_{\perp}^{1-n}} \Delta_{\perp}^{-n} \right)^{\beta_1(n)} \right]^{1/\beta_1(n)} \quad (197)'$$

$$\Omega_1^{\perp}(n) = \frac{3}{4\Gamma\left(\frac{5-n}{2}\right)} \left[ \left( \frac{1}{\pi} \frac{a_{\perp}^2}{a_{||}^2} I_{00,2} \right)^{\beta_2(n)} + \left( \frac{\sqrt{\pi}}{2} \frac{a_{||}}{a_{\perp}^{1-n}} \Delta_{\perp}^{-n} \right)^{\beta_2(n)} \right]^{1/\beta_2(n)} \quad (199)'$$

$$\Omega_2^{\perp}(n) = \frac{3}{4\Gamma\left(\frac{5-n}{2}\right)} \left[ \left( \frac{2}{\pi} I_{20,0} \right)^{\beta_3(n)} + \left( \sqrt{\pi} \frac{a_{||}}{a_{\perp}^{3-n}} \Delta_{\perp}^{2-n} \right)^{\beta_3(n)} \right]^{1/\beta_3(n)} \quad (200)'$$

Where the  $\alpha$ 's and  $\beta$ 's are constants, depending only on the interparticle force law index  $n$ . They are to be chosen to minimize the relative error between the exact and the approximate expressions. This will be discussed in more detail below.

### 3.1. Coulomb interaction

If the mutual force between the interacting particles obeys the inverse square law ( $a=2, n=3$ ), the integrals in equations (193)-(200) can be evaluated numerically. Tables 1 - 6 give the numerical values with a 1% accuracy for wide ranges of "Mach numbers" and parallel-to-

Table 1. The numerical values of  $\phi_{33}(3)$  (Coulomb interaction and parallel relative drift) for different values of  $\Delta/a_{\perp}$  and  $T_{\parallel}/T_{\perp}$ .

$T_{\parallel}/T_{\perp} =$	1/16	1/9	1/4	1/3	1/2	1	2	3	4	9	16
$\Delta/a_{\perp}$											
1/64	2.11	1.91	1.58	1.46	1.29	1.00	7.40(-1)	6.06(-1)	5.21(-1)	3.26(-1)	2.26(-1)
1/32	2.10	1.90	1.58	1.46	1.29	9.99(-1)	7.39(-1)	6.06(-1)	5.21(-1)	3.26(-1)	2.26(-1)
1/16	2.05	1.88	1.57	1.46	1.28	9.98(-1)	7.38(-1)	6.05(-1)	5.20(-1)	3.26(-1)	2.26(-1)
1/8	1.90	1.79	1.53	1.43	1.26	9.91(-1)	7.36(-1)	6.04(-1)	5.19(-1)	3.26(-1)	2.26(-1)
1/4	1.42	1.49	1.40	1.33	1.20	9.63(-1)	7.25(-1)	5.97(-1)	5.15(-1)	3.24(-1)	2.26(-1)
1/2	6.22(-1)	8.04(-1)	9.86(-1)	1.00	9.85(-1)	8.63(-1)	6.82(-1)	5.73(-1)	4.99(-1)	3.19(-1)	2.23(-1)
1	1.66(-1)	2.24(-1)	3.56(-1)	4.12(-1)	4.92(-1)	5.68(-1)	5.39(-1)	4.86(-1)	4.39(-1)	3.00(-1)	2.16(-1)
2	3.19(-2)	4.28(-2)	6.66(-2)	7.80(-2)	1.00(-1)	1.59(-1)	2.33(-1)	2.61(-1)	2.69(-1)	2.36(-1)	1.87(-1)
4	4.79(-3)	6.38(-3)	9.73(-3)	1.13(-2)	1.41(-2)	2.08(-2)	3.26(-2)	4.48(-2)	5.70(-2)	9.62(-2)	1.08(-1)
8	6.35(-4)	8.44(-4)	1.28(-3)	1.47(-3)	1.81(-3)	2.60(-3)	3.76(-3)	4.73(-3)	5.61(-3)	1.01(-2)	1.89(-2)
16	8.07(-5)	1.07(-4)	1.62(-4)	1.86(-4)	2.29(-4)	3.25(-4)	4.62(-4)	5.69(-4)	6.61(-4)	1.02(-3)	1.43(-3)
32	1.01(-5)	1.34(-5)	2.03(-5)	2.33(-5)	2.87(-5)	4.06(-5)	5.75(-5)	7.05(-5)	8.15(-5)	1.23(-4)	1.66(-4)
64	1.27(-5)	1.68(-6)	2.54(-6)	2.91(-6)	3.59(-6)	5.07(-6)	7.17(-6)	8.79(-6)	1.01(-5)	1.53(-5)	2.04(-5)

Table 2. The numerical values of  $\Omega_{\perp}^{II}(3)$  (Coulomb interaction and parallel relative drift) for different values of  $\Delta/a_{\perp}$  and  $T_{\parallel}/T_{\perp}$ .

$T_{\parallel}/T_{\perp} =$	1/16	1/9	1/4	1/3	1/2	1	2	3	4	9	16
$\Delta/a_{\perp}$											
1/64	1.06	9.56(-1)	7.91(-1)	7.32(-1)	6.44(-1)	5.00(-1)	3.70(-1)	3.03(-1)	2.60(-1)	1.63(-1)	1.13(-1)
1/32	1.07	9.60(-1)	7.92(-1)	7.33(-1)	6.44(-1)	5.00(-1)	3.70(-1)	3.03(-1)	2.60(-1)	1.63(-1)	1.13(-1)
1/16	1.10	9.75(-1)	7.97(-1)	7.36(-1)	6.46(-1)	5.00(-1)	3.70(-1)	3.03(-1)	2.60(-1)	1.63(-1)	1.13(-1)
1/8	1.22	1.03	8.14(-1)	7.47(-1)	6.50(-1)	5.02(-1)	3.70(-1)	3.03(-1)	2.60(-1)	1.63(-1)	1.13(-1)
1/4	1.61	1.23	8.75(-1)	7.86(-1)	6.70(-1)	5.06(-1)	3.70(-1)	3.03(-1)	2.60(-1)	1.63(-1)	1.13(-1)
1/2	2.30	1.67	1.05	9.04(-1)	7.30(-1)	5.21(-1)	3.72(-1)	3.02(-1)	2.59(-1)	1.62(-1)	1.13(-1)
1	2.55	1.91	1.23	1.05	8.27(-1)	5.52(-1)	3.74(-1)	2.99(-1)	2.55(-1)	1.59(-1)	1.11(-1)
2	2.02	1.52	1.01	8.81(-1)	7.16(-1)	5.03(-1)	3.46(-1)	2.75(-1)	2.34(-1)	1.48(-1)	1.05(-1)
4	1.22	9.22(-1)	6.14(-1)	5.35(-1)	4.36(-1)	3.12(-1)	2.25(-1)	1.87(-1)	1.64(-1)	1.12(-1)	8.45(-2)
8	6.50(-1)	4.90(-1)	3.26(-1)	2.83(-1)	2.31(-1)	1.64(-1)	1.16(-1)	9.59(-2)	8.37(-2)	5.88(-2)	4.65(-2)
16	3.30(-1)	2.49(-1)	1.65(-1)	1.44(-1)	1.17(-1)	8.28(-2)	5.86(-2)	4.80(-2)	4.16(-2)	2.80(-2)	2.13(-2)
32	1.66(-1)	1.25(-1)	8.30(-2)	7.22(-2)	5.87(-2)	4.15(-2)	2.94(-2)	2.40(-2)	2.08(-2)	1.39(-2)	1.04(-2)
64	8.31(-2)	6.26(-2)	4.15(-2)	3.62(-2)	2.94(-2)	2.08(-2)	1.47(-2)	1.20(-2)	1.04(-2)	6.93(-3)	5.20(-3)

Table 3. The numerical values of  $\Omega_2^{||}(z)$  (Coulomb interaction and parallel relative drift) for different values of  $\Delta/a_{\perp}$  and  $T_{||}/T_{\perp}$ .

$T_{  }/T_{\perp} =$	1/16	1/9	1/4	1/3	1/2	1	2	3	4	9	16
$\Delta/a_{\perp}$											
1/64	4.44(-1)	5.45(-1)	7.09(-1)	7.67(-1)	8.56(-1)	1.00	1.13	1.20	1.24	1.34	1.39
1/32	4.43(-1)	5.44(-1)	7.08(-1)	7.67(-1)	8.55(-1)	1.00	1.13	1.20	1.24	1.34	1.39
1/16	4.38(-1)	5.39(-1)	7.05(-1)	7.64(-1)	8.53(-1)	9.98(-1)	1.13	1.20	1.24	1.34	1.39
1/8	4.18(-1)	5.22(-1)	6.92(-1)	7.52(-1)	8.43(-1)	9.91(-1)	1.12	1.19	1.24	1.34	1.39
1/4	3.59(-1)	4.62(-1)	6.42(-1)	7.07(-1)	8.04(-1)	9.63(-1)	1.11	1.18	1.23	1.33	1.38
1/2	2.26(-1)	3.11(-1)	4.88(-1)	5.59(-1)	6.72(-1)	8.63(-1)	1.04	1.13	1.18	1.31	1.37
1	9.53(-2)	1.31(-1)	2.21(-1)	2.68(-1)	3.61(-1)	5.68(-1)	8.06(-1)	9.38(-1)	1.02	1.22	1.31
2	2.52(-2)	3.41(-2)	5.46(-2)	6.50(-2)	8.68(-2)	1.59(-1)	3.22(-1)	4.68(-1)	5.86(-1)	9.19(-1)	1.11
4	4.43(-3)	5.92(-3)	9.12(-3)	1.06(-2)	1.34(-2)	2.07(-2)	3.66(-2)	5.82(-2)	9.15(-2)	3.12(-1)	5.75(-1)
8	6.11(-4)	8.12(-4)	1.23(-3)	1.42(-3)	1.76(-3)	2.56(-3)	3.81(-3)	4.92(-3)	6.03(-3)	1.45(-2)	5.22(-2)
16	8.02(-5)	1.07(-4)	1.61(-4)	1.85(-4)	2.28(-4)	3.24(-4)	4.64(-4)	5.76(-4)	6.73(-4)	1.08(-3)	1.60(-3)
32	1.01(-5)	1.34(-5)	2.02(-5)	2.33(-5)	2.86(-5)	4.06(-5)	5.75(-5)	7.07(-5)	8.18(-5)	1.25(-4)	1.70(-4)
64	1.27(-6)	1.68(-6)	2.53(-6)	2.91(-6)	3.59(-6)	5.07(-6)	7.18(-6)	8.80(-6)	1.02(-5)	1.53(-5)	2.05(-5)

Table 4. The numerical values of  $\phi_{11}(3)$  (Coulomb interaction and perpendicular relative drift) for different values of  $\Delta/a_{\perp}$  and  $T_{\parallel}/T_{\perp}$ . ( $\phi_{11}=\phi_{22}$ )

$T_{\parallel}/T_{\perp} =$	1/16	1/9	1/4	1/3	1/2	1	2	3	4	9	16
$\Delta/a_{\perp}$											
1/64	4.45(-1)	5.45(-1)	7.10(-1)	7.68(-1)	8.57(-1)	1.00	1.13	1.20	1.24	1.34	1.39
1/32	4.44(-1)	5.45(-1)	7.09(-1)	7.67(-1)	8.56(-1)	9.99(-1)	1.13	1.20	1.24	1.34	1.39
1/16	4.44(-1)	5.44(-1)	7.07(-1)	7.66(-1)	8.54(-1)	9.98(-1)	1.13	1.19	1.24	1.33	1.38
1/8	4.40(-1)	5.39(-1)	7.02(-1)	7.60(-1)	8.48(-1)	9.91(-1)	1.12	1.19	1.23	1.33	1.38
1/4	4.26(-1)	5.23(-1)	6.81(-1)	7.38(-1)	8.24(-1)	9.64(-1)	1.09	1.16	1.20	1.29	1.34
1/2	3.75(-1)	4.62(-1)	6.04(-1)	6.56(-1)	7.34(-1)	8.63(-1)	9.81(-1)	1.04	1.08	1.17	1.22
1	2.31(-1)	2.88(-1)	3.84(-1)	4.20(-1)	4.75(-1)	5.68(-1)	6.58(-1)	7.06(-1)	7.37(-1)	8.12(-1)	8.51(-1)
2	5.14(-2)	6.62(-2)	9.40(-2)	1.05(-1)	1.24(-1)	1.59(-1)	1.96(-1)	2.19(-1)	2.34(-1)	2.75(-1)	2.99(-1)
4	5.45(-3)	7.21(-3)	1.08(-2)	1.23(-2)	1.50(-2)	2.08(-2)	2.81(-2)	3.32(-2)	3.71(-2)	4.89(-2)	5.75(-2)
8	6.56(-4)	8.70(-4)	1.31(-3)	1.50(-3)	1.85(-3)	2.60(-3)	3.63(-3)	4.40(-3)	5.02(-3)	7.19(-3)	9.06(-3)
16	8.14(-5)	1.08(-4)	1.63(-4)	1.87(-4)	2.30(-4)	3.25(-4)	4.58(-4)	5.59(-4)	6.44(-4)	9.52(-4)	1.25(-3)
32	1.01(-5)	1.35(-5)	2.03(-5)	2.33(-5)	2.87(-5)	4.06(-5)	5.73(-5)	7.02(-5)	8.09(-5)	1.21(-4)	1.60(-4)
64	1.27(-6)	1.68(-6)	2.54(-6)	2.91(-6)	3.59(-6)	5.07(-6)	7.17(-6)	8.78(-6)	1.01(-5)	1.52(-5)	2.02(-5)

Table 5. The numerical values of  $\Omega_{\perp}^{\perp}(3)$  (Coulomb interaction and perpendicular relative drift) for different values of  $\Delta/a_{\perp}$  and  $T_{\parallel}/T_{\perp}$ .

$T_{\parallel}/T_{\perp} =$	1/16	1/9	1/4	1/3	1/2	1	2	3	4	9	16
$\Delta/a_{\perp}$											
1/64	1.05	9.53(-1)	7.91(-1)	7.32(-1)	6.44(-1)	5.00(-1)	3.70(-1)	3.03(-1)	2.60(-1)	1.63(-1)	1.13(-1)
1/32	1.05	9.53(-1)	7.90(-1)	7.31(-1)	6.43(-1)	5.00(-1)	3.70(-1)	3.03(-1)	2.60(-1)	1.63(-1)	1.13(-1)
1/16	1.05	9.52(-1)	7.88(-1)	7.30(-1)	6.42(-1)	4.99(-1)	3.69(-1)	3.02(-1)	2.60(-1)	1.63(-1)	1.13(-1)
1/8	1.04	9.43(-1)	7.81(-1)	7.24(-1)	6.37(-1)	4.95(-1)	3.67(-1)	3.01(-1)	2.59(-1)	1.62(-1)	1.12(-1)
1/4	1.00	9.08(-1)	7.54(-1)	7.00(-1)	6.17(-1)	4.82(-1)	3.57(-1)	2.94(-1)	2.53(-1)	1.59(-1)	1.11(-1)
1/2	8.56(-1)	7.81(-1)	6.59(-1)	6.14(-1)	5.45(-1)	4.31(-1)	3.24(-1)	2.69(-1)	2.33(-1)	1.48(-1)	1.04(-1)
1	4.63(-1)	4.37(-1)	3.90(-1)	3.71(-1)	3.40(-1)	2.84(-1)	2.26(-1)	1.93(-1)	1.70(-1)	1.15(-1)	8.32(-2)
2	5.62(-2)	7.23(-2)	7.35(-2)	7.52(-2)	7.76(-2)	7.93(-2)	7.69(-2)	7.29(-2)	6.93(-2)	5.57(-2)	4.47(-2)
4	3.02(-3)	3.98(-3)	5.84(-3)	6.62(-3)	7.92(-3)	1.04(-2)	1.30(-2)	1.43(-2)	1.50(-2)	1.60(-2)	1.54(-2)
8	3.36(-4)	4.45(-4)	6.67(-4)	7.64(-4)	9.34(-4)	1.30(-3)	1.78(-3)	2.10(-3)	2.36(-3)	3.09(-3)	3.53(-3)
16	4.09(-5)	5.42(-5)	8.17(-5)	9.38(-5)	1.15(-4)	1.62(-4)	2.28(-4)	2.76(-4)	3.16(-4)	4.56(-4)	5.76(-4)
32	5.08(-6)	6.74(-6)	1.02(-5)	1.17(-5)	1.44(-5)	2.03(-5)	2.86(-5)	3.50(-5)	4.03(-5)	5.98(-5)	7.86(-5)
64	6.34(-7)	8.41(-7)	1.27(-6)	1.46(-6)	1.79(-6)	2.54(-6)	3.58(-6)	4.39(-6)	5.06(-6)	7.57(-6)	1.01(-5)

Table 6. The numerical values of  $\Omega_2^\perp(z)$  (Coulomb interaction and perpendicular relative drift) for different values of  $\Delta/a_\perp$  and  $T_{||}/T_\perp$ .

$T_{  }/T_\perp =$	1/16	1/9	1/4	1/3	1/2	1	2	3	4	9	16
$\Delta/a_\perp$											
1/64	4.44(-1)	5.45(-1)	7.09(-1)	7.68(-1)	8.56(-1)	1.00	1.13	1.20	1.24	1.34	1.39
1/32	4.44(-1)	5.45(-1)	7.09(-1)	7.68(-1)	8.56(-1)	1.00	1.13	1.20	1.24	1.34	1.39
1/16	4.44(-1)	5.44(-1)	7.09(-1)	7.67(-1)	8.55(-1)	9.99(-1)	1.13	1.20	1.24	1.34	1.39
1/8	4.42(-1)	5.42(-1)	7.06(-1)	7.65(-1)	8.53(-1)	9.97(-1)	1.13	1.19	1.24	1.34	1.39
1/4	4.34(-1)	5.34(-1)	6.97(-1)	7.54(-1)	8.43(-1)	9.88(-1)	1.12	1.19	1.23	1.33	1.38
1/2	4.06(-1)	5.01(-1)	6.60(-1)	7.18(-1)	8.06(-1)	9.52(-1)	1.09	1.16	1.21	1.31	1.37
1	3.19(-1)	4.02(-1)	5.46(-1)	6.00(-1)	6.86(-1)	8.36(-1)	9.83(-1)	1.06	1.12	1.25	1.32
2	1.76(-1)	2.29(-1)	3.32(-1)	3.75(-1)	4.46(-1)	5.83(-1)	7.36(-1)	8.29(-1)	8.95(-1)	1.07	1.18
4	8.42(-2)	1.11(-1)	1.67(-1)	1.91(-1)	2.33(-1)	3.22(-1)	4.37(-1)	5.17(-1)	5.78(-1)	7.66(-1)	9.04(-1)
8	4.17(-2)	5.53(-2)	8.32(-2)	9.54(-2)	1.17(-1)	1.65(-1)	2.30(-1)	2.79(-1)	3.19(-1)	4.57(-1)	5.76(-1)
16	2.08(-2)	2.76(-2)	4.15(-2)	4.77(-2)	5.87(-2)	8.29(-2)	1.17(-1)	1.43(-1)	1.64(-1)	2.43(-1)	3.19(-1)
32	1.04(-2)	1.38(-2)	2.08(-2)	2.39(-2)	2.94(-2)	4.15(-2)	5.87(-2)	7.18(-2)	8.29(-2)	1.24(-1)	1.64(-1)
64	5.19(-3)	6.89(-3)	1.04(-2)	1.19(-2)	1.47(-2)	2.08(-2)	2.94(-2)	3.60(-2)	4.15(-2)	6.22(-2)	9.29(-2)

perpendicular temperature ratios. However, the approximate expressions (193)'-(200)' may be used instead of these tables. The values for the  $\alpha$ 's and  $\beta$ 's, which minimize the relative error, are given in Table 13.

The accuracy of the approximate expressions is given in Table 14. In general, for the case of parallel relative drift, the relative error does not exceed 63% when the parallel-to-perpendicular temperature ratio ( $T_{\parallel}/T_{\perp}$ ) ranges from 1/4 to 4, and is less than 110% for  $T_{\parallel}/T_{\perp}$  values from 1/16 to 16. In the case of perpendicular drift, the error is less than 26% for  $1/4 \leq T_{\parallel}/T_{\perp} \leq 4$  and less than 96% for  $1/16 \leq T_{\parallel}/T_{\perp} \leq 16$ . However, the closer to the isotropic condition ( $T_{\parallel} = T_{\perp}$ ), the better the approximate expressions. Also, when the relative drift is much higher, or much lower, than the average thermal speed (i.e.,  $\Delta \gg a_{\parallel}$ ,  $a_{\perp}$  or  $\Delta \ll a_{\parallel}$ ,  $a_{\perp}$ ) the approximate expressions become very accurate.

To evaluate the collision terms on the right-hand-side of equations (146) - (148) in the case of a Coulomb-force interaction, the following steps are to be taken. First, Tables 1-6 are to be used to find the  $\phi$ 's and  $\Omega$ 's, or alternatively, the approximate expressions given in equations (193)' - (200)' can be used, taking  $n=3$  and the values of the  $\alpha$ 's and  $\beta$ 's given in Table 13. Second,  $\Psi_{\parallel}$  and  $\Psi_{\perp}$  are calculated using equations (171) and (172), and the momentum transfer collision frequency  $\nu_{st}$  is determined from equation (63), with  $A_1(2)$  equal to the Coulomb logarithm. Third, the substitution of the above quantities into equations (167) - (169) yields the desired collision terms  $\delta \underline{M}_s / \delta t$ ,  $\delta \underline{E}_s / \delta t$  and  $\delta \underline{E}_s / \delta t$ .



### 3.2. Hard sphere interaction

In the case of a hard sphere interaction ( $a=\infty$ ,  $n=-1$ ) the integrals in equations (193) - (200) can also be evaluated numerically. Tables 7 - 12 give the numerical values for wide ranges of "Mach numbers" and parallel-to-perpendicular temperature ratios. However, the approximate expressions (193)' - (200)' may be used instead of these tables. The values for the  $\alpha$ 's and  $\beta$ 's, which minimize the relative error, are given in Table 13.

The accuracy of these approximate expressions for a hard sphere interaction is much better than that obtained for a Coulomb interaction. For parallel relative drift the error is less than 10% when  $1/4 \leq T_{\parallel}/T_{\perp} \leq 4$  and does not exceed 26% when  $1/16 \leq T_{\parallel}/T_{\perp} \leq 16$ . As was mentioned in the previous subsection, the accuracy gets better as we approach the isotropic case and as  $\Delta$  becomes much greater, or much less, than  $a_{\parallel}$  and  $a_{\perp}$ .

To evaluate the collision terms ( $\delta \underline{M}_s / \delta t$ ,  $\delta \underline{E}_{s\parallel} / \delta t$ , and  $\delta \underline{E}_{s\perp} / \delta t$ ), steps similar to that mentioned for the Coulomb interaction are to be followed. However, in this case we use  $n=-1$  and  $a=\infty$ .

Table 7. The numerical values of  $\phi_{33}(-1)$  (hard sphere interaction and parallel relative drift) for different values of  $\Delta/a_{\perp}$  and  $T_{\parallel}/T_{\perp}$ .

$T_{\parallel}/T_{\perp} =$	1/16	1/9	1/4	1/3	1/2	1	2	3	4	9	16
$\Delta/a_{\perp}$											
1/64	1.58(-1)	2.19(-1)	3.65(-1)	4.40(-1)	5.89(-1)	1.00	1.78	2.55	3.31	7.09	1.24(+1)
1/32	1.58(-1)	2.19(-1)	3.65(-1)	4.40(-1)	5.89(-1)	1.00	1.78	2.55	3.31	7.09	1.24(+1)
1/16	1.56(-1)	2.19(-1)	3.65(-1)	4.40(-1)	5.90(-1)	1.00	1.78	2.55	3.31	7.09	1.24(+1)
1/8	1.60(-1)	2.21(-1)	3.67(-1)	4.42(-1)	5.92(-1)	1.00	1.79	2.55	3.31	7.09	1.24(+1)
1/4	1.64(-1)	2.26(-1)	3.74(-1)	4.50(-1)	6.00(-1)	1.01	1.80	2.56	3.33	7.10	1.24(+1)
1/2	1.81(-1)	2.47(-1)	4.01(-1)	4.79(-1)	6.32(-1)	1.05	1.84	2.61	3.37	7.14	1.24(+1)
1	2.34(-1)	3.15(-1)	4.95(-1)	5.81(-1)	7.49(-1)	1.19	1.99	2.77	3.54	7.32	1.26(+1)
2	3.73(-1)	4.97(-1)	7.60(-1)	8.81(-1)	1.10	1.64	2.54	3.36	4.16	8.01	1.33(+1)
4	6.86(-1)	9.11(-1)	1.38	1.59	1.97	2.82	4.11	5.18	6.14	1.04(+1)	1.59(+1)
8	1.34	1.78	2.68	3.09	3.80	5.40	7.70	9.50	1.11(+1)	1.72(+1)	2.41(+1)
16	2.66	3.54	5.33	6.13	7.54	1.07(+1)	1.51(+1)	1.86(+1)	2.15(+1)	3.25(+1)	4.40(+1)
32	5.32	7.06	1.06(+1)	1.22(+1)	1.51(+1)	2.13(+1)	3.01(+1)	3.69(+1)	4.26(+1)	6.41(+1)	8.58(+1)
64	1.06(+1)	1.41(+1)	2.13(+1)	2.44(+1)	3.01(+1)	4.25(+1)	6.02(+1)	7.37(+1)	8.51(+1)	1.28(+2)	1.71(+2)

Table 8. The numerical values of  $\Omega_{\parallel}^{\parallel}(-1)$  (hard sphere interaction and parallel relative drift) for different values of  $\Delta/a_{\perp}$  and  $T_{\parallel}/T_{\perp}$ .

$T_{\parallel}/T_{\perp} =$	1/16	1/9	1/4	1/3	1/2	1	2	3	4	9	16
$\Delta/a_{\perp}$											
1/64	7.97(-2)	1.10(-1)	1.83(-1)	2.20(-1)	2.95(-1)	5.00(-1)	8.91(-1)	1.27	1.65	3.54	6.17
1/32	8.16(-2)	1.12(-1)	1.84(-1)	2.21(-1)	2.96(-1)	5.01(-1)	8.92(-1)	1.28	1.66	3.54	6.17
1/16	8.95(-2)	1.18(-1)	1.89(-1)	2.26(-1)	3.00(-1)	5.05(-1)	8.96(-1)	1.28	1.66	3.55	6.18
1/8	1.21(-1)	1.44(-1)	2.09(-1)	2.44(-1)	3.17(-1)	5.21(-1)	9.11(-1)	1.29	1.67	3.56	6.19
1/4	2.52(-1)	2.49(-1)	2.90(-1)	3.20(-1)	3.86(-1)	5.82(-1)	9.68(-1)	1.35	1.73	3.61	6.24
1/2	8.35(-1)	7.11(-1)	6.37(-1)	6.40(-1)	6.74(-1)	8.35(-1)	1.20	1.58	1.95	3.83	6.46
1	3.92	3.10	2.34	2.18	2.02	1.96	2.19	2.52	2.87	4.78	7.32
2	2.42(+1)	1.85(+1)	1.28(+1)	1.14(+1)	9.78	7.91	7.02	6.90	7.03	8.44	1.09(+1)
4	1.76(+2)	1.34(+2)	8.97(+1)	7.86(+1)	6.48(+1)	4.78(+1)	3.66(+1)	3.22(+1)	2.99(+1)	2.66(+1)	2.72(+1)
8	1.37(+3)	1.04(+3)	6.90(+2)	6.02(+2)	4.91(+2)	3.51(+2)	2.54(+2)	2.12(+2)	1.87(+2)	1.38(+2)	1.18(+2)
16	1.09(+4)	8.23(+3)	5.46(+3)	4.76(+3)	3.87(+3)	2.74(+3)	1.95(+3)	1.60(+3)	1.40(+3)	9.57(+2)	7.46(+2)
32	8.72(+4)	6.57(+4)	4.36(+4)	3.80(+4)	3.08(+4)	2.18(+4)	1.55(+4)	1.26(+4)	1.10(+4)	7.36(+3)	5.58(+3)
64	6.97(+5)	5.26(+5)	3.49(+5)	3.03(+5)	2.47(+5)	1.74(+5)	1.23(+5)	1.01(+5)	8.72(+4)	5.83(+4)	4.38(+4)

Table 9. The numerical values of  $\Omega_2^{\parallel}(-1)$  (hard sphere interaction and parallel relative drift) for different values of  $\Delta/a_{\perp}$  and  $T_{\parallel}/T_{\perp}$ .

$T_{\parallel}/T_{\perp} =$	1/16	1/9	1/4	1/3	1/2	1	2	3	4	9	16
$\Delta/a_{\perp}$											
1/64	2.23(-1)	2.98(-1)	4.59(-1)	5.33(-1)	6.69(-1)	1.00	1.54	2.03	2.48	4.61	7.43
1/32	2.23(-1)	2.98(-1)	4.59(-1)	5.33(-1)	6.70(-1)	1.00	1.54	2.03	2.48	4.61	7.43
1/16	2.23(-1)	2.99(-1)	4.59(-1)	5.33(-1)	6.70(-1)	1.00	1.54	2.03	2.49	4.61	7.43
1/8	2.24(-1)	2.99(-1)	4.61(-1)	5.35(-1)	6.72(-1)	1.00	1.55	2.03	2.49	4.61	7.43
1/4	2.27(-1)	3.04(-1)	4.66(-1)	5.41(-1)	6.80(-1)	1.01	1.56	2.05	2.50	4.63	7.45
1/2	2.40(-1)	3.19(-1)	4.91(-1)	5.66(-1)	7.09(-1)	1.05	1.60	2.09	2.55	4.69	7.51
1	2.82(-1)	3.75(-1)	5.69(-1)	6.57(-1)	8.16(-1)	1.19	1.77	2.28	2.75	4.91	7.75
2	4.05(-1)	5.37(-1)	8.11(-1)	9.33(-1)	1.15	1.64	2.36	2.95	3.48	5.78	8.69
4	7.05(-1)	9.35(-1)	1.41	1.62	1.99	2.82	4.00	4.91	5.68	8.70	1.21(+1)
8	1.35	1.79	2.70	3.10	3.82	5.40	7.64	9.35	1.08(+1)	1.62(+1)	2.17(+1)
16	2.67	3.54	5.34	6.13	7.55	1.07(+1)	1.51(+1)	1.85(+1)	2.14(+1)	3.20(+1)	4.27(+1)
32	5.32	7.06	1.06(+1)	1.22(+1)	1.51(+1)	2.13(+1)	3.01(+1)	3.69(+1)	4.26(+1)	6.39(+1)	8.52(+1)
64	1.06(+1)	1.41(+1)	2.13(+1)	2.45(+1)	3.01(+1)	4.26(+1)	6.02(+1)	7.37(+1)	8.51(+1)	1.28(+2)	1.70(+2)

Table 10. The numerical values of  $\phi_{11}(-1)$  (hard sphere interaction and perpendicular relative drift) for different values of  $\Delta/a_{\perp}$  and  $T_{\parallel}/T_{\perp}$ . ( $\phi_{11}=\phi_{22}$ )

$T_{\parallel}/T_{\perp} =$	1/16	1/9	1/4	1/3	1/2	1	2	3	4	9	16
$\Delta/a_{\perp}$											
1/64	2.23(-1)	2.98(-1)	4.59(-1)	5.33(-1)	6.70(-1)	1.00	1.54	2.03	2.49	4.61	7.43
1/32	2.23(-1)	2.98(-1)	4.59(-1)	5.33(-1)	6.70(-1)	1.00	1.54	2.03	2.49	4.61	7.42
1/16	2.23(-1)	2.98(-1)	4.59(-1)	5.33(-1)	6.70(-1)	1.00	1.54	2.03	2.49	4.61	7.43
1/8	2.24(-1)	2.99(-1)	4.60(-1)	5.34(-1)	6.72(-1)	1.00	1.55	2.03	2.49	4.62	7.43
1/4	2.31(-1)	3.08(-1)	4.65(-1)	5.40(-1)	6.92(-1)	1.01	1.56	2.05	2.51	4.64	7.46
1/2	2.37(-1)	3.16(-1)	4.85(-1)	5.62(-1)	7.06(-1)	1.05	1.61	2.11	2.57	4.72	7.56
1	2.74(-1)	3.65(-1)	5.58(-1)	6.46(-1)	8.07(-1)	1.19	1.79	2.32	2.81	5.04	7.94
2	3.94(-1)	5.24(-1)	7.94(-1)	9.16(-1)	1.14	1.64	2.41	3.05	3.63	6.15	9.29
4	6.96(-1)	9.24(-1)	1.40	1.61	1.98	2.82	4.05	5.02	5.87	9.30	1.32(+1)
8	1.35	1.78	2.69	3.09	3.81	5.40	7.67	9.42	1.09(+1)	1.67(+1)	2.27(+1)
16	2.67	3.51	5.33	6.13	7.55	1.07(+1)	1.51(+1)	1.85(+1)	2.14(+1)	3.23(+1)	4.33(+1)
32	5.32	7.06	1.06(+1)	1.22(+1)	1.51(+1)	2.13(+1)	3.01(+1)	3.69(+1)	4.26(+1)	6.40(+1)	8.55(+1)
64	1.06(+1)	1.41(+1)	2.13(+1)	2.44(+1)	3.01(+1)	4.25(+1)	6.02(+1)	7.37(+1)	8.51(+1)	1.28(+2)	1.70(+2)

Table 11. The numerical values of  $\Omega_1^\perp(-1)$  (hard sphere interaction and perpendicular relative drift) for different values of  $\Delta/a_\perp$  and  $T_{||}/T_\perp$ .

$T_{  }/T_\perp =$	1/16	1/9	1/4	1/3	1/2	1	2	3	4	9	16
$\Delta/a_\perp$											
1/64	7.90(-2)	1.09(-1)	1.82(-1)	2.20(-1)	2.94(-1)	5.00(-1)	8.91(-1)	1.27	1.65	3.54	6.17
1/32	7.90(-2)	1.09(-1)	1.83(-1)	2.20(-1)	2.95(-1)	5.00(-1)	8.91(-1)	1.27	1.65	3.54	6.17
1/16	7.91(-2)	1.09(-1)	1.83(-1)	2.20(-1)	2.95(-1)	5.00(-1)	8.92(-1)	1.27	1.66	3.54	6.17
1/8	7.95(-2)	1.10(-1)	1.83(-1)	2.21(-1)	2.96(-1)	5.01(-1)	8.93(-1)	1.28	1.66	3.54	6.18
1/4	8.12(-2)	1.12(-1)	1.86(-1)	2.24(-1)	2.99(-1)	5.06(-1)	8.99(-1)	1.28	1.66	3.55	6.18
1/2	8.74(-2)	1.20(-1)	1.98(-1)	2.37(-1)	3.14(-1)	5.25(-1)	9.21(-1)	1.31	1.69	3.58	6.21
1	1.10(-1)	1.50(-1)	2.40(-1)	2.83(-1)	3.69(-1)	5.94(-1)	1.00	1.40	1.78	3.69	6.33
2	1.79(-1)	2.40(-1)	3.70(-1)	4.30(-1)	5.43(-1)	8.21(-1)	1.29	1.72	2.13	4.10	6.78
4	3.39(-1)	4.50(-1)	6.83(-1)	7.88(-1)	9.77(-1)	1.41	2.08	2.63	3.14	5.40	8.28
8	6.68(-1)	8.37(-1)	1.34	1.54	1.90	2.70	3.86	4.78	5.58	8.79	1.24(+1)
16	1.33	1.77	2.66	3.06	3.77	5.34	7.57	9.30	1.08(+1)	1.64(+1)	2.23(+1)
32	2.66	3.53	5.32	6.11	7.53	1.06(+1)	1.51(+1)	1.85(+1)	2.13(+1)	3.21(+1)	4.30(+1)
64	5.32	7.05	1.06(+1)	1.22(+1)	1.50(+1)	2.13(+1)	3.01(+1)	3.69(+1)	4.26(+1)	6.39(+1)	8.53(+1)

Table 12. The numerical values of  $\Omega_{\perp}^{\perp}(-1)$  (hard sphere interaction and perpendicular relative drift) for different values of  $\Delta/a_{\perp}$  and  $T_{\parallel}/T_{\perp}$ .

$T_{\parallel}/T_{\perp} =$	1/16	1/9	1/4	1/3	1/2	1	2	3	4	9	16
$\Delta/a_{\perp}$											
1/64	2.23(-1)	2.98(-1)	4.59(-1)	5.33(-1)	6.70(-1)	1.00	1.54	2.03	2.49	4.61	7.43
1/32	2.23(-1)	2.99(-1)	4.59(-1)	5.33(-1)	6.70(-1)	1.00	1.55	2.03	2.49	4.62	7.43
1/16	2.24(-1)	3.00(-1)	4.61(-1)	5.35(-1)	6.73(-1)	1.00	1.55	2.04	2.50	4.63	7.46
1/8	2.28(-1)	3.05(-1)	4.69(-1)	5.45(-1)	6.85(-1)	1.02	1.58	2.07	2.54	4.70	7.56
1/4	2.44(-1)	3.26(-1)	5.01(-1)	5.81(-1)	7.30(-1)	1.09	1.67	2.23	2.68	4.96	7.96
1/2	3.09(-1)	4.12(-1)	6.32(-1)	7.32(-1)	9.18(-1)	1.36	2.08	2.71	3.28	6.01	9.58
1	5.95(-1)	7.92(-1)	1.21	1.40	1.74	2.55	3.83	4.92	5.94	1.05(+1)	1.64(+1)
2	2.11	2.80	4.24	4.89	6.06	8.73	1.28(+1)	1.61(+1)	1.91(+1)	3.21(+1)	4.81(+1)
4	1.21(+1)	1.61(+1)	2.44(+1)	2.80(+1)	3.46(+1)	4.92(+1)	7.05(+1)	8.74(+1)	1.02(+2)	1.62(+2)	2.29(+2)
8	8.81(+1)	1.17(+2)	1.76(+2)	2.03(+2)	2.50(+2)	3.54(+2)	5.02(+2)	6.17(+2)	7.15(+2)	1.09(+3)	1.49(+3)
16	6.87(+2)	9.11(+2)	1.37(+3)	1.58(+3)	1.94(+3)	2.75(+3)	3.89(+3)	4.77(+3)	5.51(+3)	8.31(+3)	1.12(+4)
32	5.46(+3)	7.24(+3)	1.09(+4)	1.25(+4)	1.54(+4)	2.18(+4)	3.09(+4)	3.78(+4)	4.37(+4)	6.56(+4)	8.77(+4)
64	4.36(+4)	5.78(+4)	8.72(+4)	1.00(+5)	1.23(+5)	1.74(+5)	2.47(+5)	3.02(+5)	3.49(+5)	5.23(+5)	6.98(+5)

Table 13. Optimum values of  $\alpha$ 's and  $\beta$ 's.

$\ell$	Coulomb Interaction		Hard Sphere Interaction	
	Parallel Drift $\alpha_\ell$	Perpendicular Drift $\beta_\ell$	Parallel Drift $\alpha_\ell$	Perpendicular Drift $\beta_\ell$
1	-1.0	-1.051	2.0	2.0
2	-6.0	-1.07	0.58	2.0
3	-1.07	-2.35	2.08	0.62



Table 14. Maximum percentage error of the approximate expressions given in equations (193)-(200).

	Coulomb Interaction			Hard Sphere Interaction		
	$\frac{T_{  }}{T_{\perp}} = 1$	$\frac{1}{4} \leq \frac{T_{  }}{T_{\perp}} \leq 4$	$\frac{1}{16} \leq \frac{T_{  }}{T_{\perp}} \leq 16$	$\frac{T_{  }}{T_{\perp}} = 1$	$\frac{1}{4} \leq \frac{T_{  }}{T_{\perp}} \leq 4$	$\frac{1}{16} \leq \frac{T_{  }}{T_{\perp}} \leq 16$
$\phi_{11}$	10.0	32.5	73.5	1.3	2.0	2.4
$\Omega_1^{  }$	9.5	35.7	108	2.1	9.6	26
$\Omega_2^{  }$	7.7	62.6	109	0.2	3.1	6.3
$\phi_{22}$	8.4	19.6	55.1	1.4	1.7	1.9
$\Omega_1^{\perp}$	8.0	25.9	95.8	1.5	3.0	3.9
$\Omega_2^{\perp}$	0.7	6.6	12.5	0.9	3.6	7.8

Table 15. The  $I_{LM,N}$  for Coulomb and Hard sphere interactions.

L	M	N	$I_{LM,N}$
Coulomb			
0	0	2	$\frac{2\pi}{\lambda} [1 - \phi'(\lambda)]$
2	0	0	$\frac{\pi}{\lambda} [-1 + (1 + \lambda)\phi'(\lambda)]$
Hard Sphere			
0	0	2	$\frac{\pi}{2\lambda} \left[ \frac{1}{1+\lambda} - \frac{2}{(1+\lambda)^2} + \phi'(\lambda) \right]$
2	0	0	$\frac{\pi}{4\lambda} \left[ 3 - \frac{2}{1+\lambda} + (3\lambda - 1)\phi'(\lambda) \right]$

$$\phi'(\lambda) = \frac{1}{\sqrt{\lambda}} \tan^{-1} \sqrt{\lambda} \quad ; \quad \lambda = \frac{a^2}{a^2} - 1$$

## CHAPTER IV

COMPARISON OF TRANSPORT EQUATIONS BASED ON MAXWELLIAN  
AND BI-MAXWELLIAN DISTRIBUTIONS  
FOR ANISOTROPIC PLASMAS

## 1. Theoretical formulation

For a weakly-ionized homogeneous ( $\nabla f = 0$ ) plasma, the steady state ( $\frac{\partial}{\partial t} = 0$ ) distribution function for ions ( $s=i$ ) is governed by the following equation;

$$\frac{e_i}{m_i} \left[ \underline{E} + \frac{1}{c} \underline{v}_i \times \underline{B} \right] \cdot \underline{v}_i f_i = \frac{\delta f_i}{\delta t} \quad (201)$$

Moreover, if a simple relaxation model is used to describe ion neutral collisions (Tanenbaum 1967), the right-hand-side of Boltzman's equation takes the form

$$\frac{\delta f_i}{\delta t} = -\nu_i (f_i - f_{im}) \quad (202)$$

where

$$f_{im} = n_i \left[ \frac{m_i}{2\pi k T_n} \right]^{3/2} e^{-(m_i v_i^2 / 2k T_n)} \quad (203)$$

is a Maxwellian distribution function at the temperature of the neutral gas ( $T_n$ ),  $n_i$  is the ion density, and  $\nu_i$  is the velocity independent ion-neutral collision frequency. This collision term acts to drive the ion distribution toward the Maxwellian distribution at a rate governed by the relaxation time  $\nu_i^{-1}$ .

1.1. Closed form solution

Equations (201) and (202) can be integrated into a closed form for general electric and magnetic fields. However, this general case is not

of immediate interest to the purpose of this work. I will consider the two special cases when the electric field is parallel or perpendicular to the magnetic field. The equations related to the case of parallel electric and magnetic fields will be designated by an 'L' next to their numbers, while the ones related to the case of perpendicular fields will be designated by a 'T' next to their numbers.

The coordinates were chosen such that

$$\underline{B} = B \underline{e}_3 \quad (204)$$

$$\underline{E} = E_{||} \underline{e}_3 \quad (205)L$$

or

$$\underline{E} = E_{\perp} \underline{e}_2 \quad (206)T$$

For parallel electric and magnetic fields, the integration of equations (201) and (202) yields,

$$f_i = n_i \frac{m_i}{4\pi k T_n u_d} \exp \left[ -\frac{m_i v_i^2}{2k T_n} \right] \exp(\psi^2) \operatorname{erfc}(\psi) \quad (207)L$$

where

$$u_d = \frac{e_i E_{||}}{m_i v_i} \quad (208)L$$

$$\psi = \sqrt{\frac{k T_n}{2 m_i}} \cdot \frac{1}{u_d} - \sqrt{\frac{m_i}{2k T_n}} v_{i3} \quad (209)L$$

and "erfc" is the complementary error function.

For perpendicular electric and magnetic fields, the solution is given by

$$f_i = n_i \left( \frac{m_i}{2\pi k T_n} \right)^{3/2} \exp \left\{ -\frac{m_i}{2k T_n} [(v_{i1} - u_E)^2 + v_{i2}^2 + v_{i3}^2 + u_E^2] \right\} \\ \cdot \alpha \int_0^{\infty} dn e^{-\alpha n} \exp \left\{ -\frac{m_i}{2k T_n} [2u_E (v_{i1} - u_E) \cos n - 2u_E v_{i2} \sin n] \right\} \quad (210)T$$

where

$$\alpha = \frac{v_i m_i c}{e_i B} \quad (211)T$$

$$u_E = \frac{E \perp c}{B} \quad (212)T$$

Equation (210) is consistent with the results given by St.-Maurice and Schunk (1973), and by Whealton and Woo (1972) for the case of  $\underline{B} = 0$ .

### 1.2. Expansion based on a Maxwellian distribution

According to Grad (1958),  $f_i$  can be expanded about a zeroth-order function  $f_i^{(0)}$  as follows

$$f_i = f_i^{(0)} \sum_{\gamma} a_{\gamma}(\underline{r}) M_{\gamma}(\underline{r}, \underline{c}_i) \quad (213)$$

where  $f_i^{(0)}$  is chosen to represent a local Maxwellian distribution function

$$f_i^{(0)} = n_i \left( \frac{m_i}{2\pi k T_i} \right)^{3/2} \exp \left[ -\frac{m_i c_i^2}{2k T_i} \right], \quad (214)$$

$M_{\gamma}$ 's are a set of complete orthogonal polynomials,  $a_{\gamma}$ 's are the expansion coefficients, and the subscript  $\gamma$  is used to indicate that the summation is generally over more than one variables. In equations (213) and (214)  $\underline{c}_i$  is the random ion velocity and  $T_i$  is the ion temperature, defined below.

The expansion is truncated by setting all expansion coefficients of order higher than some value to zero, and the remaining set of coefficients are found in terms of the lower-order moments of the distribution function, such as

$$\underline{u}_i = \langle \underline{v}_i \rangle \quad (\text{Bulk drift velocity}) \quad (215)$$

$$\underline{P}_i = n_i m_i \langle \underline{c}_i \underline{c}_i \rangle \quad (\text{Pressure tensor}) \quad (216)$$

$$p_i = \frac{1}{3} n_i m_i \langle c_i^2 \rangle \quad (\text{Pressure}) \quad (217)$$

$$\underline{\tau}_i = \underline{P}_i - p_i \underline{I} \quad (\text{Stress tensor}) \quad (218)$$

$$\underline{Q}_i = n_i m_i \langle \underline{c}_i c_i c_i \rangle \quad (\text{Heat flow tensor}) \quad (219)$$

$$\underline{q}_i = \frac{1}{2} n_i m_i \langle c_i^2 \underline{c}_i \rangle \quad (\text{Heat flow vector}) \quad (220)$$

In the above equations, the angle brackets denote the average in velocity space, and  $\underline{c}_i$  is defined as

$$\underline{c}_i = \underline{v}_i - \underline{u}_i \quad (221)$$

Within Grad's formulation, various levels of approximations (such as 5-, 13-, and 20-moment approximation) are possible depending upon the number of terms retained in the series expansion for the distribution function.

The 5-moment approximation. At this level of approximation the species distribution function is assumed to be represented adequately by the first term in the series expansion, that is, by the Maxwellian given in equation (214).

To find the equations which govern the relevant moments, we multiply equation (201) by 1,  $m_i \underline{c}_i$  and  $m_i c_i^2/2$  and integrate over velocity space.

These 'moment equations' are

Continuity

$$0 = 0 \quad (222)$$

Momentum

$$- n_i e_i \left( \underline{E} + \frac{1}{c} \underline{u}_i \times \underline{B} \right) = - \underline{v}_i n_i m_i \underline{u}_i \quad (223)$$

Energy

$$0 = -v_i \left[ \frac{3}{2} n_i k (T_i - T_n) - \frac{1}{2} n_i m_i u_i^2 \right] \quad (224)$$

Solving equations (222) - (224) for the required moments, we get

$$\underline{u}_i = u_d \underline{e}_3 \quad (225)L$$

$$T_i = T_n + \frac{1}{3} \left( \frac{m_i}{k} \right) u_d^2 \quad (226)L$$

for parallel electric and magnetic fields and

$$\underline{u}_i = \frac{u_E}{1 + \alpha} (\underline{e}_1 + \alpha \underline{e}_2) \quad (227)T$$

$$T_i = T_n + \frac{1}{3} \left( \frac{m_i}{k} \right) \frac{u_E^2}{1 + \alpha} \quad (228)T$$

for perpendicular electric and magnetic fields.

Alternatively, the relations (225)-(228), as well as all of the moments in this section, may be found by taking the proper velocity moments of the exact distribution functions given in equations (207) and (210). In practice, however, series expansions are needed only when exact solutions are not available, and therefore, in general it is necessary to obtain the velocity moments from the appropriate moment equations.

The 13-moment approximation. The level of approximation that properly accounts for the stress tensor and heat flow vector is the 13-moments approximation. For this approximation, the ion distribution function takes the form

$$f_i = f_i^{(0)} \left[ 1 + \frac{m_i}{2kT_i p_i} \underline{r}_i \cdot \underline{c}_i \underline{c}_i - \left( 1 - \frac{m_i c_i^2}{5kT_i} \right) \frac{m_i}{kT_i p_i} \underline{q}_i \cdot \underline{c}_i \right] \quad (229)$$

where  $f_i^{(0)}$  is defined in equation (214).

The corresponding set of moment equations is (222) - (224) in addition to the following equations:

Stress

$$\frac{e_i}{m_i c} (\underline{B} \times \underline{\tau}_i - \underline{\tau}_i \times \underline{B}) = -v_i \left[ \underline{\tau}_i - n_i m_i (\underline{u}_i \underline{u}_i - \frac{1}{3} u_i^2 \underline{I}) \right] \quad (230)$$

Heat flow

$$\begin{aligned} -\frac{e_i}{m_i} \left( \underline{E} + \frac{1}{c} \underline{u}_i \times \underline{B} \right) \cdot \left( \underline{\tau}_i + \frac{5}{2} p_i \underline{I} \right) - \frac{e_i}{m_i c} \underline{q}_i \times \underline{B} = \\ = -v_i \left[ \underline{q}_i + \frac{5}{2} n_i^k T_n \underline{u}_i + \frac{1}{2} n_i m_i u_i^2 \underline{u}_i \right] \end{aligned} \quad (231)$$

which can be solved for the relevant set of moments.

For the case of parallel fields, the required moments are given by (225), (226), and

$$\underline{\tau}_i = n_i m_i u_d^2 (3 \underline{e}_3 \underline{e}_3 - \underline{I}) \quad (232)$$

$$\underline{q}_i = n_i m_i u_d^3 \underline{e}_3 \quad (233) \text{L}$$

while for the case of perpendicular fields they are given by (227), (233) and

$$(\underline{\tau}_i)_{11} = \frac{1}{3} n_i m_i u_d^2 \frac{2 + 10 \alpha^2 - \alpha^4}{(1 + \alpha^2)^2 (4 + \alpha^2)} \quad (234) \text{T}$$

$$(\underline{\tau}_i)_{22} = \frac{1}{3} n_i m_i u_d^2 \frac{2 - 5 \alpha^2 + 2 \alpha^4}{(1 + \alpha^2)^2 (4 + \alpha^2)} \quad (235) \text{T}$$



$$(\underline{\tau}_i)_{33} = -\frac{1}{3} n_i m_i u_E^2 \frac{1}{(1 + \alpha^2)} \quad (236)T$$

$$(\underline{\tau}_i)_{12} = (\underline{\tau}_i)_{21} = n_i m_i u_E^2 \frac{\alpha (2\alpha^2 - 1)}{(1 + \alpha^2)^2 (4 + \alpha^2)} \quad (237)T$$

$$(\underline{\tau}_i)_{13} = (\underline{\tau}_i)_{31} = (\underline{\tau}_i)_{23} = (\underline{\tau}_i)_{32} = 0 \quad (238)T$$

$$\underline{q}_i = n_i m_i u_E^3 \frac{\alpha}{(1 + \alpha^2)^2 (4 + \alpha^2)} [3\alpha \underline{e}_1 + (\alpha^2 - 2)\underline{e}_2] \quad (239)T$$

The 20-moment approximation. At this level of approximation the ion heat flow tensor is properly accounted for. The ion distribution function takes the form

$$f_i = f_i^{(0)} \left\{ 1 + \left[ \frac{m_i}{2kT_i p_i} \right] \underline{\tau}_i : \underline{c}_i \underline{c}_i + \left[ \frac{m_i^2}{6k^2 T_i^2 p_i} \right] \underline{Q}_i : \underline{c}_i \underline{c}_i \underline{c}_i - \left[ \frac{m_i}{kT_i p_i} \right] \underline{q}_i \cdot \underline{c}_i \right\} \quad (240)$$

The moment equations that are associated with this distribution function are (222) - (224), (230) and

$$-3 \frac{e_i}{m_i} \left[ \left( \underline{E} + \frac{1}{c} \underline{u}_i \times \underline{B} \right) \underline{P}_i \right]^s + 3 \frac{e_i}{m_i c} (\underline{B} \times \underline{Q}_i)^s = -\underline{v}_i \left[ \underline{Q}_i + 3 n_i k T_n (\underline{u}_i \underline{I})^s + n_i m_i \underline{u}_i \underline{u}_i \underline{u}_i \right] \quad (241)$$

where the superscript "s" denotes that the tensor is symmetrized (e.g.)

$$(\underline{A}^s)_{\alpha\beta} = \frac{1}{2} (A_{\alpha\beta} + A_{\beta\alpha})$$

$$(\underline{A}^s)_{\alpha\beta\gamma} = \frac{1}{6} (A_{\alpha\beta\gamma} + A_{\alpha\gamma\beta} + A_{\beta\alpha\gamma} + A_{\gamma\alpha\beta} + A_{\beta\gamma\alpha} + A_{\gamma\beta\alpha})$$

The resulting velocity moments are similar to those of the 13-moment approximation, except for

$$\underline{Q}_i = 2n_i m_i u_i^3 \underline{e}_3 \underline{e}_3 \underline{e}_3 \quad (242)L$$

and

$$(\underline{Q}_i)_{111} = n_i m_i u_i^3 \frac{26\alpha^2 + 74\alpha^4}{(1 + \alpha^2)^3 (4 + \alpha^2) (9 + \alpha^2)} \quad (243)T$$

$$(\underline{Q}_i)_{112} = n_i m_i u_i^3 \frac{-6 - 34\alpha^2 + 20\alpha^4}{(1 + \alpha^2)^3 (4 + \alpha^2) (9 + \alpha^2)} \quad (244)T$$

$$(\underline{Q}_i)_{122} = n_i m_i u_i^3 \frac{28\alpha^2 - 14\alpha^4 + 6\alpha^6}{(1 + \alpha^2)^3 (4 + \alpha^2) (9 + \alpha^2)} \quad (245)T$$

$$(\underline{Q}_i)_{222} = n_i m_i u_i^3 \frac{-30\alpha + 12\alpha^3 - 4\alpha^4 + 2\alpha^6}{(1 + \alpha^2)^3 (4 + \alpha^2) (9 + \alpha^2)} \quad (246)T$$

$$(\underline{Q}_i)_{113} = (\underline{Q}_i)_{123} = (\underline{Q}_i)_{223} = (\underline{Q}_i)_{133} = (\underline{Q}_i)_{233} = (\underline{Q}_i)_{333} = 0 \quad (247)T$$

and  $\underline{Q}_i$  is symmetric with respect to a change in any two coordinate indices (e.g.  $(\underline{Q}_i)_{\alpha\beta\gamma} = (\underline{Q}_i)_{\alpha\gamma\beta}$ )

### 1.3. Expansion based on a bi-Maxwellian distribution

With regard to anisotropic plasmas, Grad's approximations have limited applicability because they cannot be used to describe distribution functions that are characterized by large temperature anisotropies. These cases are better described by expanding the distribution function about a two-temperature (or bi-Maxwellian) zeroth-order distribution function.

Following a line parallel to that in subsection (1.2), the ion distribution function is expanded about a bi-Maxwellian function. Then, the expansion coefficients, of order higher than some value, are set to zero. The remaining coefficients are found in terms of the lower-order moments, e.g.,

$$\underline{u}_i = \langle v_i \rangle \quad (\text{Bulk drift velocity}) \quad (248)$$

$$\underline{P}_i = n_i m_i \langle \underline{c}_i \underline{c}_i \rangle \quad (\text{Pressure tensor}) \quad (249)$$

$$p_{i\parallel} = n_i m_i \langle c_{i\parallel}^2 \rangle \quad (\text{Parallel pressure}) \quad (250)$$

$$p_{i\perp} = \frac{1}{2} n_i m_i \langle c_{i\perp}^2 \rangle \quad (\text{Perpendicular pressure}) \quad (251)$$

$$\underline{\tau}_i' = \underline{P}_i - p_i \underline{I} - (p_{i\parallel} - p_{i\perp}) \underline{e}_z \underline{e}_z \quad (\text{Stress tensor}) \quad (252)$$

$$\underline{q}_i^{\parallel} = n_i m_i \langle c_{i\parallel}^2 \underline{c}_i \rangle \quad (\text{Heat flow vector for parallel energy}) \quad (253)$$

$$\underline{q}_i^{\perp} = \frac{1}{2} n_i m_i \langle c_{i\perp}^2 \underline{c}_i \rangle \quad (\text{Heat flow vector for perpendicular energy}) \quad (254)$$

where the prime on  $\underline{\tau}_i'$  is used to distinguish the two definitions given in equations (218) and (252).

Various levels of approximations (such as 6- and 16- moment approximations) can be obtained depending on the number of terms retained in the series expansion of the distribution function.

The 6-moment approximation. In this case the approximate expression for the ion distribution function takes the form

$$f_i = f_i^{(b)} = n_i (2\pi)^{-3/2} \beta_{\perp} (\beta_{\parallel})^{1/2} \exp\left(-\frac{1}{2} \beta_{\perp} c_{i\perp}^2 - \frac{1}{2} \beta_{\parallel} c_{i\parallel}^2\right) \quad (255)$$

where

$$\beta_{\parallel} = \frac{m_i}{k T_{i\parallel}} \quad (256)$$

$$\beta_{\perp} = \frac{m_i}{k T_{i\perp}} \quad (257)$$

The required moment equations are (222), (223) and ;

Parallel energy

$$0 = -v_i \left[ n_i k (T_{i\parallel} - T_n) - n_i m_i u_{i\parallel}^2 \right] \quad (258)$$

Perpendicular energy

$$0 = -v_i \left[ n_i k (T_{i\perp} - T_n) - \frac{1}{2} n_i m_i u_{i\perp}^2 \right] \quad (259)$$

The moments, found by solving this set of equations, are given by equations (225) and

$$T_{i\parallel} = T_n + \left( \frac{m_i}{k} \right) u_d^2 \quad (260)L$$

$$T_{i\perp} = T_n \quad (261)L$$

when the electric field is parallel to the magnetic field, and by equations (227) and

$$T_{i\parallel} = T_n \quad (262)T$$

$$T_{i\perp} = T_n + \frac{1}{2} \frac{m_i}{k} \frac{u_E^2}{1 + \alpha^2} \quad (263)T$$

when the electric field is perpendicular to the magnetic field.

The 16-moment approximation. For the 16-moment approximation, the ion distribution function takes the form

$$f_i = f_i^{(b)} [1 + \phi_i] \quad (264)$$

where  $f_i^{(b)}$  is defined in equation (255) and  $\phi_i$  is given by

$$\begin{aligned} \phi_i = & \frac{\beta_{\perp}}{2n_i m_i} \left[ \beta_{\perp} (c_{i1}^2 - c_{i2}^2) (\tau_i' : e_1 e_1) + 2\beta_{\perp} (\tau_i' : e_1 e_2) c_{i1} c_{i2} + 2\beta_{\parallel} \tau_i' : c_i c_{i\parallel} \right] \\ & - \frac{\beta_{\perp}^2}{n_i m_i} \left( 1 - \frac{\beta_{\perp} c_{i\perp}^2}{4} \right) \underline{q}_i \cdot c_{i\perp} - \frac{\beta_{\perp} \beta_{\parallel}}{n_i m_i} \left( 1 - \frac{\beta_{\perp} c_{i\perp}^2}{2} \right) \underline{q}_i \cdot c_{i\parallel} - \frac{\beta_{\parallel}^2}{2n_i m_i} \\ & \left( 1 - \frac{\beta_{\parallel} c_{i\parallel}^2}{3} \right) \underline{q}_i \cdot c_{i\parallel} - \frac{\beta_{\perp} \beta_{\parallel}}{2n_i m_i} \left( 1 - \beta_{\parallel} c_{i\parallel}^2 \right) \underline{q}_i \cdot c_{i\perp} \end{aligned} \quad (265)$$

The corresponding moment equations are (222), (223), (258), (259)

and

Stress tensor

$$\frac{e_i}{m_i c} (\underline{B} \times \underline{\tau}'_i - \underline{\tau}'_i \times \underline{B}) = -v_i [\underline{\tau}'_i - \frac{u_i u_i}{c} + \frac{u_{i3} u_{i3}}{c} + \frac{1}{2} u_{i\perp}^2 (\underline{I} - e_3 e_3)] \quad (266)$$

Parallel heat flow

$$\begin{aligned} \frac{e_i}{m_i c} \underline{B} \times \underline{q}_i^{\parallel} - \frac{e_i}{m_i} (\underline{E} + \frac{1}{c} \underline{u}_i \times \underline{B}) \cdot [p_{i\parallel} \underline{I} + 2e_3 e_3 \cdot (\underline{\tau}'_i + p_{i\parallel} \underline{I})] = \\ = -v_i [q_i^{\parallel} + 2n_i kT_{n-i3} + n_i kT_{n-i} + n_i m_i u_{i3}^2 u_i] \end{aligned} \quad (267)$$

Perpendicular heat flow

$$\begin{aligned} \frac{e_i}{m_i c} \underline{B} \times \underline{q}_i^{\perp} - \frac{e_i}{m_i} (\underline{E} + \frac{1}{c} \underline{u}_i \times \underline{B}) \cdot [p_{i\perp} \underline{I} + (\underline{I} - e_3 e_3) \cdot (\underline{\tau}'_i + p_{i\perp} \underline{I})] = \\ = -v_i [q_i^{\perp} + n_i kT_{n-i\perp} + n_i kT_{n-i} + \frac{1}{2} n_i m_i u_{i\perp}^2 u_i] \end{aligned} \quad (268)$$

For the case of parallel electric and magnetic fields, the velocity moments that are obtained from these equations are given by (225), (260), (261) and

$$\underline{\tau}'_i = 0 \quad (269)L$$

$$\underline{q}_i^{\parallel} = 2 n_i m_i u_d^3 e_3 \quad (270)L$$

$$\underline{q}_i^{\perp} = 0 \quad (271)L$$

while for perpendicular electric and magnetic fields they are given by equations (227), (262), (263) and

$$(\underline{\tau}'_i)_{11} = -(\underline{\tau}'_i)_{22} = n_i m_i u_E^2 \frac{\alpha^2 (5 - \alpha^2)}{2(1 + \alpha^2)^2 (4 + \alpha^2)} \quad (272)T$$

$$(\underline{\tau}'_i)_{12} = (\underline{\tau}'_i)_{21} = n_i m_i u_E^2 \frac{\alpha (2\alpha^2 - 1)}{(1 + \alpha^2)^2 (4 + \alpha^2)} \quad (273)T$$

$$(\underline{\tau}'_i)_{33} = (\underline{\tau}'_i)_{13} = (\underline{\tau}'_i)_{31} = (\underline{\tau}'_i)_{23} = (\underline{\tau}'_i)_{32} = 0 \quad (274)T$$

$$\underline{a}_i^i = 0 \quad (275) \text{T}$$

$$\underline{a}_i^1 = n_i m_i u_E^3 \frac{\alpha}{(1 + \alpha^2)^2 (4 + \alpha^2)} [3\alpha \underline{e}_1 + (\alpha^2 - 2) \underline{e}_2] \quad (276) \text{T}$$

## 2. Comparison of transport equations

In this section I compare different series expansions of the ion distribution function. These expansions fall into two categories; Maxwellian-based and bi-Maxwellian-based expansions. The Maxwellian-based expansions, which depend on the technique developed by Grad (1949), include the 5-moment, the 13-moment and the 20-moment approximations. The 5-moment approximation assumes that the distribution function can be represented by the local Maxwellian given by equation (214). This level of approximation only accounts for the bulk drift velocity  $\underline{u}_i$  and temperature  $T_i$ , which are given by equations (225) and (226) for the case of parallel electric and magnetic fields, or equations (227) and (228) for the case of perpendicular fields. In the 13-moment approximation, the expression for the ion distribution function contains a local Maxwellian term in addition to correction terms proportional to the stress tensor  $\underline{\tau}_i$  and the heat flow vector  $\underline{q}_i$ . These corrections allow for temperature anisotropy and asymmetry in the distribution function. At this level of approximation the appropriate expression for the distribution function is given by equation (229) and the relevant moments are given by equations (225), (226), (232), and (233) for the case of parallel fields or equations (227), (228), and (234) - (239) for the case of perpendicular fields. The 20-moment approximation accounts for the heat flow more accurately because it represents the heat flow by a tensor  $\underline{Q}_i$  instead of the vector  $\underline{q}_i$  used in the 13-moment approximation. At this level, the ion distribution function is given by equation (240) and the moments that enter into this

expression are given by equations (225), (226), (232), and (242) for parallel electric and magnetic fields and by equations (227), (228), (234) - (238), and (243) - (247) for perpendicular fields.

The bi-Maxwellian-based expansions include the 6-moment and the 16-moment approximations. The 6-moment approximation represents the ion distribution function by a local bi-Maxwellian (255). It accounts only for the bulk drift velocity  $\underline{u}_i$ , parallel temperature  $T_{i\parallel}$  and perpendicular temperature  $T_{i\perp}$ , which are given by equations (225), (260), and (261) for parallel electric and magnetic fields or by equations (227), (262), and (263) for perpendicular fields. The 16-moment approximation contains, in addition to the local bi-Maxwellian term, corrections proportional to the stress tensor  $\underline{\tau}'_i$  and the heat flow vectors for parallel and perpendicular energy  $q_i^{\parallel}$  and  $q_i^{\perp}$ . For this approximation, the distribution function is given by equations (255), (264), and (265) and the relevant moments are given by equations (225), (260), (261), and (269) - (271) or by equations (227), (262), (263), and (272) - (276) for the case of parallel or perpendicular fields, respectively. Since the approximations based on a bi-Maxwellian are found by expanding about an anisotropic function, they are expected to handle large anisotropies better than those based on a Maxwellian.

In the following subsections, the different levels of approximation are compared among themselves and with the closed form solution. I consider a wide range of conditions; that is, both parallel and perpendicular electric and magnetic fields, and different values for the electric field and for the collision-to-cyclotron frequency ratio. The different conditions produce a range of non-Maxwellian characteristics.



The comparison of the different expressions for the ion distribution function is shown in Figures 3 to 12, which are obtained as follows. The relevant moments are computed and the distribution function in the required plane is found by substituting for the moments and taking the component of the random velocity perpendicular to this plane equal to zero. Finally, the distribution function is represented by contours at levels decreasing by a factor of  $e^{1/2}$  starting from the maximum.

### 2.1. Parallel electric and magnetic fields

Figure 3 shows a comparison between different expansions based on a Maxwellian; namely, the 5-moment, 13-moment and 20-moment approximations. As mentioned earlier, the 5-moment approximation only accounts for the bulk drift velocity  $\underline{u}_i$  and the temperature  $T_i$ . As the electric field strength increases, both  $\underline{u}_i$  and  $T_i$  increase. However, the increase in the bulk drift velocity does not show up because the contours are plotted against the ion random velocity  $\underline{c}_i$ . The 13-moment approximation allows for anisotropic and asymmetric features through corrections proportional to the stress tensor and the heat flow vector. As the electric field strength increases, these correction terms increase. At moderate and high electric field strengths ( $D_{||} = 1$  and 3), the distribution function differs significantly from that for the 5-moment approximation, where  $D_{||} [\equiv (e_i E_{||} / m_i v_i) / (2kT_n / m_i)^{1/2}]$  is the normalized drift velocity. The 20-moment approximation is similar to the 13-moment approximation, however, it describes the heat flow better through the tensor  $\underline{Q}_i$ . For intermediate and high values of  $E_{||}$ , the

Figure 3. Contours of the ion distribution function in the principal velocity plane parallel to the electric field for the Maxwellian-based expansions and for parallel electric and magnetic fields. Three series expansions are shown, including the 5-moment (top row), the 13-moment (middle row), and the 20-moment (bottom row). In addition, three values of the normalized parallel drift velocity were considered;  $D_{\parallel} = 0.3$  (left column), 1.0 (middle column), and 3.0 (right column), where  $D_{\parallel} = (e_i E / m_i v_i) / (2kT_n / m_i)^{1/2}$ . The contours are plotted against the normalized random velocity  $c_i / (2kT_n / m_i)^{1/2}$ . The contour levels decrease by a factor of  $e^{1/2}$  starting from the maximum, shown by the dot. Contour numbers have been omitted whenever they are obvious.

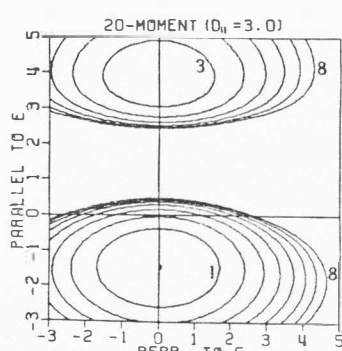
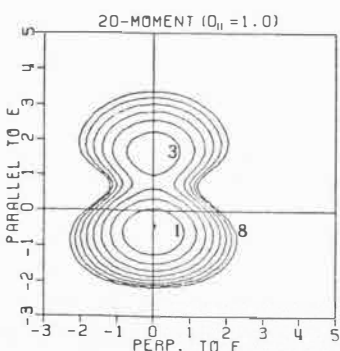
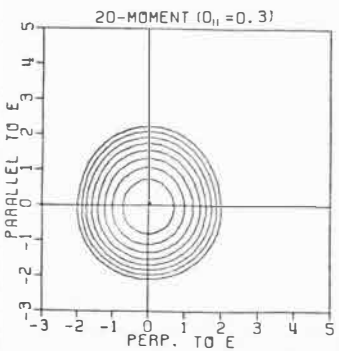
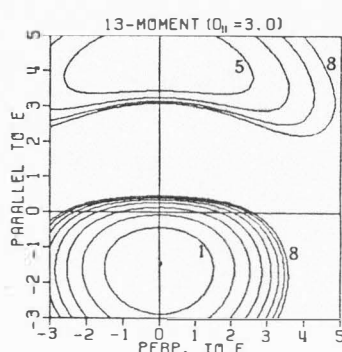
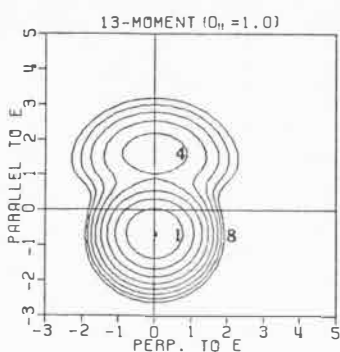
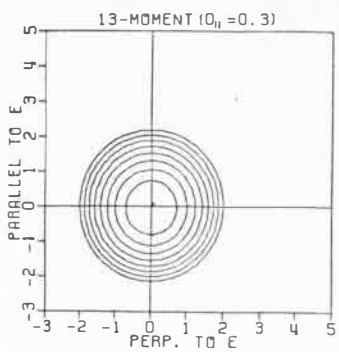
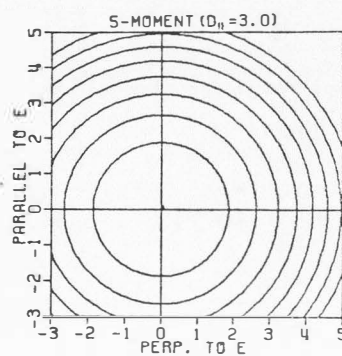
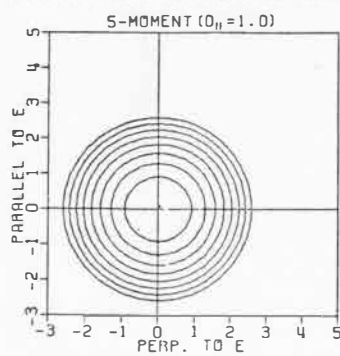
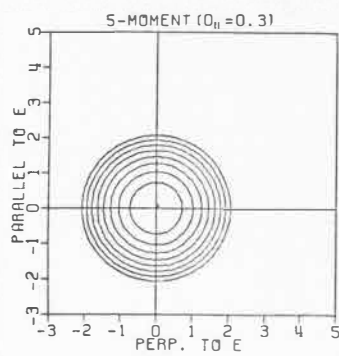


Figure 4. Contours of the ion distribution function in the principal velocity plane parallel to the electric field for the bi-Maxwellian-based expansions and for parallel electric and magnetic fields. Two expansions are shown, including the 6-moment (top row) and 16-moment (bottom row). In addition, three values of the normalized parallel drift velocity were considered;  $D_{\parallel} = 0.3$  (left column), 1.0 (middle column), and 3.0 (right column), where  $D_{\parallel} = (e_i E / m_i v_i) / (2kT_n / m_i)^{1/2}$ . The plotting format is the same as that for Figure 3.

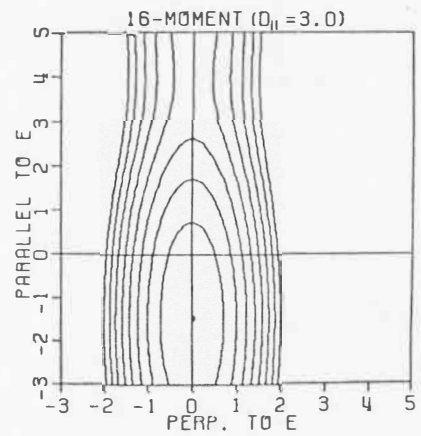
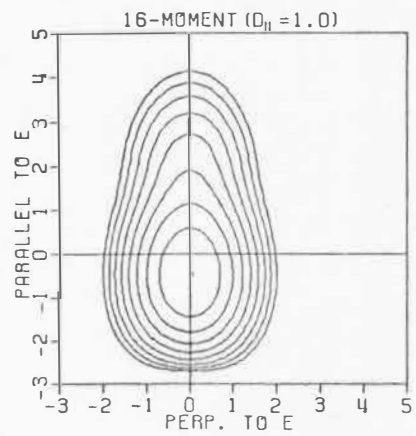
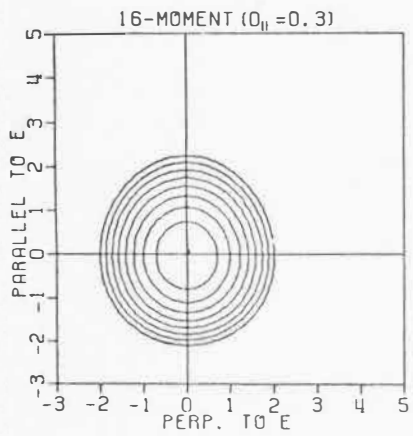
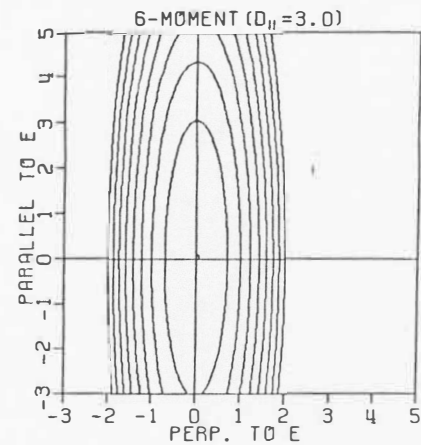
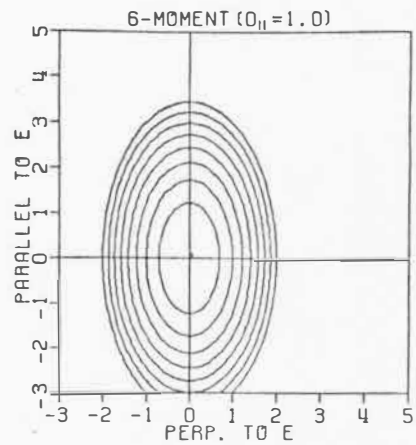
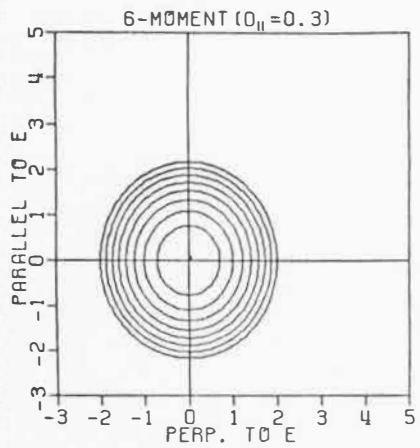


Figure 5. Comparison of the exact form with the 15-moment and the 20-moment expansions for the ion distribution function in the principal velocity plane parallel to the electric field for the case of parallel electric and magnetic fields. Three values of the normalized parallel drift velocity were considered,  $D_{||} = 0.3$  (left column), 1.0 (middle column) and 3.0 (right column), where  $D_{||} = (e_i E / m_i v_i) / (2kT_n / m_i)^{1/2}$ . The plotting format is the same as that for Figure 3.

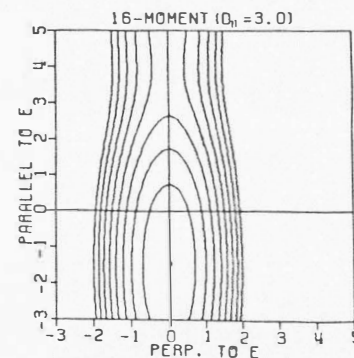
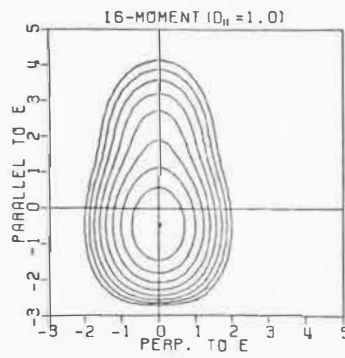
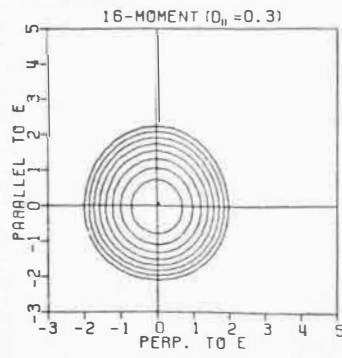
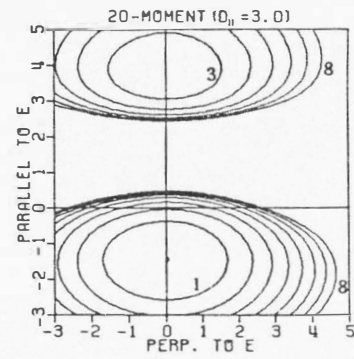
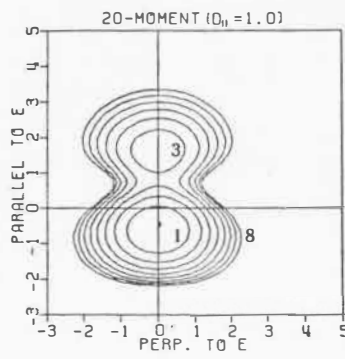
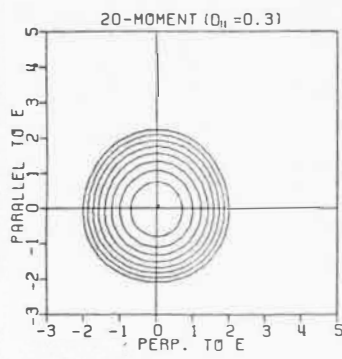
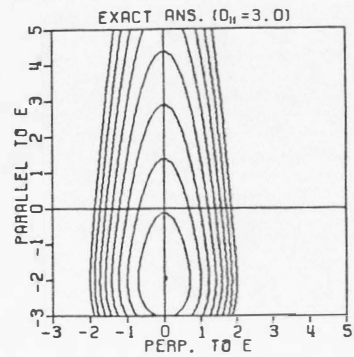
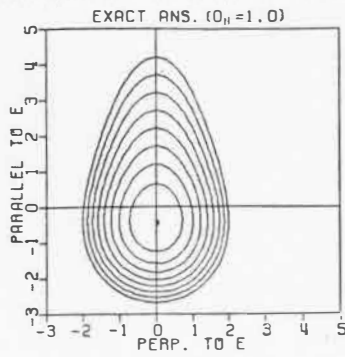
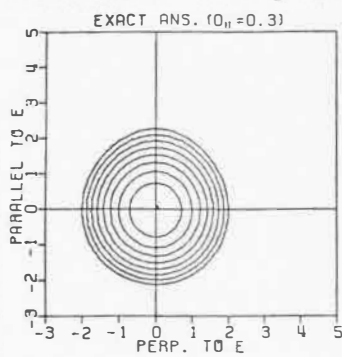


Figure 6. Contours of the exact ion distribution function in the principal velocity ( $\underline{E}-\underline{E} \times \underline{B}$ ) plane for the case of perpendicular electric and magnetic fields. Three values of the collision-to-gyro frequency ratio were used;  $\alpha = 0.1$  (bottom row), 1.0 (middle row), and 10 (top row), where  $\alpha = v_i m_i c / e_i B$ . In addition, three values of the normalized perpendicular drift velocity were considered;  $D_{\perp} = 0.3$  (left column), 1.0 (middle column), and 3.0 (right column), where  $D_{\perp} = (c E_{\perp} / B) / (2 k T_n / m_i)^{1/2}$ . The plotting format is the same as that for Figure 3.



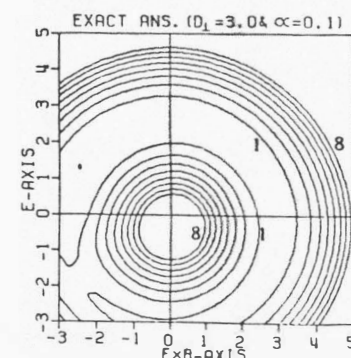
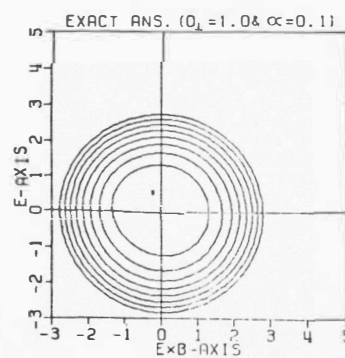
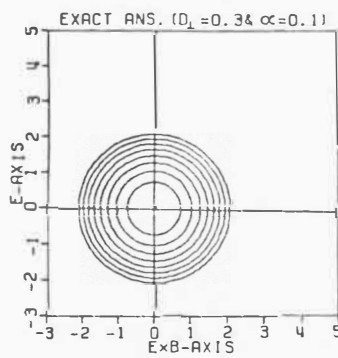
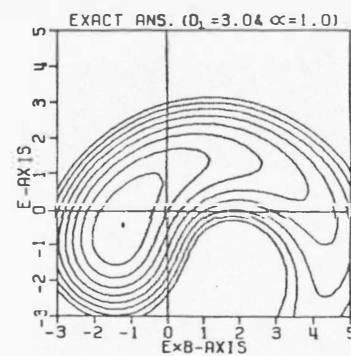
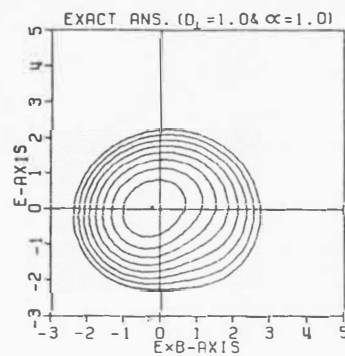
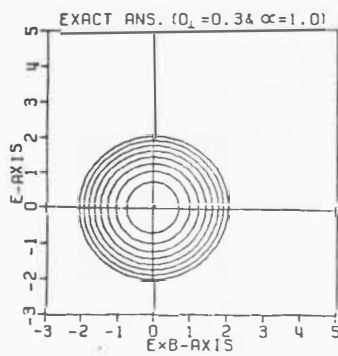
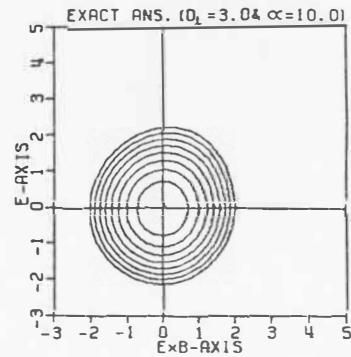
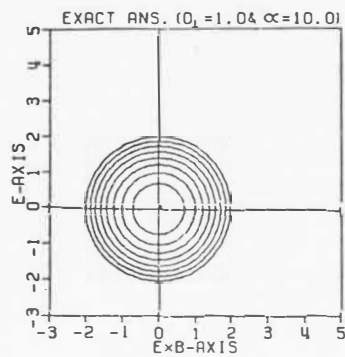
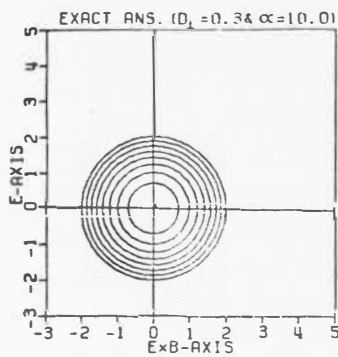


Figure 7. Contours of the ion distribution function in the principal velocity ( $\underline{B}-\underline{E}\times\underline{B}$ ) plane for the exact form and the Maxwellian-based expansions and for perpendicular electric and magnetic fields. The exact form (top row) is compared with the 5-moment (second row), the 13-moment (third row), and the 20-moment (bottom row) expansions. In addition, three combinations of  $D_{\perp}$  and  $\alpha$  were considered; [ $D_{\perp}=1.0, \alpha=0.1$ ] (left column), [ $D_{\perp}=1.0, \alpha=1.0$ ] (middle column), and [ $D_{\perp}=3.0, \alpha=1.0$ ] (right column), where  $D_{\perp}=(cE_{\perp}/B)/(2kT_n/m_i)^{1/2}$  and  $\alpha=v_i m_i c/e_i B$ . The plotting format is the same as that for Figure 3.

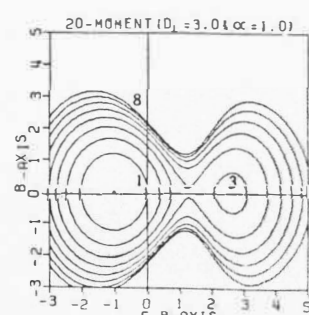
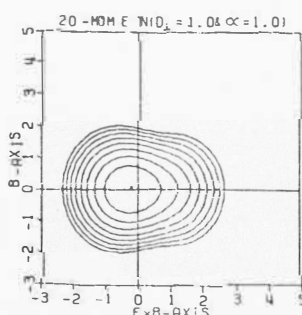
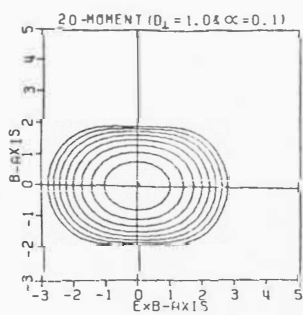
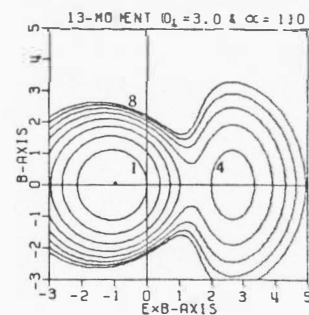
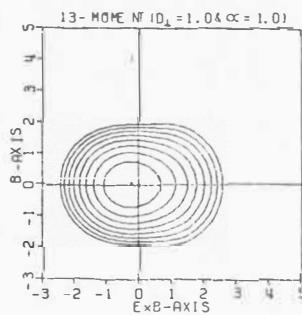
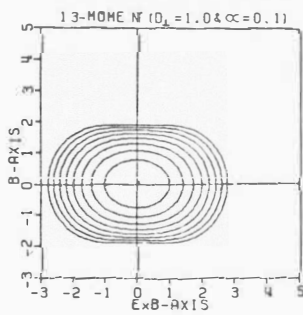
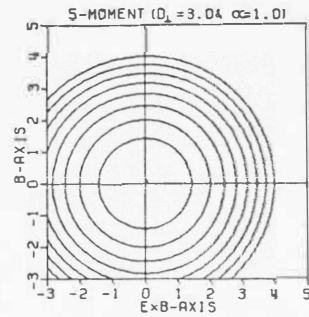
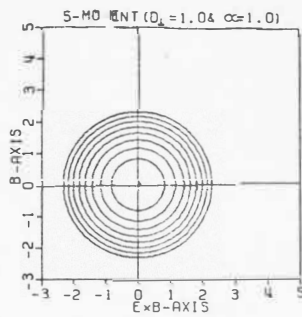
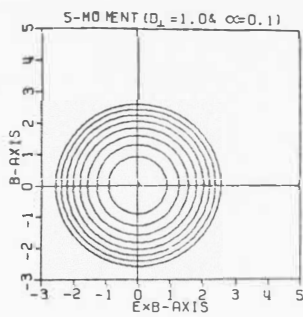
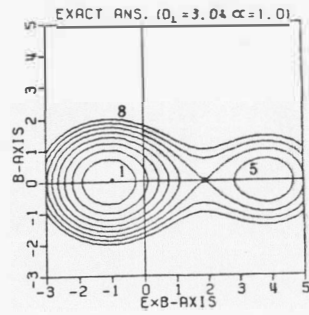
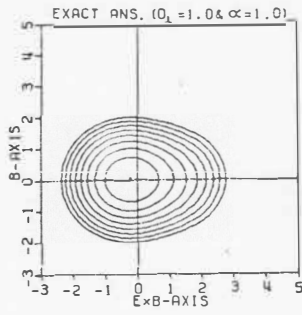
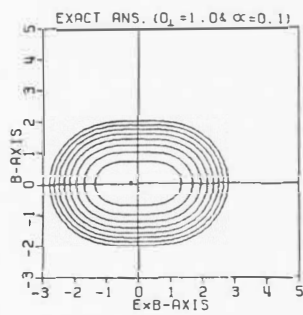


Figure 8. Contours of the ion distribution function in the principal velocity ( $\underline{B}-\underline{E} \times \underline{B}$ )-plane for the exact form and the bi-Maxwellian-based expansions and for perpendicular electric and magnetic fields. The exact form (top row) is compared with the 6-moment (middle row) and the 16-moment (bottom row) expansions. In addition, three combinations of  $D_{\perp}$  and  $\alpha$  were considered; [ $D_{\perp} = 1.0, \alpha = 0.1$ ] (left column), [ $D_{\perp} = 1.0, \alpha = 1.0$ ] (middle column), and [ $D_{\perp} = 3.0, \alpha = 1.0$ ] (right column), where  $D_{\perp} = (cE_{\perp}/B)/(2kT_n/m_i)^{1/2}$  and  $\alpha = v_i m_i c / e_i B$ . The plotting format is the same as that for Figure 3.

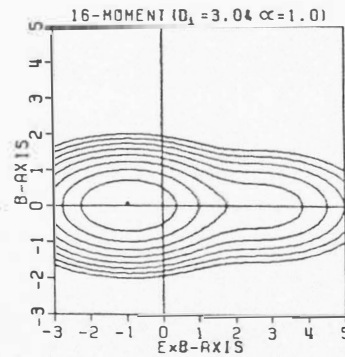
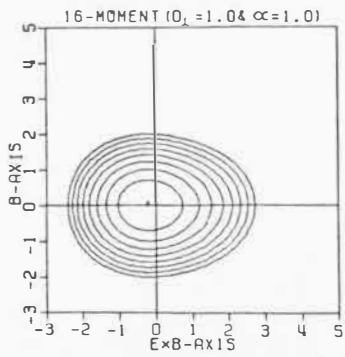
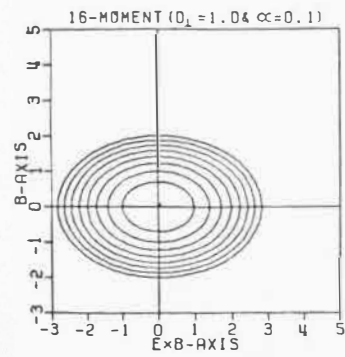
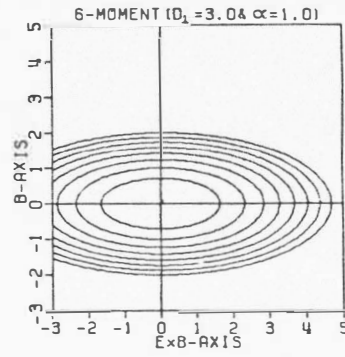
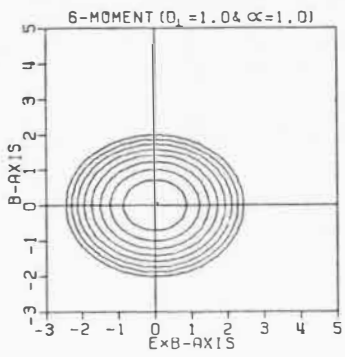
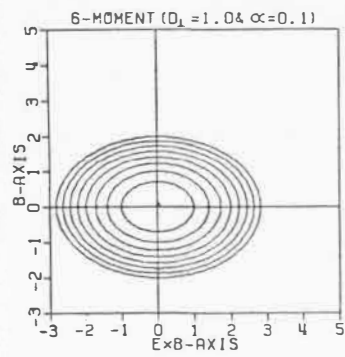
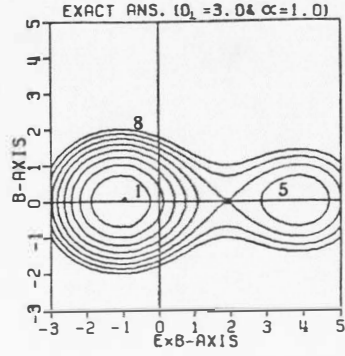
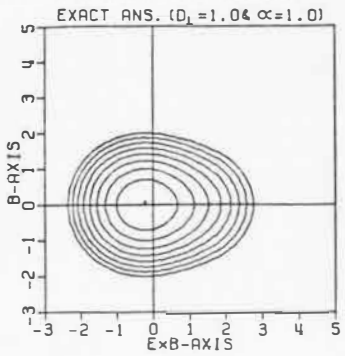
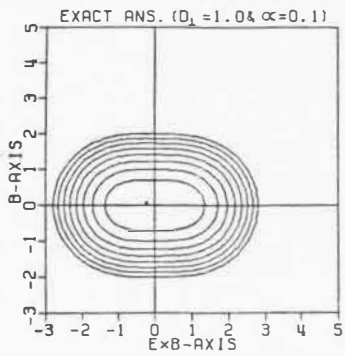


Figure 9. Comparison of the exact form with the 16-moment and the 20-moment expansions of the ion distribution function for the case of perpendicular electric and magnetic fields and for  $D_{\perp} = 1.0$  and  $\alpha = 0.1$ . The contours are plotted in the three principal velocity planes. The plotting format is the same as that for Figure 3.

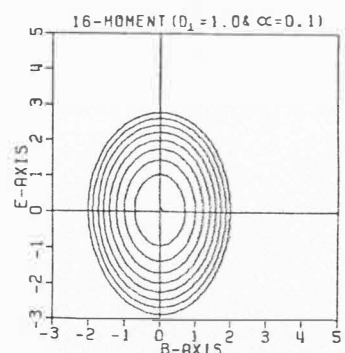
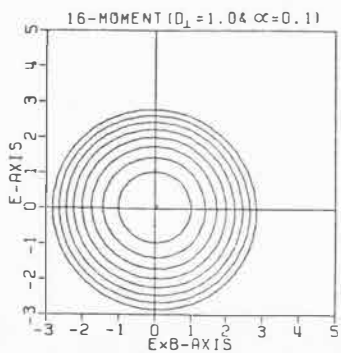
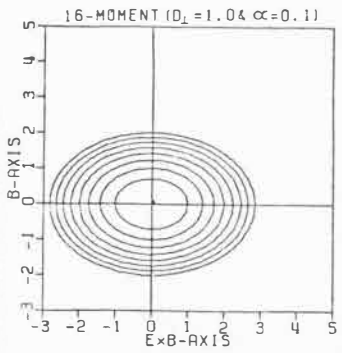
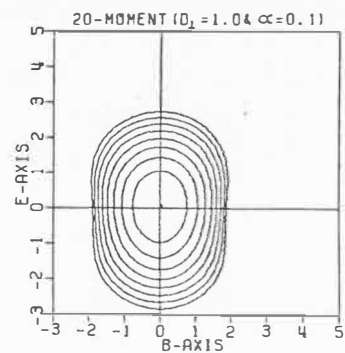
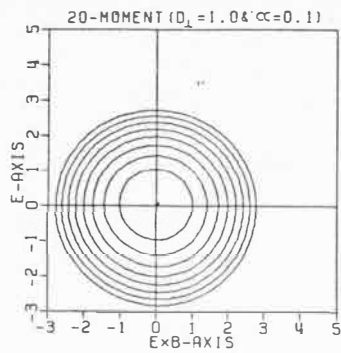
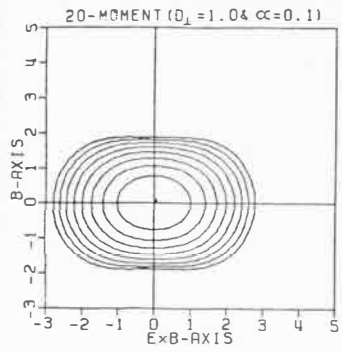
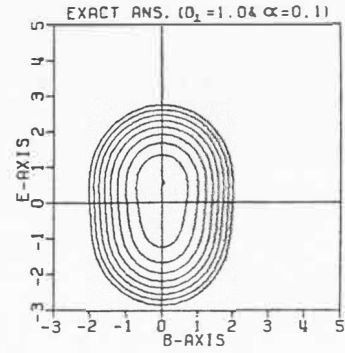
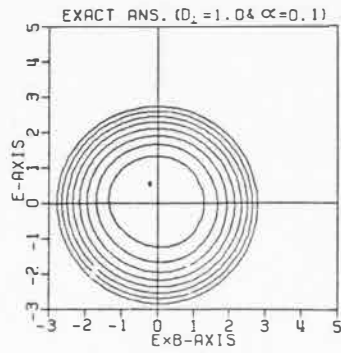
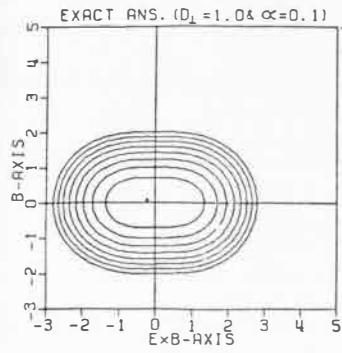


Figure 10. Comparison of the exact form with the 16-moment and the 20-moment expansions of the ion distribution function for the case of perpendicular electric and magnetic fields and for  $D_{\perp} = 1.0$  and  $\alpha = 1.0$ . The contours are plotted in the three principal velocity planes. The plotting format is the same as that for Figure 3.



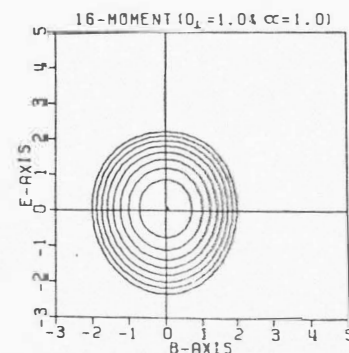
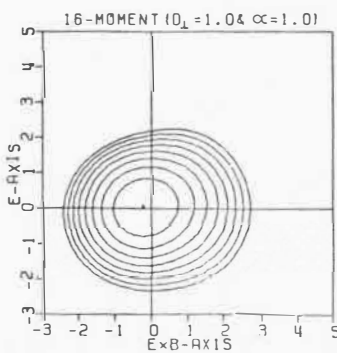
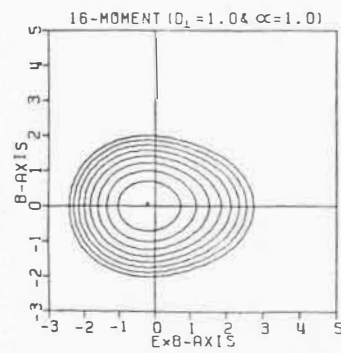
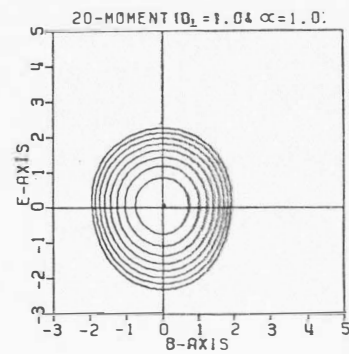
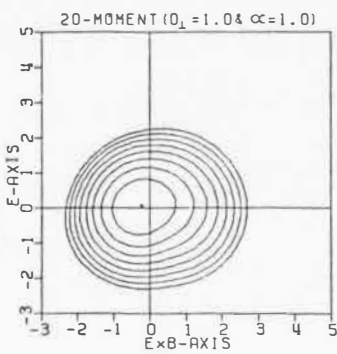
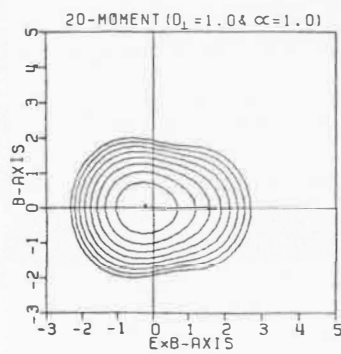
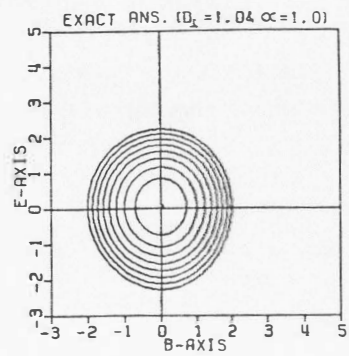
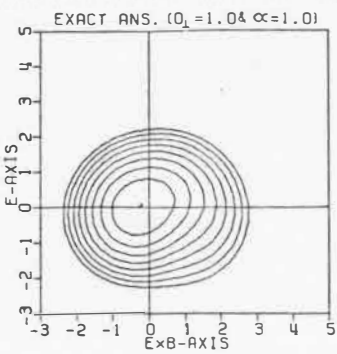
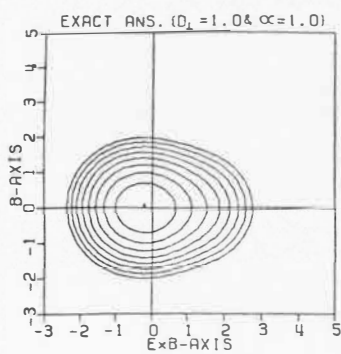


Figure 11. Comparison of the exact form with the 16-moment and the 20-moment expansions of the ion distribution function for the case of perpendicular electric and magnetic fields and for  $D_{\perp} = 3.0$  and  $\alpha = 1.0$ . The contours are plotted in the three principal velocity planes. The plotting format is the same as that for Figure 3.

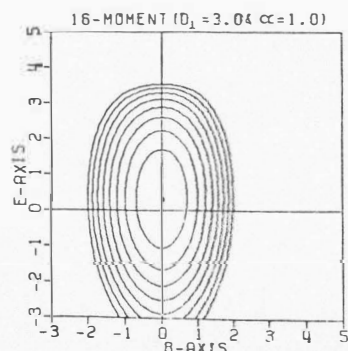
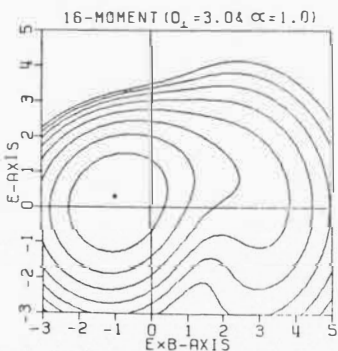
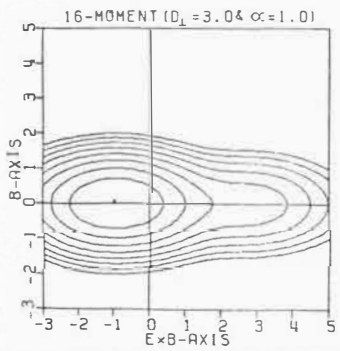
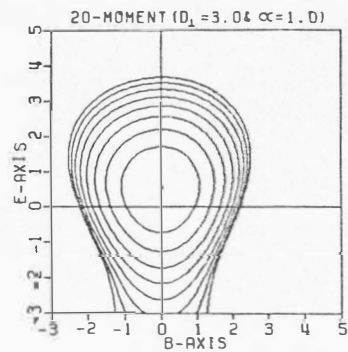
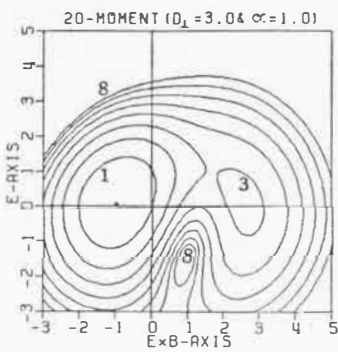
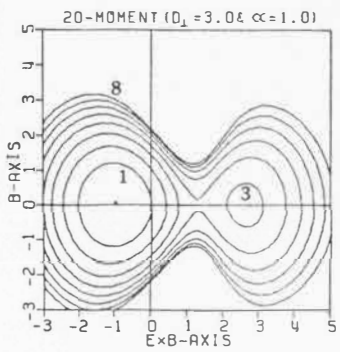
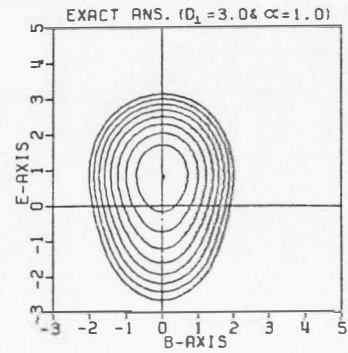
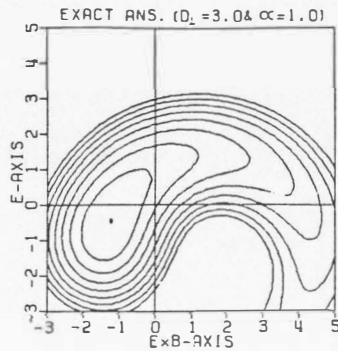
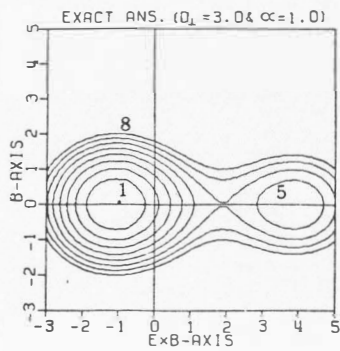
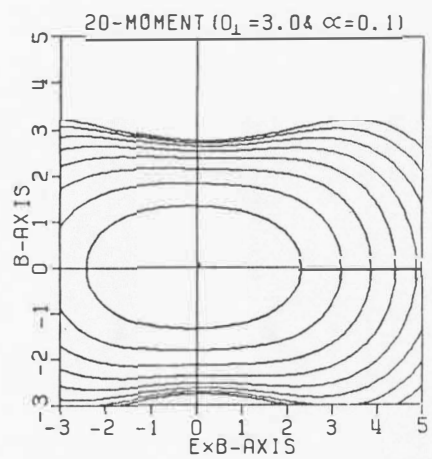
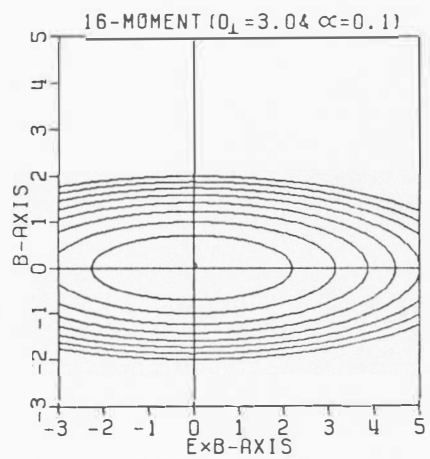
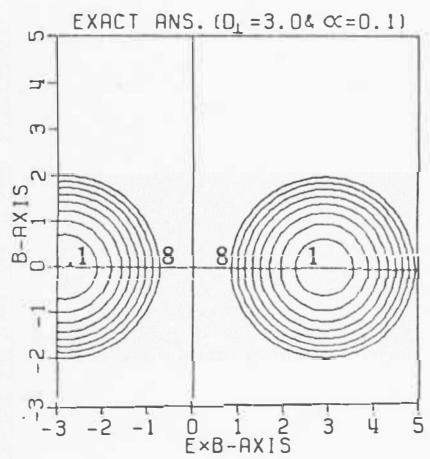


Figure 12. Comparison of the exact form with the 16-moment and the 20-moment expansions of the ion distribution function for the case of perpendicular electric and magnetic fields and for  $D_{\perp} = 3.0$  and  $\alpha = 0.1$ . The contours are plotted in the principal velocity ( $\underline{B}$ - $\underline{ExB}$ )-plane. The plotting format is the same as that for Figure 3.



effect of the 20-moment correction terms becomes significant, but the results are qualitatively similar to those of the 13-moment approximation. Finally, when the electric field is weak ( $D_{\parallel} = 0.3$ ) the distribution is close to Maxwellian and all three levels of approximation are acceptable.

In Figure 4, expansions based on a bi-Maxwellian (6- and 16-moments) are compared. The 6-moment approximation accounts for the bulk drift velocity  $\underline{u}_i$  and parallel and perpendicular temperatures,  $T_{i\parallel}$  and  $T_{i\perp}$ . As  $E_{\parallel}$  increases,  $\underline{u}_i$  and  $T_{i\parallel}$  increase while  $T_{i\perp}$  stays constant because of the absence of any mechanism to transfer the parallel energy, absorbed from the electric field, to the perpendicular direction. The increase in the drift velocity does not show up in this case for reasons similar to those mentioned in the previous paragraph. The 16-moment expansion allows for skewness through the correction terms proportional to  $q_i^{\parallel}$  and  $q_i^{\perp}$ . When  $D_{\parallel} = 0.3$ , the two expansions are near to Maxwellian. As  $E_{\parallel}$  increases ( $D_{\parallel} = 1$  and 3), the effect of the correction terms becomes apparent and the 16-moment result departs significantly from that of the 6-moment.

The 20-moment approximation, having more terms is expected to be better than the 5- and 13-moment approximations. By the same token, the 16-moment approximation should be better than the 6-moment approximation. A detailed comparison indicates that this is indeed the case. Furthermore, for anisotropic plasmas, we would expect that an expansion based on a bi-Maxwellian is better than one based on a Maxwellian. In Figure 5 I compare the 20-moment and the 16-moment approximations to the exact distribution function. For small values of

$E_{\parallel}$  ( $D_{\parallel} = 0.3$ ), both approximations are close to the exact solution which is close to Maxwellian. As  $E_{\parallel}$  increases, and hence the anisotropy increases, the 16-moment approximation gives much better results than those given by the 20-moment approximation even though the former contains fewer terms. The 16-moment approximation is in excellent agreement with the exact solution for  $D_{\parallel} = 1$  and in good agreement for  $D_{\parallel} = 3$ . Therefore, the 16-moment approximation is capable of describing temperature anisotropies as large as 19 (see Table 16).

From the previous discussion, it is apparent that expansions based on a bi-Maxwellian are better than those based on a Maxwellian in describing anisotropic plasmas even if fewer terms are retained. Also, the 16-moment approximation can handle very large anisotropies ( $T_{\perp i} / T_{\parallel i}$  20).

## 2.2. Perpendicular electric and magnetic fields

For the case of parallel electric and magnetic fields, the main effect of the electric field is to cause a parallel-to-perpendicular temperature anisotropy. However, when the fields are perpendicular, significant deviations from the Maxwellian shape can occur in the direction perpendicular to the magnetic field in addition to the unequal temperatures in the directions parallel and perpendicular to the magnetic field. Therefore, the 16-moment approximation is not expected to describe the distribution function as well as when the fields are parallel, especially in the velocity plane perpendicular to  $\underline{B}$ .

Figure 6 shows the behavior of the exact solution for the ion distribution function in the principal velocity plane perpendicular to

Table 16. Ion temperature anisotropy ( $T_{i\parallel}/T_{i\perp}$ ).

$\underline{E} \parallel \underline{B}$		$\alpha$	$\underline{E} \perp \underline{B}$		
$D_{\parallel}$	$D_{\perp}$		0.1	1.0	10.0
0.3	1.18	0.3	0.91	0.95	1.00
1.0	3.00	1.0	0.50	0.66	0.99
3.0	19.00	3.0	0.09	0.17	0.91



B. The distribution function is shown for  $\alpha = 10, 1, 0.1$  (from top to bottom) and for  $D_{\perp} = 0.3, 1, 3$  (from left to right), where  $\alpha [\equiv v_{i\perp} m_i c / e_i B]$  is the collision-to-cyclotron frequency ratio and  $D_{\perp} [\equiv (c E_{\perp} / B) / (2 k T_n / m_i)^{1/2}]$  is the normalized perpendicular drift velocity. As shown, when  $\alpha = 10$  (large collision frequency) and when  $D_{\perp} = 0.3$  (weak electric field) the distribution function is very close to the Maxwellian shape. However, when  $D_{\perp}$  approaches or exceeds unity and  $\alpha$  approaches or becomes less than unity, the distribution function shows significant deviation from the Maxwellian form. For example, the distribution function takes a bean shape ( $D_{\perp} = 3, \alpha = 1$ ) and a toroidal shape ( $D_{\perp} = 3, \alpha = 0.1$ ), as noted by St-Maurice and Schunk (1974). Also, for the cases ( $D_{\perp} = 1, \alpha = 1$ ) and ( $D_{\perp} = 1, \alpha = 0.1$ ), as well as for the two cases mentioned above, the peak of the distribution function (marked by the dot) does not coincide with the average drift velocity (at the origin). In addition to the non-Maxwellian characteristics that occur for these four cases in the plane perpendicular to B, the ion velocity distribution also exhibits a pronounced temperature anisotropy, with  $T_{i\perp} > T_{i\parallel}$  (see Table 16).

From the four cases that display significant non-Maxwellian characteristics, I select three cases (namely,  $D_{\perp} = 1, \alpha = 0.1$ ;  $D_{\perp} = 1, \alpha = 1$ ;  $D_{\perp} = 3, \alpha = 1$ ) for my comparison of the different expansions for the ion distribution function. The fourth case ( $D_{\perp} = 3, \alpha = 0.1$ ), where all expansions fail, will be discussed later.

The 5-moment, the 13-moment and the 20-moment approximations are compared with the exact form of the distribution function in Figure 7. The distribution function is plotted in the plane perpendicular to E.

The 5-moment approximation is unacceptable in all three cases. On the other hand, the results of the 13-moment and the 20-moment approximations are comparable, although the 20-moment approximation is slightly better. Generally, when the distribution function is not too far from Maxwellian, the 13-moment and 20-moment approximations are in good agreement with the exact solution (left and middle columns).

In Figure 8, the 6- and 16-moment approximations are compared with the exact answer for the same three cases and the same velocity plane considered above. It is clear that the 16-moment expansion can account for all three cases. Although it fails to handle the bean feature for the case ( $D_{\perp} = 3, \alpha = 1$ ), it still accounts very well for the temperature anisotropy. Moreover, the 6-moment approximation is not that bad considering its very few degrees of freedom.

In the previous two figures, the comparisons were between distribution functions displayed in one velocity plane. However, it is necessary to consider the three principal velocity planes in order to see the 3-dimensional structure of the distribution function. The 20- and 16-moment expansions (as the best candidates from the Maxwellian-based and bi-Maxwellian-based expansions) are compared with the exact solution in Figure 9 ( $D_{\perp} = 1, \alpha = 0.1$ ), Figure 10 ( $D_{\perp} = 1, \alpha = 1$ ) and Figure 11 ( $D_{\perp} = 3, \alpha = 1$ ). For each case the distribution function is plotted in the three principal planes. In the first two cases, both series expansions are quite acceptable in all three planes; that is, the three-dimensional shape is well represented. However, in the third case (Figure 11), the 16-moment expansion is better in the two planes parallel to the magnetic field because it provides a better description

for the temperature anisotropy, which is the major feature in these planes. On the other hand, both expansions tend to produce the bean shape appearing in the plane perpendicular to the magnetic field (middle column of Figure 11). Since this shape is produced by the terms proportional to the heat flow, the 20-moment expansion produces it slightly better because it accounts for the heat flow tensor accurately.

Figure 12 shows the case ( $D_{\perp} = 3$ ,  $\alpha = 0.1$ ) where the distribution function takes the form of a torus with the major axis parallel to  $\underline{B}$ . The figure shows the intersection of this torus with a plane passing through this axis. The toroidal character can be accounted for only by expansions including moments higher than the third order. Consequently, both the 20-moment and 16-moment approximations fail in producing this shape.

## CHAPTER V

COMPARISON OF MAXWELLIAN AND BI-MAXWELLIAN EXPANSIONS  
WITH MONTE CARLO SIMULATIONS FOR ANISOTROPIC  
PLASMAS

Although the results of chapter (IV) were obtained for a homogeneous plasma and a simple collision model, they should be useful in providing clues as to the extent to which a given series expansion can account for the anisotropic character of a plasma. However, a more realistic collision model will produce a smaller temperature anisotropy than the simple collision model for given electric and magnetic fields, and it is not clear to what extent this will affect the results. Therefore, in this chapter I use more rigorous collision models and compare Maxwellian and bi-Maxwellian expansions with Monte Carlo simulations in order to determine the adequacy of a given series expansion.

## 1. Monte Carlo simulation

My aim is to use the Monte Carlo Simulation (referred to hereafter as MCS) to find the velocity distribution function of a system of ions moving under the influence of electric and magnetic fields in a neutral gas. The neutrals are assumed to have a non-drifting Maxwellian velocity distribution function and the ion density is assumed to be much smaller than that of the neutrals, so that ion-ion collisions can be neglected.

### 1.1. The Monte Carlo technique

The standard procedure of the MCS is to follow the motion of one ion for a large number of collisions, and its velocity is continually monitored. Then, various kinds of time averages for the ion are computed, which can be equated to the corresponding ensemble averages of the system.

In practice, the ion motion is simulated as follows. The time interval between every two successive collisions is found via a proper random number generator. The ion trajectories during these intervals are determined by the classical laws of motion of a charged particle under the influence of electric and magnetic fields. Changes of ion velocity due to collisions are determined using another set of random numbers having the statistical properties determined according to the chosen collision model. Then, a suitable grid in velocity space is used to register the ion's behavior. The time that an ion spends in each bin, divided by the bin's volume, is taken to be proportional to the ion velocity distribution function at its center. Moreover, the individual segments of the trajectory can be directly used to find different velocity moments, as will be explained later. The general aspects of this technique are discussed in more detail by Lin and Bardsley (1977), while some fine details, which depend on the specific collision model, are discussed later.

### 1.2. Relaxation model

For this collision model, the total collision cross section  $\sigma_T$  is inversely proportional to the relative velocity ( $g$ ) between colliding

particles. That is, the collision rate  $K(g) [\equiv \sigma_T(g)g]$  is independent of the colliding particles' velocities. In this case the time intervals between successive collisions have an exponential probability density function and can be generated easily. Also, according to this model, the colliding particles exchange their velocities (or equivalently, exchange identities) during a collision. This is equivalent to assuming that the ions and neutrals have the same mass (ions in their parent gas) and that the differential scattering cross section varies as

$$\sigma(g, \chi) \propto \delta(\chi - \pi) / g \quad (277)$$

where  $\chi$  is the scattering angle in the center-of-mass frame of reference and  $\delta(x)$  is the delta function.

For this simple model, a closed-form expression can be found for the ion velocity distribution function (see chapter (IV)). However, the MCS was used to find the ion velocity distribution functions and the corresponding velocity moments for a couple of cases. The ion was followed for  $10^5$  collisions in each case. The results were compared with the closed-form solutions as a check on the simulation process, and excellent agreement was found. This shows that the MCS, with the probe ion followed for  $10^5$  collisions, is accurate enough for our purpose. Therefore, in all of the cases presented in this work the computations were performed for  $10^5$  'real' collisions.

### 1.3. Polarization model

For the polarization collision model, the collision rate  $K$  is constant as in the case of the relaxation model. On the other hand, the collisional scattering is assumed to be isotropic in the center-of-mass

frame of reference. This approximation, used by Wannier (1953), introduces about a 10% error for relative energies that are sufficiently small, compared to the minimum of the interaction potential (St.-Maurice 1975).

I adopt this approximation for some reasons beyond computational simplicity. First, I am mainly interested in the comparison between transport equations and the results of MCS, rather than their absolute values. Second, this 10% error introduced by this approximation is lower than the uncertainties in the interaction potentials. Third, in the limit of high relative velocity, where this approximation fails, the collision properties can be approximated by using the hard sphere model discussed below.

#### 1.4. Hard sphere model

For the hard sphere collision model, the total collision cross section  $\sigma_T$  is independent of the colliding particles' velocities; that is, the collision rate  $K$  is proportional to their relative velocity ( $g$ ). Contrary to the two previous cases, it is difficult to generate, directly, the time intervals between collisions. I use the concept of 'null collision' explained in detail by Lin and Bardsley (1977). This technique requires the existence of an upper bound  $K_{\max}$  for the collision rate, i.e.,  $K(g) \leq K_{\max}$  for all values of  $g$ . In the case under consideration,  $K_{\max}$  is infinite, which causes a computational problem. This problem can be overcome by using a finite value for  $K_{\max}$ , which introduces an error through collisions corresponding to relative velocities greater than a certain value. However, the resulting error can be arbi-

trarily reduced by taking  $K_{\max}$  large enough, although still finite, such that the error-causing collisions are highly improbable.

The collisional scattering is isotropic in the center-of-mass frame of reference. This is a typical characteristic of hard sphere collisions.



## 2. Velocity distributions for the polarization model

In this section, the ion velocity distribution functions resulting from the MCS are compared with those of the 20- and 16-moment approximations for a variety of cases. For parallel electric and magnetic fields, different values of the normalized parallel drift velocity ( $D_{\parallel}$ ) are considered, while for perpendicular electric and magnetic fields different combinations of the normalized perpendicular drift velocity ( $D_{\perp}$ ) and the collision-to-cyclotron frequency ratio ( $\alpha$ ) are considered. The different parameters produce a range of non-Maxwellian characteristics for the ion velocity distribution function.

It is important to choose the values of these parameters to match the cases presented in chapter (IV) to facilitate comparison with the results for the relaxation collision model used there. Unfortunately, the definitions used in that chapter are not useful for the collision models considered here. On the other hand, the relevant definitions available in the literature (e.g., the definition of collision frequency  $\nu_i$  presented by Schunk (1977)) are limited to specific forms of the distribution function. Different, yet more general, definitions are used here when necessary. For example, the normalized parallel drift velocity ( $D_{\parallel}$ ) is defined as

$$D_{\parallel} = u_i / (2kT_n / m_n)^{1/2} \quad (278)$$

The normalized perpendicular drift velocity ( $D_{\perp}$ ) is

$$D_{\perp} = (c E_{\perp} / B) / (2kT_n / m_n)^{1/2} \quad (279)$$

and  $\alpha$  is defined as

$$\alpha^{-1} = \text{av} [t_c (e_i B / m_i c)] / \text{av} [(1 - \cos \chi) \frac{m_n}{m_i + m_n}] \quad (280)$$

where  $u_i$  is the ion drift velocity,  $T_n$  and  $m_n$  are the neutral temperature and mass, respectively,  $E_{\perp}$  and  $B$  are the electric and magnetic fields,  $c$  is the speed of light,  $e_i$  and  $m_i$  are the ion charge and mass,  $t_c$  is the time interval between two successive collisions,  $\chi$  is the scattering angle in the center-of-mass frame of reference and the "av" denotes an average over the path of the probe ion in the MCS.

These definitions are chosen such that they satisfy certain guidelines. First, they are consistent with the corresponding definitions given in chapter (IV). Second, when the collision frequency  $\nu_i$  is independent of the distribution function ( $K(g) = \text{const}$ ), they are consistent with those in the literature (Schunk 1977). Finally, they account for the angular dependence of the differential cross section and for the 'velocity persistence', mentioned by Chapman and Cowling (1970), through the weighting factor  $\frac{m_n}{m_i + m_n} (1 - \cos \chi)$  in equation (280).

The comparison between the ion distribution functions resulting from the MCS, the 20-moment, and the 16-moment approximations is presented in Figures 13-18, which are obtained as follows. The MCS is used to follow the probe ion for  $10^5$  collisions so that the ion distribution function can be calculated. Also, the resulting velocity moments are found as explained in the next two subsections. These velocity moments are substituted into equations (240) and (264) for the 20- and 16-moment approximations of the distribution function, respectively. Finally, the ion distribution functions are represented by contours at levels decreasing by a factor of  $e^{1/2}$  starting from the maximum.

Figure 13. Comparison of the MCS with the 16-moment and 20-moment expansions of  $f_i$  in the principal velocity plane parallel to the electric field for the polarization collision model, equal ion and neutral masses, and parallel electric and magnetic fields. Two values of the normalized parallel drift velocity were considered,  $D_{\parallel}=1$  (left column) and 3 (right column), where  $D_{\parallel}=u_{\parallel}/(2kT_n/m_n)^{1/2}$ . The contours are plotted against the normalized random velocity  $c_i/(kT_i/m_i)^{1/2}$ . The contour levels decrease by a factor of  $e^{1/2}$  starting from the maximum, shown by the dot.

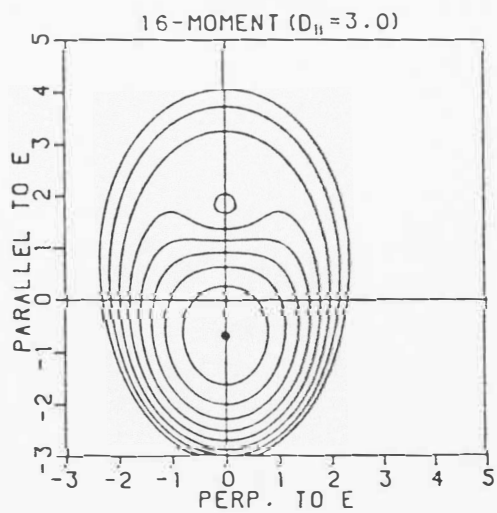
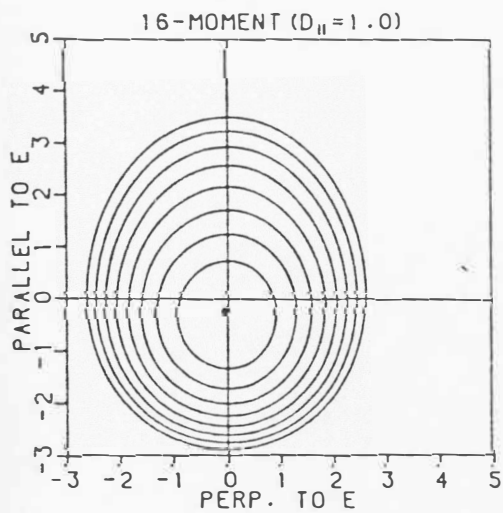
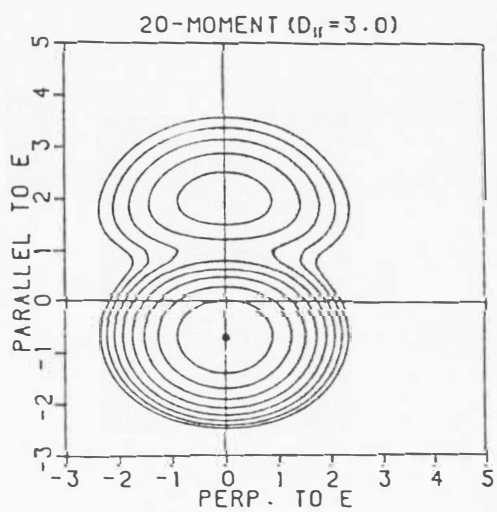
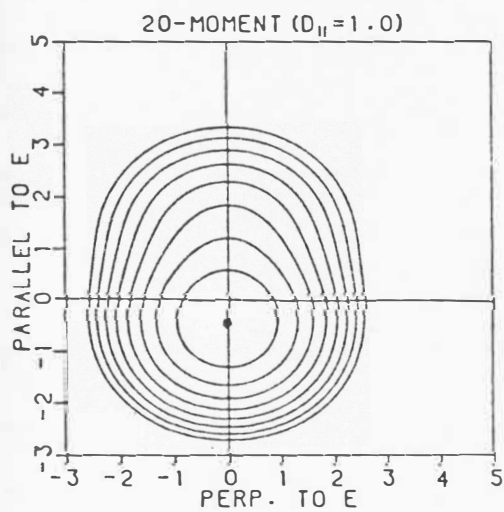
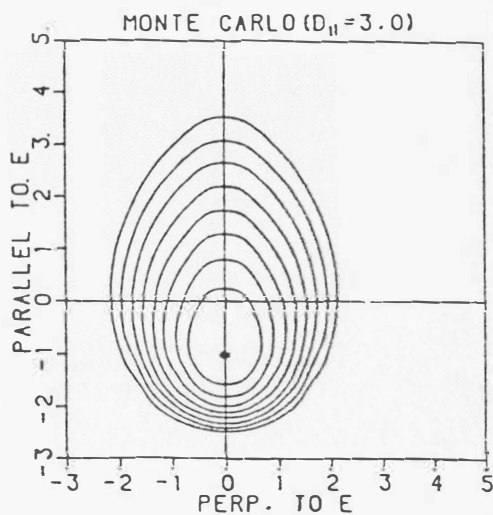
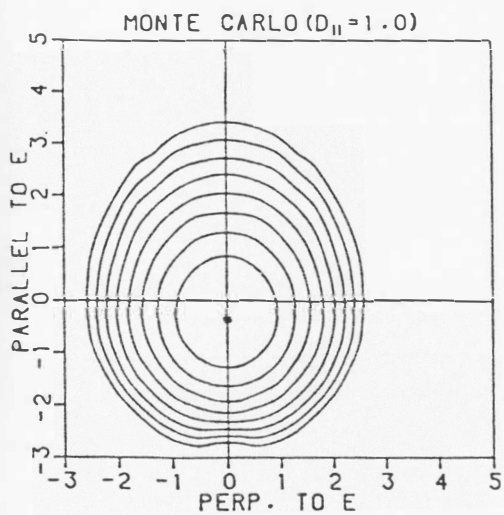


Figure 14. Contours of  $f_i$  obtained from the MCS in the principal velocity ( $\underline{E} - \underline{E} \times \underline{B}$ ) plane for the polarization collision model, equal ion and neutral masses, and perpendicular electric and magnetic fields. Two values of the collision-to-cyclotron frequency ratio were used;  $\alpha=0.1$  (bottom) and 1 (top), where  $\alpha$  is defined in equation (280). In addition, two values of the normalized perpendicular drift velocity were considered;  $D_{\perp}=1$  (left) and 3 (right), where  $D_{\perp} = (cE_{\perp}/B)/(2kT_n/m_n)^{1/2}$ . The plotting format is the same as that for Figure 13, but the dotted contour (bottom, right panel) is lower than the maximum by a factor of  $2/(e^{-1/2}+1)$ .

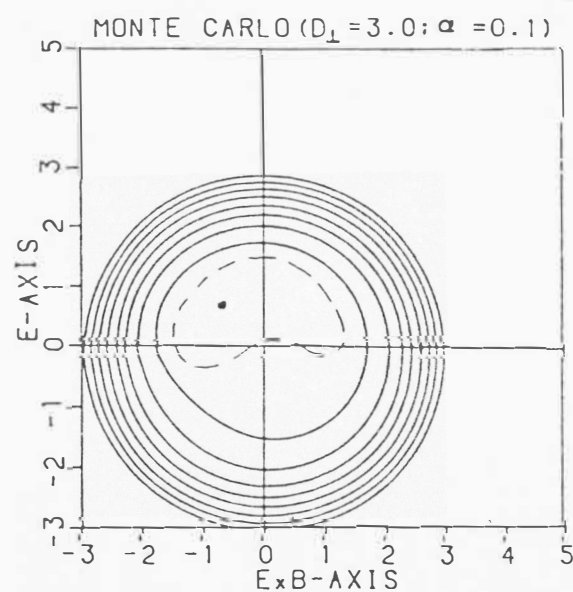
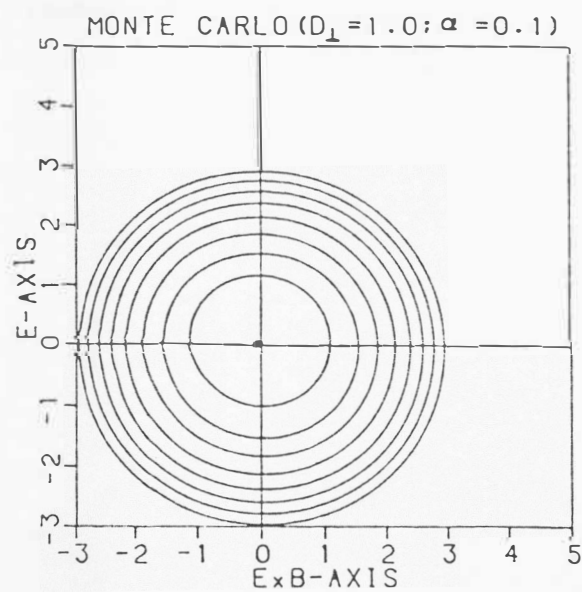
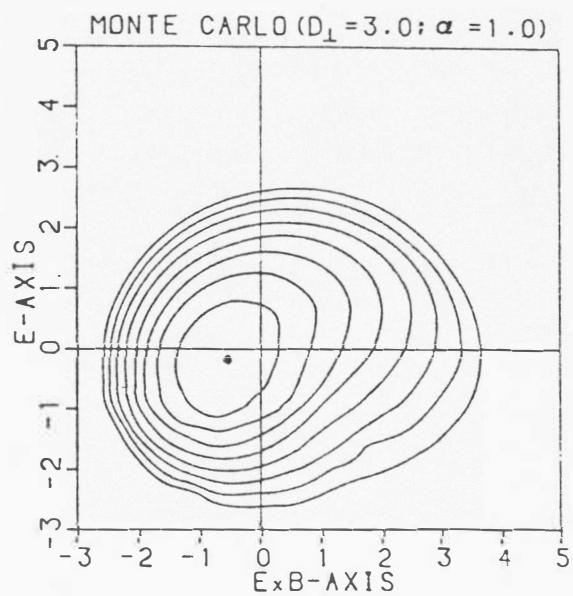
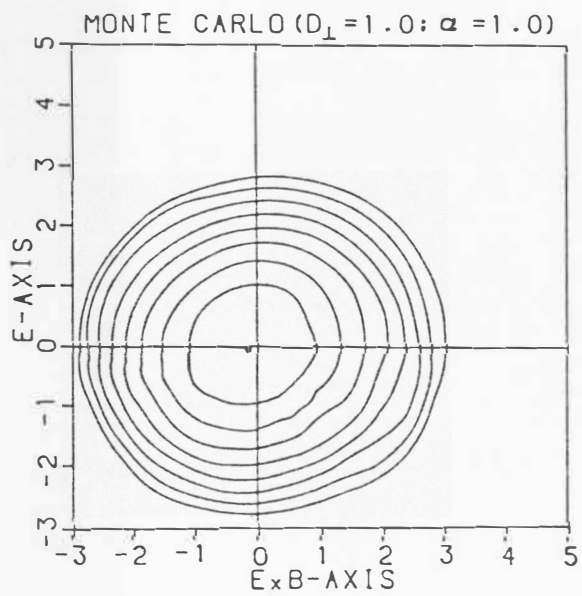


Figure 15. Comparison of the MCS with the 16-moment and 20-moment expansions of  $f_i$  for the polarization collision model, equal ion and neutral masses, perpendicular electric and magnetic fields,  $D_{\perp}=3$ , and  $\alpha=0.1$ . The contours are plotted in the three principal velocity planes. The plotting format is the same as that for Figure 13.

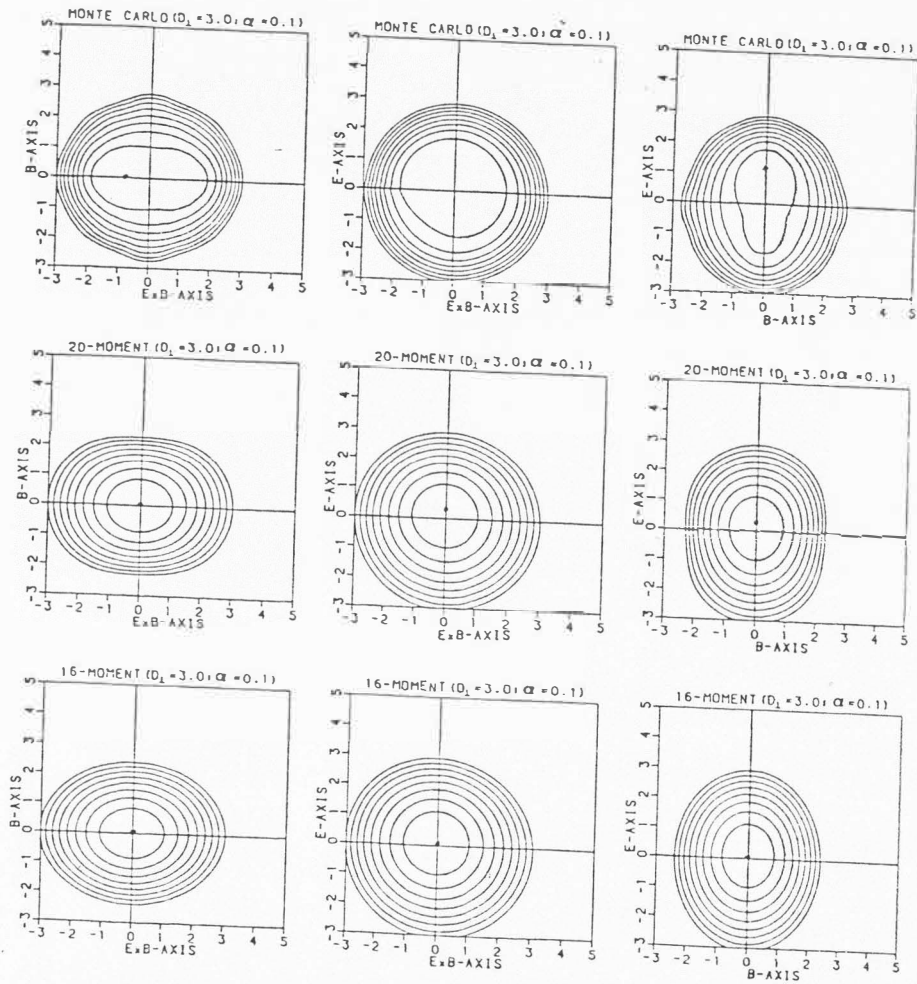




Figure 16. Comparison of the MCS with the 16-moment and 20-moment expansions of  $f_i$  for the polarization collision model, equal ion and neutral masses, perpendicular electric and magnetic fields,  $D_{\perp}=1$ , and  $\alpha=0.1$ . The contours are plotted in the three principal velocity planes. The plotting format is the same as that for Figure 13.

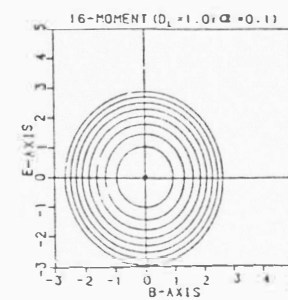
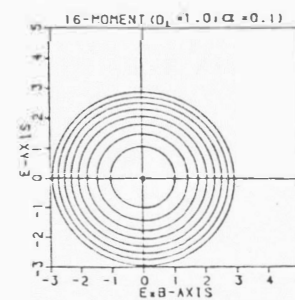
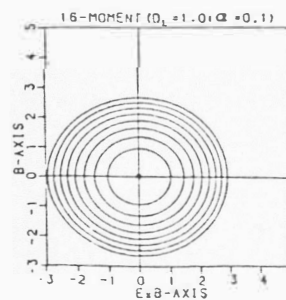
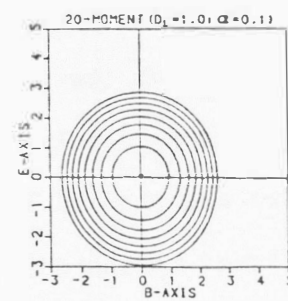
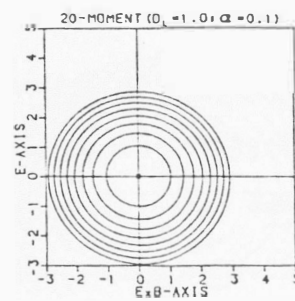
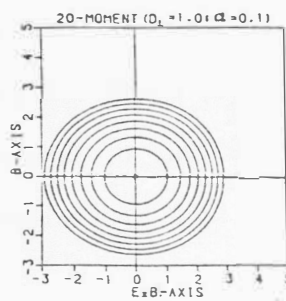
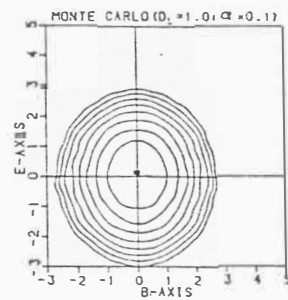
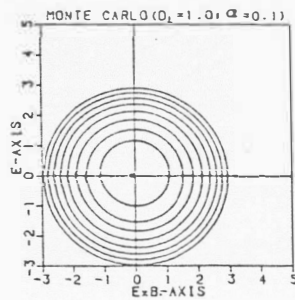
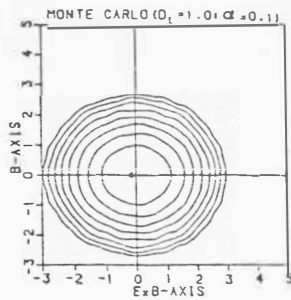


Figure 17. Comparison of the MCS with the 16-moment and 20-moment expansions of  $f_i$  for the polarization collision model, equal ion and neutral masses, perpendicular electric and magnetic fields,  $D_{\perp}=3$ , and  $\alpha=1$ . The contours are plotted in the principal velocity ( $\underline{E} - \underline{E} \times \underline{B}$ ) plane. The plotting format is the same as that for Figure 13.

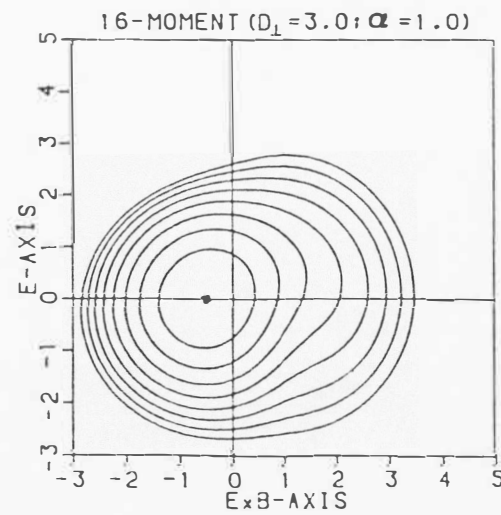
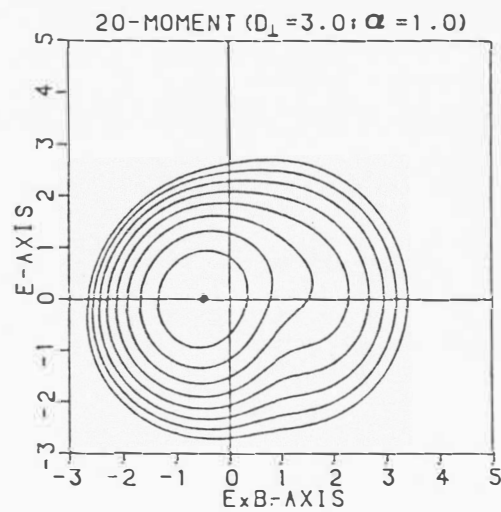
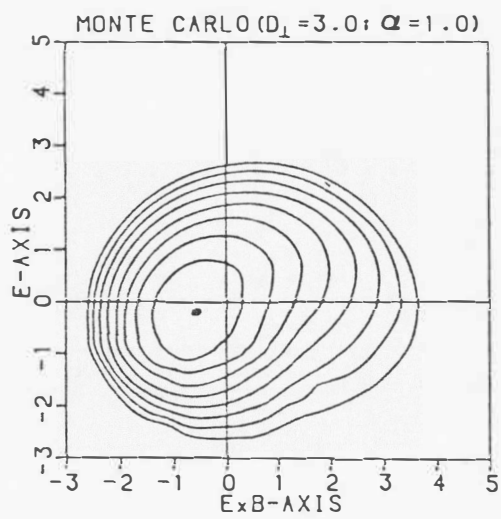
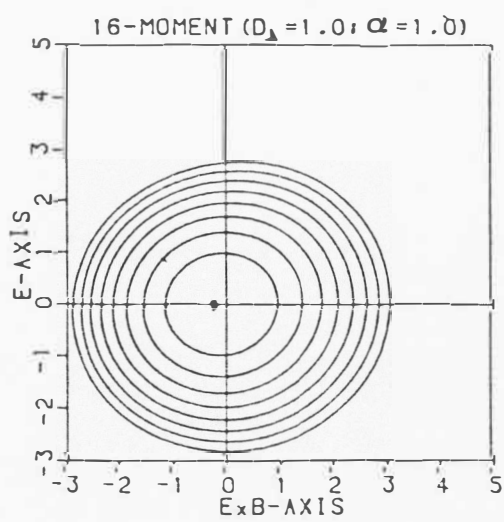
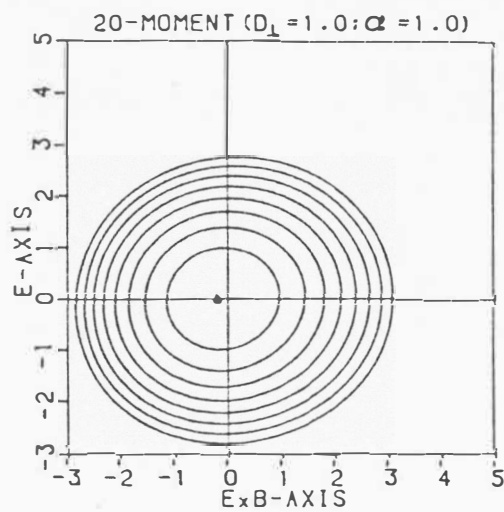
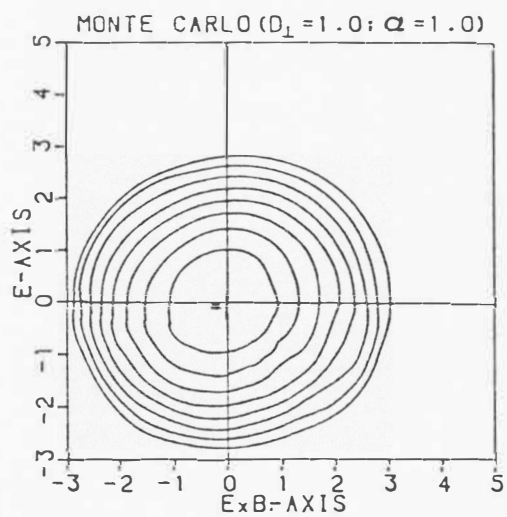


Figure 13. Comparison of the MCS with the 16-moment and 20-moment expansions of  $f_i$  for the polarization collision model, equal ion and neutral masses, perpendicular electric and magnetic fields,  $D_{\perp}=1$ , and  $\alpha=1$ . The contours are plotted in the principal velocity ( $\underline{E} - \underline{E} \times \underline{B}$ ) plane. The plotting format is the same as that for Figure 13.



Although a closed form expression for the ion distribution function cannot be found for realistic collision models, the velocity moments can be found directly by solving the proper transport equations. These 'exact' values for the moments were compared with those computed by the MCS as follows. Each set of moments was substituted into equations (240) and (264) and the results were plotted in a contour form. The difference in the resulting distribution functions, due to using different sets of moments (the exact and the MCS), was almost undetectable. This is another indication that the MCS is adequate for the purpose of this work.

### 2.1. Parallel electric and magnetic fields

As mentioned earlier, in the MCS a suitable grid is used to record the probe ion's velocities. In the case of parallel electric and magnetic fields, the grid has the velocity components parallel and perpendicular to the magnetic field as coordinates, while the azimuthal dependence is taken care of by virtue of cylindrical symmetry. Between collisions the motion of the ion is represented, on the grid, by a straight line parallel to the fields. The time spent by the ion in a certain bin is proportional to the length of that portion of the line lying inside the bin.

The ion distribution function can be represented as

$$f_i = C \sum_{\ell} (\phi_i)_{\ell} \quad (281)$$

where

$$(\phi_i)_\ell = \begin{cases} \delta(v_\perp - (v_\perp)_\ell) / v_\perp & \text{for } (v_{\parallel s})_\ell \leq v_{\parallel} \leq (v_{\parallel f})_\ell \\ 0 & \text{elsewhere} \end{cases} \quad (282)$$

and where  $\delta(x)$  is the Dirac Delta function,  $v_{\parallel s}$  and  $v_{\parallel f}$  are the initial and final parallel velocities,  $v_\perp$  is the perpendicular velocity,  $C$  is a constant, and the subscript  $\ell$  is used to denote that the summation is over all continuous segments of the probe ion trajectory in velocity space. With this expression, it is possible to accumulate the data necessary to compute the velocity moments while following the probe ion's motion. For example, the ion drift velocity is simply

$$\underline{u}_i = \frac{1}{2} \sum_\ell [(v_{\parallel f})_\ell^2 - (v_{\parallel s})_\ell^2] / \sum_\ell [(v_{\parallel f})_\ell - (v_{\parallel s})_\ell] \quad (283)$$

Figure 13 shows a comparison between the MCS and the 20- and 16-moment approximations of the ion distribution function for the polarization collision model and for parallel electric and magnetic fields. Two values of the normalized parallel drift velocity ( $D_{\parallel}$ ) were considered; namely,  $D_{\parallel}=1$  and 3. The case of  $D_{\parallel}=0.3$ , corresponding to that presented in chapter (IV), is not shown here because in this case the ion distribution function is sufficiently close to Maxwellian that it can be handled by any level of approximation. Comparing the polarization model results shown in Figure 13 with the relaxation model results, we find that for the polarization collision model, the ion distribution functions are closer to Maxwellian for a given value of  $D_{\parallel}$ . For example, in the case of  $D_{\parallel}=3$ , the parallel-to-perpendicular temperature anisotropy is 2.2 for the polarization model, which is much less than that found for the relaxation model ( $\approx 20$ ). This is due to the fact that the



polarization model permits the transfer of kinetic energy between the parallel and perpendicular directions, while the relaxation model does not.

As the electric field strength increases, the drift velocity ( $\underline{u}_i$ ) and the temperature ( $T_i$ ) increase. These changes do not appear in Figure 13 because the contours are plotted against the normalized ion random velocity  $\underline{c}_i / (kT_i/m_i)^{1/2}$ . However, the ion parallel temperature increases more rapidly than the perpendicular temperature (i.e., the temperature anisotropy increases), and such changes show up because of their relative nature. For  $D_{\parallel} > 3$ , the shape of the ion distribution function does not change significantly with  $D_{\parallel}$  and starts to 'saturate'. The shape of the distribution function for  $D_{\parallel} = \infty$ , given by Wannier (1953), does not differ much from that shown in Figure 13 for  $D_{\parallel} = 3$ . This saturation does not occur for the relaxation model; the temperature anisotropy increases indefinitely with  $D_{\parallel}$ .

For  $D_{\parallel} = 1$  (left column), the 16-moment approximation of  $f_i$  shows an excellent agreement with the MCS, while the 20-moment approximation shows a good agreement. As  $D_{\parallel}$  increases and the ion distribution function deviates more from the Maxwellian, the approximate distribution functions deviate from those found by the MCS. When  $D_{\parallel} = 3$  (right column), the 20-moment approximation starts to fail, while the 16-moment approximation still compares favorably with the MCS. Further increases of  $D_{\parallel}$  are not expected to result in significant changes in the degree of agreement due to the shape saturation mentioned earlier.

In general, for the case of parallel electric and magnetic fields, the bi-Maxwellian-based 16-moment approximation shows better agreement (ranging from excellent ( $D_{\parallel}=1$ ) to acceptable ( $D_{\parallel}>3$ )) with the MCS than does the Maxwellian-based 20-moment approximation. However, both approximations did much better for the polarization collision model than for the relaxation model, for which a greater temperature anisotropy occurs for the same  $D_{\parallel}$ .

## 2.2. Perpendicular electric and magnetic fields

In this case, between collisions the probe ion moves in circles in velocity space with constant angular velocity ( $\Omega_i = e_i B / m_i c$ ). These circles are centered at the  $\underline{E} \times \underline{B}$  drift velocity  $\underline{u}_E$ . Therefore, in the MCS we used a three-dimensional grid whose coordinates are the parallel and perpendicular velocities relative to  $\underline{u}_E$  and the azimuthal angle  $\theta$ . The time spent by an ion in one bin is proportional to the angular distance it scans while lying inside this bin. Using this criterion we can compute the time that the probe ion spends in each bin.

The ion velocity distribution function is

$$f_i = C \sum_{\ell} (\phi_i)_{\ell} \quad (284)$$

where

$$(\phi_i)_{\ell} = \begin{cases} \delta(v_{\parallel}^{\ell} - (v_{\parallel}^{\ell})_{\ell}) \frac{\delta(v_{\perp}^{\ell} - (v_{\perp}^{\ell})_{\ell})}{v_{\perp}} & \text{for } (\theta_s)_{\ell} \leq \theta \leq (\theta_f)_{\ell} \\ 0 & \text{elsewhere} \end{cases} \quad (285)$$

where  $\delta(x)$  is the Dirac delta function,  $v_{\parallel}^{\ell}$  and  $v_{\perp}^{\ell}$  are the parallel and perpendicular components of  $\underline{v}^{\ell} [\equiv \underline{v}_i - \underline{u}_E]$ ,  $\ell$  denotes that the summation is taken over all continuous segments of the ion trajectory, and  $\theta_s$  and  $\theta_f$

are the initial and final azimuthal angles for such a segment. This expression is used to accumulate the data required to calculate the velocity moments in a way similar to that discussed in the previous subsection.

Of the nine cases considered in chapter (IV) for the relaxation collision model, I only chose the four cases that showed significant deviations from a Maxwellian because the polarization model is expected to produce much smaller non-Maxwellian deviations for a given  $D_{\perp}$ . These cases correspond to the following parameter values:  $D_{\perp}=1$ ,  $\alpha=1$ ;  $D_{\perp}=3$ ,  $\alpha=1$ ;  $D_{\perp}=1$ ,  $\alpha=0.1$ ; and  $D_{\perp}=3$ ,  $\alpha=0.1$ . For the relaxation model, the resulting distribution functions showed some interesting non-Maxwellian characteristics, i.e., bean and toroidal shapes.

Figure 14 shows the ion distribution functions resulting from the MCS for the four cases mentioned above. In general, they show less deviations from a Maxwellian compared with the distribution functions obtained from the relaxation model for the same values of  $D_{\perp}$  and  $\alpha$ . As mentioned in the previous subsection, this is due to energy transfer between the parallel and perpendicular directions.

For the case ( $D_{\perp}=1$ ,  $\alpha=1$ ), the distribution function is the closest to Maxwellian. As  $D_{\perp}$  increases or  $\alpha$  decreases, the deviation from a Maxwellian increases. For the case ( $D_{\perp}=3$ ,  $\alpha=1$ ), the bean shape starts to appear, while weak toroidal features (e.g., flat maximum) appear as the collision frequency decreases ( $\alpha=0.1$ ). As  $D_{\perp}$  increases from 1 to 3, the maximum of  $f_i$  in the plane perpendicular to  $\underline{B}$  broadens and a small dip occurs along the  $\underline{ExB}$  axis. The shape saturation mentioned in the previous subsection occurs again in this case for large values of  $D_{\perp}$  and

small values of  $\alpha$ .

The case of ( $D_{\perp}=3$ ,  $\alpha=0.1$ ) is shown in more detail in Figure 15, where the MCS (top) is compared with the 20-moment (middle) and 16-moment (bottom) approximations. The distribution functions are represented by contours in the three principal velocity planes to demonstrate their three-dimensional structure. Comparison with the relaxation model results indicates that the toroidal features are much less evident for the polarization model. Moreover, the distribution function obtained with the polarization model and ( $D_{\perp}=3$ ,  $\alpha=0.1$ ) is very similar to that obtained with the relaxation model and ( $D_{\perp}=1$ ,  $\alpha=0.1$ ). This indicates that the relaxation model can give the correct physical characteristics, provided that the proper value of the (reduced) electric field is used.

This case of ( $D_{\perp}=3$ ,  $\alpha=0.1$ ) is the worst with regard to the ability of the 20- and 16-moment expressions for  $f_i$  to approximate the MCS. This is because  $f_i$  displays its strongest toroidal features for this case, which are very difficult to account for with these levels of approximation. However, both approximations show quite reasonable agreement with the MCS (the 20-moment is a little better) in comparison with the results obtained for the relaxation model, for which the 16- and 20-moment approximations completely failed for this case.

For the other three cases, the distribution functions are expected to be closer to Maxwellian, and consequently the series expansions should be in better agreement with the MCS. Figure 16 shows that is really the case when  $D_{\perp}=1$  and  $\alpha=0.1$ . Both approximations display reasonable resemblance to the MCS result, but the 20-moment approximation han-

dles the flat maximum better.

Since the distribution function is close to Maxwellian, it is sufficient to present the distribution functions for the two remaining cases only in the plane perpendicular to the magnetic field. The case of ( $D_{\perp}=3, \alpha=1$ ) is presented in Figure 17. The distribution function generated by the MCS takes the bean shape. This feature is well accounted for by both the 20- and 16-moment approximations, but the former is a little better. Compared to the corresponding case in chapter (IV), the distribution function displays less deviations from Maxwellian; consequently, the moment approximations are in better agreement with the MCS. Also, the resemblance between this case and the case of ( $D_{\perp}=1, \alpha=1$ ) for the relaxation model supports the argument that the relaxation model, with the proper reduction in the electric field intensity, can give a qualitatively correct picture of the shape of the ion distribution function.

Figure 18 shows the comparison between the 20- and 16-moment approximations and the MCS for the case ( $D_{\perp}=1, \alpha=1$ ). The distribution function is close to Maxwellian. Therefore, the 16- and 20-moment approximations show, as expected, an excellent agreement with the MCS.

### 3. Velocity distributions for the hard sphere model

To compare the ion distribution functions of the 20- and 16-moment approximations with the MCS for the hard sphere model, a line parallel to that of the previous section is followed. The MCS code was modified to use the 'null collision' concept, mentioned earlier. A probe ion was followed for  $10^5$  'real' collisions. The grid used in this case was exactly identical to that mentioned in the previous section. Finally, the ion distribution functions obtained from the MCS and the 20- and 16-moment approximations were computed and plotted using a format similar to that of Figures 13-18.

The major difference between the polarization and hard sphere collision models is that the collision rate  $K[\equiv\sigma_T g]$  is proportional to the relative speed ( $g$ ) for the hard sphere model, while it is constant for the polarization model. That is, in the former case, faster ions collide, on the average, more rapidly and lose their energy. This inhibits the tail of the distribution function and brings it closer to Maxwellian. Therefore, better agreement is expected between the series expansions and the MCS.

#### 3.1. Parallel electric and magnetic fields

Figure 19 shows a comparison between the MCS and the 20- and 16-moment approximations of  $f_i$  for the case of parallel electric and magnetic fields. The cases of  $D_{||}=1$  (left) and 3 (right) are presented, where  $D_{||}$  is the normalized drift velocity. In general, the behavior of the ion distribution function is similar to the corresponding cases in

Figure 19. Comparison of the MCS with the 16-moment and 20-moment expressions of  $f_i$  in the principal velocity plane parallel to the electric field for the hard-sphere collision model, equal ion and neutral masses, and parallel electric and magnetic fields. Two values of the normalized parallel drift velocity were considered,  $D_{\parallel}=1$  (left) and 3 (right), where  $D_{\parallel}=u_i/(2kT_n/m_n)^{1/2}$ . The contours are plotted against the normalized random velocity  $c_i/(kT_i/m_i)^{1/2}$ . The contour levels decrease by a factor of  $e^{1/2}$  starting from the maximum, shown by the dot.

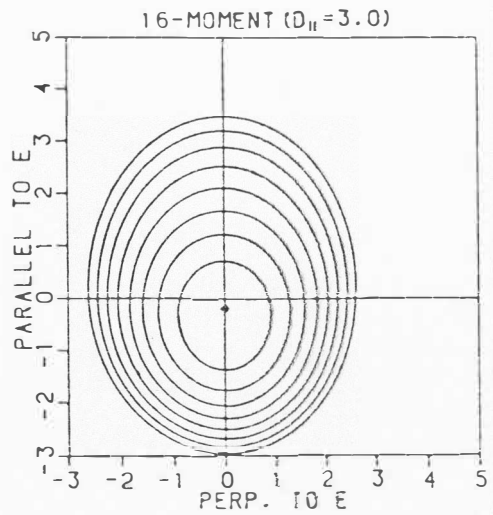
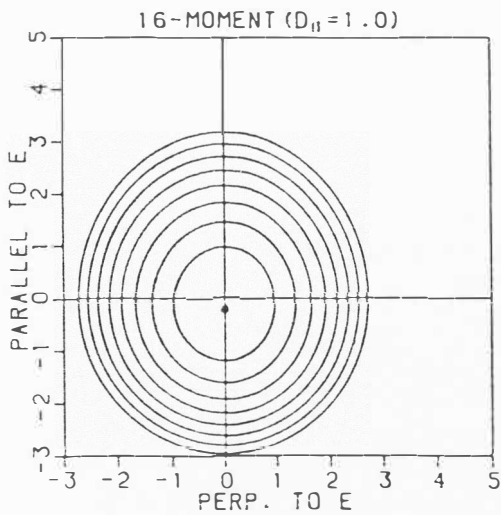
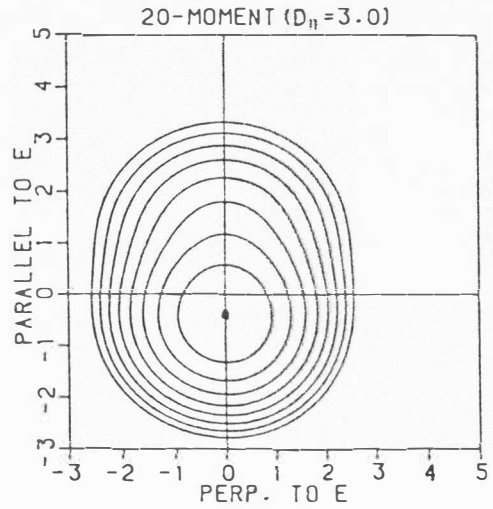
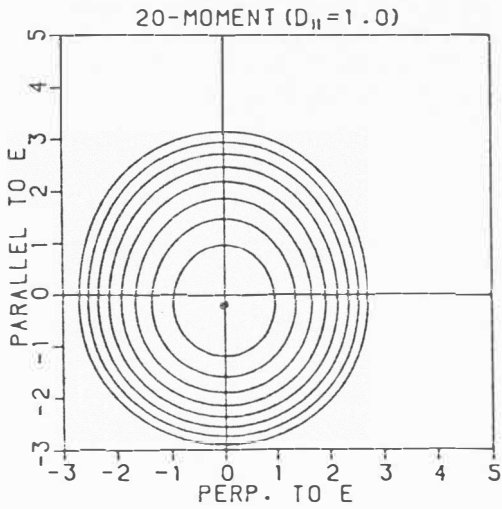
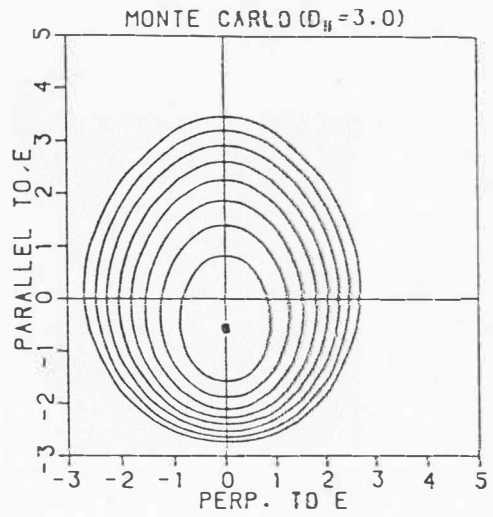
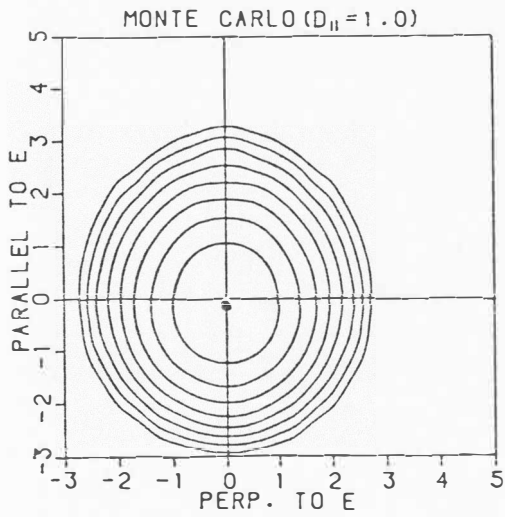




Figure 20. Contours of  $f_i$  obtained from the MCS in the principal ( $\underline{E} - \underline{E} \times \underline{B}$ ) plane for the hard-sphere collision model, equal ion and neutral masses, and perpendicular electric and magnetic fields. Two values of the collision-to-gyro frequency ratio were used;  $\alpha=0.1$  (bottom) and 1 (top), where  $\alpha$  is defined in equation (280). In addition, two values of the normalized perpendicular drift velocity were considered;  $D_{\perp}=1$  (left) and 3 (right), where  $D_{\perp}=(cE_{\perp}/B)/(2kT_n/m_n)^{1/2}$ . The plotting format is the same as that for Figure 19.

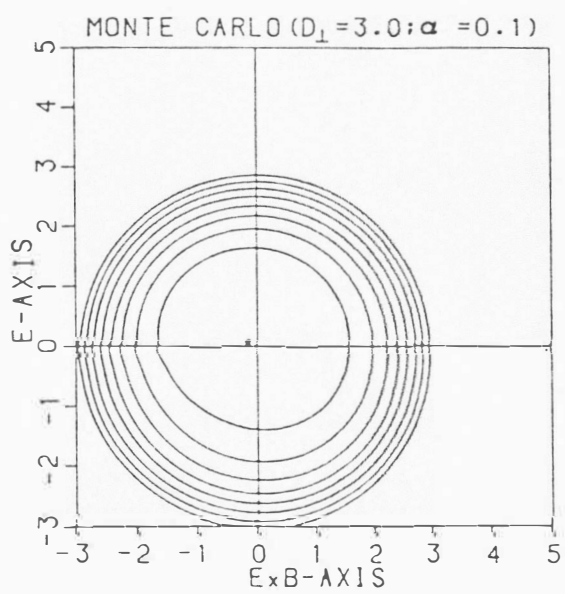
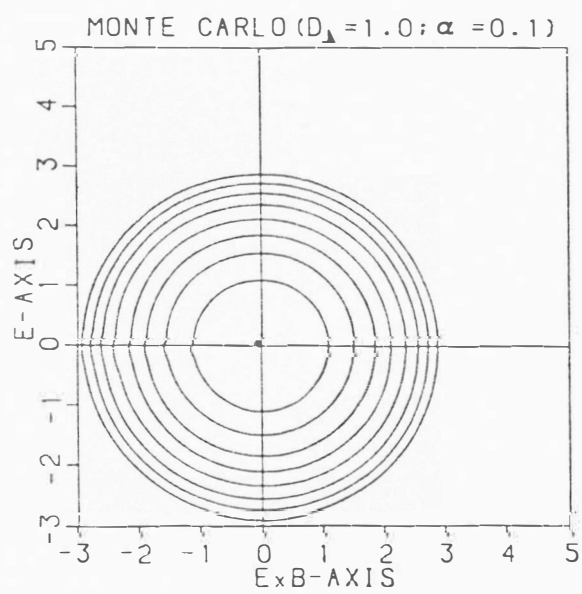
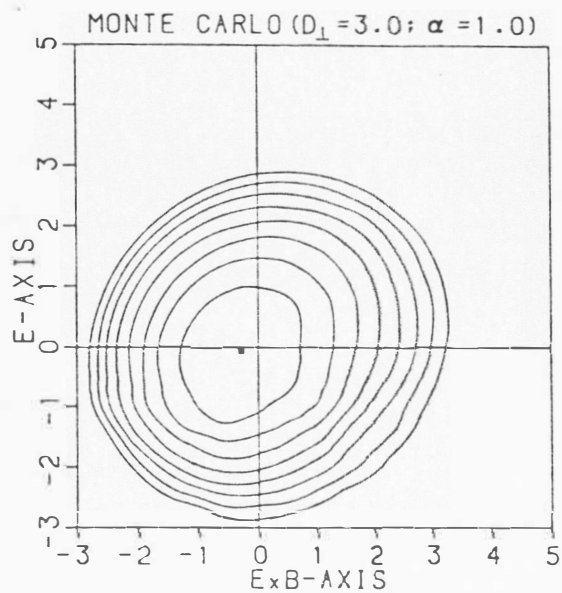
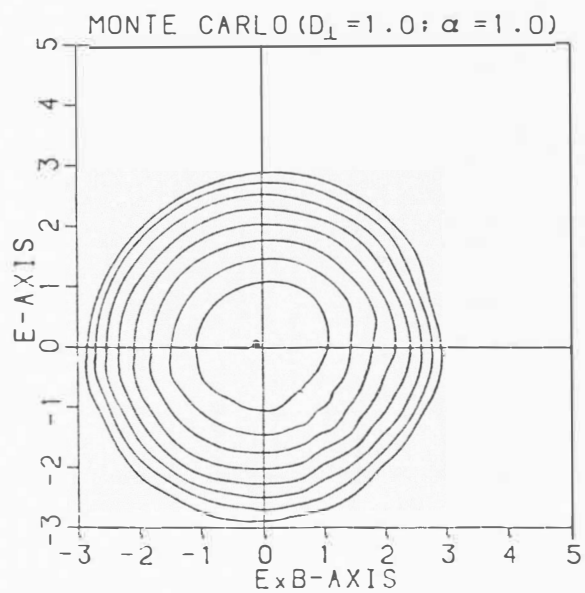


Figure 21. Comparison of the MCS with the 16-moment and 20-moment expansions of  $f_i$  for the hard-sphere collision model, equal ion and neutral masses, perpendicular electric and magnetic fields,  $D_{\perp}=3$ , and  $\alpha=0.1$ . The contours are plotted in the three principal velocity planes. The plotting format is the same as that for Figure 19.

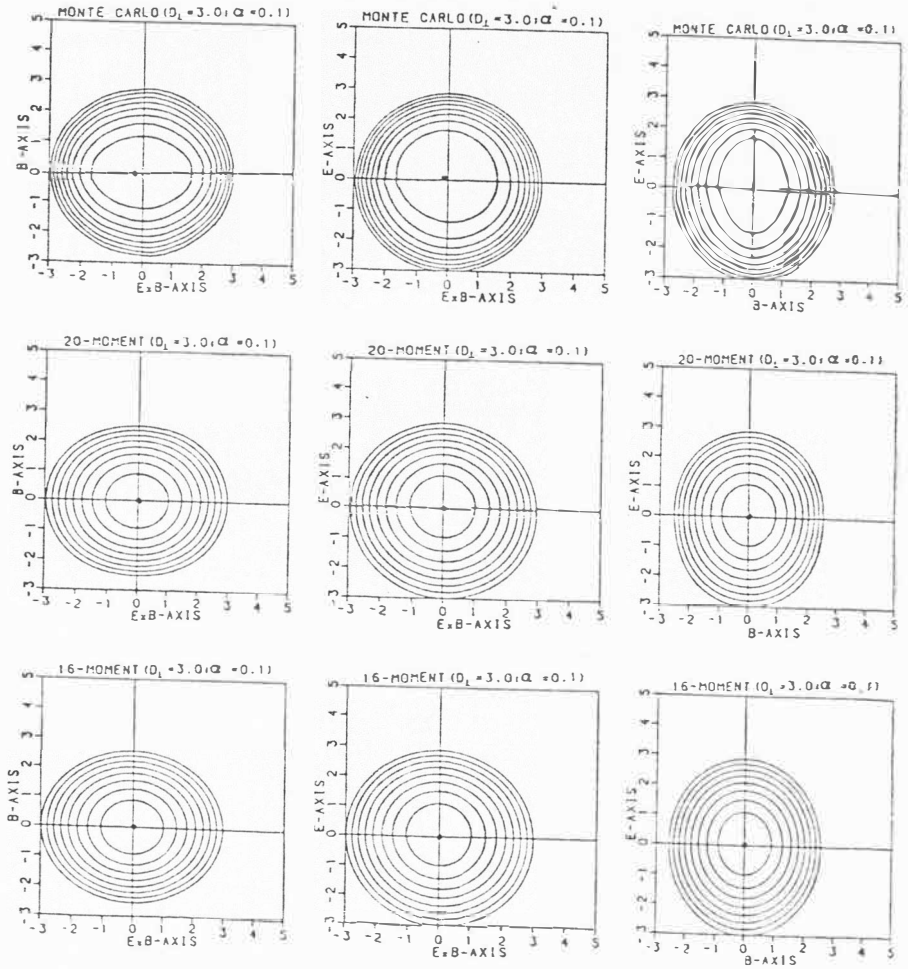


Figure 22. Comparison of the MCS with the 16-moment and 20-moment expansions of  $f_i$  for the hard-sphere collision model, equal ion and neutral masses, perpendicular electric and magnetic fields,  $D_{\perp}=1$ , and  $\alpha=0.1$ . The contours are plotted in the principal velocity ( $\underline{E} - \underline{E} \times \underline{B}$ ) plane. The plotting format is the same as that for Figure 19.

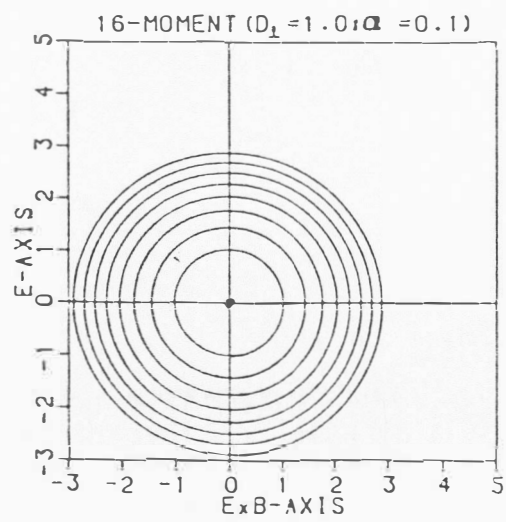
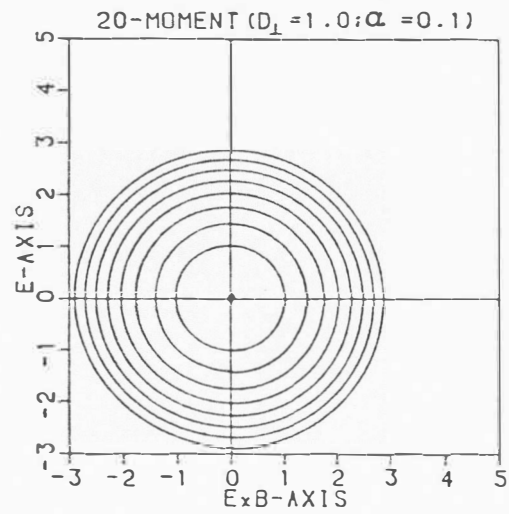
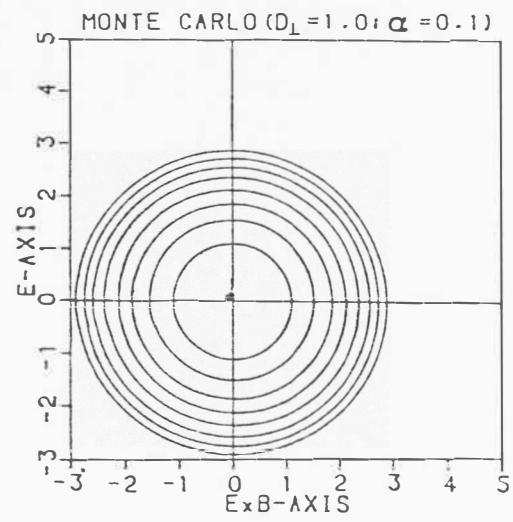


Figure 23. Comparison of the MCS with the 16-moment and 20-moment expansions of  $f_i$  for the hard-sphere collision model, equal ion and neutral masses, perpendicular electric and magnetic fields,  $D_{\perp}=3$ , and  $\alpha=1$ . The contours are plotted in the principal velocity ( $\underline{E} - \underline{E} \times \underline{B}$ ) plane. The plotting format is the same as that for Figure 19.

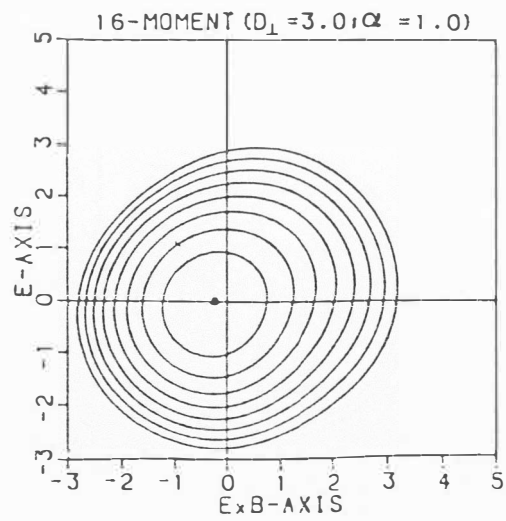
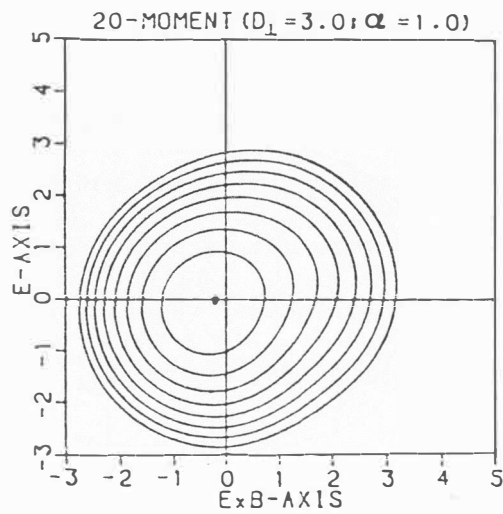
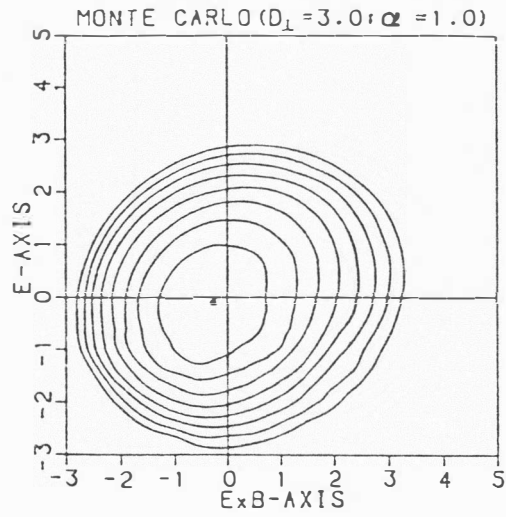
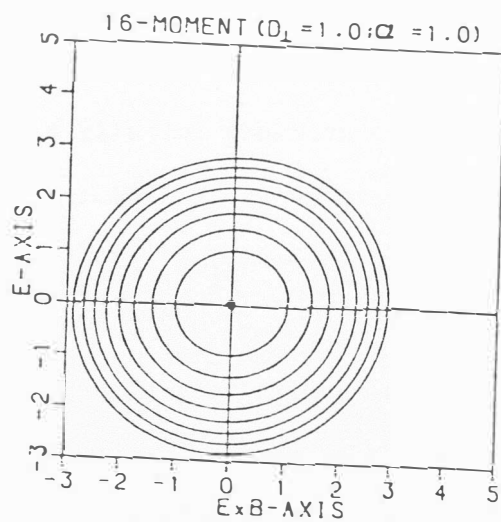
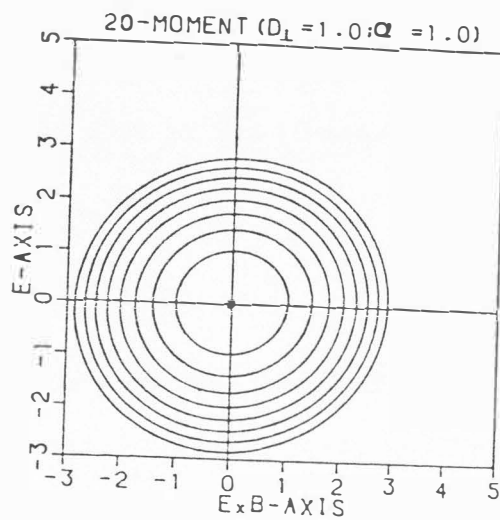
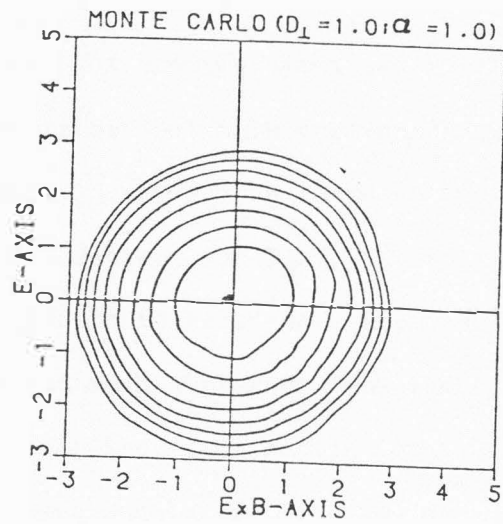




Figure 24. Comparison of the MCS with the 16-moment and 20-moment expansions of  $f_i$  for the hard-sphere collision model, equal ion and neutral masses, perpendicular electric and magnetic fields,  $D_{\perp}=1$ , and  $\alpha=1$ . The contours are plotted in the principal velocity ( $\underline{E} - \underline{E} \times \underline{B}$ ) plane. The plotting format is the same as that for Figure 19.



the previous section. For example, as the electric field intensity increases,  $u_i$  and  $T_i$  increase, but this does not show up for the same reason mentioned earlier. However, the increase of the temperature anisotropy ( $T_{i\parallel}/T_{i\perp}$ ) is noticeable. For  $D_{\parallel} > 3$ , the relative shape of the distribution function starts to saturate. The case of  $D_{\parallel} = \infty$ , presented by Scullerud (1973), is not much different from the case of  $D_{\parallel} = 3$  presented here. On the other hand, the distribution function is closer to Maxwellian and its tail is less populated. The 20- and 16-moment approximations are showing better agreement with the MCS. In fact, the 16-moment approximation is excellent in both cases, and the 20-moment approximation, although not as good as the 16-moment approximation, still shows good agreement.

### 3.2. Perpendicular electric and magnetic fields

I consider here the same four cases discussed in the previous section (namely,  $D_{\perp} = 1, \alpha = 1$ ;  $D_{\perp} = 3, \alpha = 1$ ;  $D_{\perp} = 1, \alpha = 0.1$ ; and  $D_{\perp} = 3, \alpha = 0.1$ ). The ion distribution functions obtained from the MCS for these four cases are presented in Figure 20. For the case of ( $D_{\perp} = 1, \alpha = 1$ ) the distribution function is very close to Maxwellian. For higher values of  $D_{\perp}$  ( $D_{\perp} = 3, \alpha = 1$ ), the distribution function takes the bean shape. As  $\alpha$  decreases to 0.1, weak toroidal features start to appear in the form of flat maxima in the velocity plane perpendicular to  $\underline{B}$ . This is more apparent for larger values of  $D_{\perp}$ .

The 16- and 20-moment approximations are compared with the MCS for each case in Figures 21-24. The case which shows the strongest toroidal features ( $D_{\perp} = 3, \alpha = 0.1$ ) is presented in Figure 21, where the contours in

the three principal velocity planes are shown. Compared to Figure 15 (Polarization model) the distribution function has weaker toroidal features (e.g., the maximum in the plane perpendicular to  $\underline{B}$  is less flat and the dip disappears) and, as expected, the moment approximations are in better agreement with the MCS. Although the agreement between the 20- and 16-moment approximations and the MCS is not especially good, it is still acceptable.

For the other three cases presented in Figures 22-24,  $f_i$  is closer to Maxwellian and therefore it is sufficient to show the distribution functions only in the plane perpendicular to  $\underline{B}$ . The distribution functions show similar behavior to the corresponding ones in the previous section (see Figures 16-18). However, they are closer to Maxwellian; for example, the tail of the bean distribution is inhibited in the case ( $D_{\perp}=3, \alpha=1$ ) and the toroidal features are reduced in the case ( $D_{\perp}=1, \alpha=0.1$ ). Consequently, the 20- and the 16-moment approximations show better agreement with the MCS (especially for  $D_{\perp}=3, \alpha=1$ ), with the 20-moment approximation a little better.

For the case of ( $D_{\perp}=1, \alpha=1$ ), as well as the corresponding case in the previous section, the ion distribution function is close to Maxwellian and all levels of approximation agree very well with the MCS.

I conclude that, in general, the distribution functions resulting from the hard sphere model are similar to those of the polarization model. However, the former case gives results closer to Maxwellian and consequently the 20- and 16-moment approximations show better agreement with the MCS.

## CHAPTER VI

## SUMMARY AND CONCLUSION

In chapter (II), I presented a closed system of transport equations for multicomponent anisotropic space plasmas. These general transport equations offer the opportunity to take a unified approach to the study of widely different plasma flow situations. This system of transport equations can be applied to both collision-dominated and collisionless flows and provides a continuous transition between the two regimes; it can be applied to subsonic, transonic, and supersonic flows and provides a continuous transition between the regimes; it can describe multicomponent plasmas with large temperature differences between the interacting species; it can describe plasmas that contain large temperature anisotropies; it can describe plasma flows in rapidly changing magnetic field configurations; and account is taken of Coulomb, nonresonant ion-neutral, neutral-neutral, and resonant charge exchange interactions. Furthermore, if Maxwell's equations of electricity and magnetism are added to the system of transport equations, it can be used to describe electrostatic shocks, double layers, and magnetic merging processes.

This system of generalized transport equations is based on an anisotropic bi-Maxwellian velocity distribution function and corresponds to a 16-moment approximation. The system of equations contains a continuity equation, a momentum equation, parallel and perpendicular energy equations, a stress tensor equation, and heat

flow equations for the flow of parallel and perpendicular energy for each species in the plasma.

The system of generalized transport equations reduces to Grad's 13-moment system of transport equations in the limit of small temperature anisotropies. If this latter system is ordered with respect to the collisional mean-free-path, the result is the Euler, Navier-Stokes, and Burnett equations depending on whether terms proportional to the zeroth, first, or second power of the mean-free-path are retained. At the Navier-Stokes approximation, transport processes such as ordinary diffusion, thermal diffusion, thermal conduction, diffusion-thermal heat flow, thermoelectric heat flow, and viscosity are included at a level of approximation that corresponds to either the first or second approximation of Chapman and Cowling (1970), depending on the particular transport coefficient. Also, if the plasma is treated as a single fluid and if Maxwell's equations are included, the system of generalized transport equations reduces to the familiar magnetohydrodynamic equations.

In the limit of a collisionless plasma, the system of generalized transport equations is equivalent to the level of approximation usually considered in kinetic models. These collisionless transport equations include the effects of collisionless heat flow, collisionless viscosity, and temperature anisotropies. They also contain terms which act to regulate both the heat flow and temperature anisotropy (cf. Schunk and Watkins 1979, 1981), processes which appear to be operating in the solar wind. Also, it should be noted that the system

of generalized transport equations reduces to all of the other major systems of transport equations for anisotropic plasmas that have been derived to date. The assumptions needed to derive these other sets of simplified transport equations are summarized in Figure 2.

In chapter (III), I derived a closed set of transport equations assuming that the distribution functions of the interacting gases were anisotropic bi-Maxwellian (or two-temperature) distributions. I also derived the appropriate momentum, parallel energy and perpendicular energy collision terms for Coulomb, Maxwell molecule, and constant collision cross section interaction potentials. The collision terms are valid for arbitrary temperature anisotropies, arbitrary temperature differences between interacting gases, and arbitrary relative drift velocities both parallel and perpendicular to the magnetic field.

The closed set of transport equations is given by equations (145) - (148). This set of equations contains a continuity, momentum, parallel energy, and perpendicular energy equation for each species in the plasma. For Maxwell molecule interactions, the appropriate collision terms are given by equations (167) - (169), with  $v_{st}$  given by equation (173) and the quantities  $\underline{\Lambda}$ ,  $\Omega_1$ ,  $\Omega_2$ ,  $\underline{\phi}$ ,  $\Psi_{||}$ , and  $\Psi_{\perp}$  given by equations (188) - (192).

For Coulomb and constant collision cross section interactions the collision terms had to be evaluated numerically. However, I also fitted simplified expressions to the numerical results for the convenience of users. The accuracy of the approximate collision terms

depends on both the interaction potential and the temperature anisotropy (see Table 14). The procedure for obtaining the Coulomb and constant cross section collision terms is as follows:

- (1) Tables 1-12 are to be used to find the appropriate  $\phi$ 's and  $\Omega$ 's if the 1% accuracy associated with the numerical integrations is needed. Alternatively, the approximate expressions given in equations (193)'-(200)' can be used with the values of the  $\alpha$ 's and  $\beta$ 's given in Table 13 and the  $I$ 's given in Table 15. The index  $n$  is 3 and -1 for Coulomb and hard sphere interactions, respectively.
- (2) The  $\Psi$  and  $\Psi$  are calculated using equations (171) and (172), and  $\nu_{st}$  is obtained from equation (173). In equation (173),  $A_1(2) = \ln \Lambda$  and  $A_1(\infty) = 0.5$  for Coulomb and hard sphere interactions, respectively;  $\ln \Lambda$  is the well-known Coulomb logarithm (cf. Burgers 1969, Chapman and Cowling 1970).
- (3) The substitution of these quantities into equations (167) - (169) yields the collision terms of  $\delta \underline{M}_s / \delta t$ ,  $\delta E_{s\parallel} / \delta t$  and  $\delta E_{s\perp} / \delta t$ .

In chapter (IV), I studied the extent to which transport equations based on both Maxwellian and bi-Maxwellian series expansions can describe plasma flows characterized by non-Maxwellian velocity distributions, with emphasis given to modeling the anisotropic character of the distribution function. The specific problem I considered was the steady state flow of a homogeneous, weakly-ionized plasma subjected to homogeneous electric and magnetic fields.



For parallel electric and magnetic fields, the dominant non-Maxwellian characteristic is a parallel-to-perpendicular temperature anisotropy ( $T_{i\parallel} > T_{i\perp}$ ), although there is also an appreciable asymmetry in the electric field direction. On the other hand, for perpendicular electric and magnetic fields, the temperature anisotropy is reversed ( $T_{i\perp} > T_{i\parallel}$ ) and a large non-Maxwellian deviation occurs in the velocity plane perpendicular to  $\underline{B}$  as the electric field strength is increased. For sufficiently large electric fields, the three-dimensional ion velocity distribution can be toroidal or bean-shaped, depending on the collision-to-cyclotron frequency ratio.

As expected, for the Maxwellian expansion, the 20-moment approximation can describe larger non-Maxwellian deviations than the 5- and 13-moment approximations because of the greater number of terms retained at this level of approximation. Likewise, for the bi-Maxwellian expansion, the 16-moment approximation is better than the 6-moment approximation. Also, as expected, an expansion based on a bi-Maxwellian distribution is better suited to describing anisotropic plasmas than one based on a Maxwellian, even if fewer terms are retained in the bi-Maxwellian expansion.

As far as the bulk of the particles is concerned, both Maxwellian and bi-Maxwellian-based series expansions can describe larger deviations from a Maxwellian than probably had been anticipated. For example, if the main non-Maxwellian characteristic is a temperature anisotropy, the Maxwellian-based 20-moment approximation is a reasonable approximation for temperature anisotropies up to  $T_{i\parallel}/T_{i\perp} \sim 2-3$ ,

while the bi-Maxwellian-based 16-moment approximation can describe temperature anisotropies as large as  $T_{i\parallel} / T_{i\perp} \sim 20$ . For cases when there is a significant non-Maxwellian character in the velocity plane perpendicular to  $\underline{B}$  in addition to the parallel/perpendicular temperature anisotropy, the bi-Maxwellian-based 16-moment expansion is better for describing the anisotropic character of the distribution function, but the Maxwellian-based 20-moment approximation provides a slightly better description of the distribution function in the velocity plane perpendicular to  $\underline{B}$ . Also, depending on the conditions, both Maxwellian and bi-Maxwellian-based expansions can describe non-Maxwellian distributions that do not peak at the average drift velocity point.

Finally, the same problem in chapter (IV) was solved using more rigorous collision models (chapter (V)). For the ion-neutral collision process we considered both polarization and hard sphere collision models. For each collision model, a range of non-Maxwellian distribution functions was generated by varying the magnitude and direction of the electric and magnetic fields. However, for the more rigorous collision models contained in this study, it was necessary to do Monte Carlo simulations in order to obtain ion velocity distributions which would serve as a basis for comparison. In this regard it should be noted that the Monte Carlo simulation for a weakly-ionized plasma in crossed electric and magnetic fields have not been published to date, and these results are useful in their own right.

For the polarization and hard sphere collision models, the ion distribution functions have characteristics similar to those obtained

with the simple relaxation model. For parallel electric and magnetic fields, the dominant non-Maxwellian characteristic is a parallel-to-perpendicular temperature anisotropy ( $T_{i\parallel} > T_{i\perp}$ ), although there is also an asymmetry in the electric field direction. For perpendicular electric and magnetic fields, on the other hand, the temperature anisotropy is reversed ( $T_{i\perp} > T_{i\parallel}$ ) and a non-Maxwellian deviation also occurs in the velocity plane perpendicular to  $\underline{B}$  as the electric field strength is increased. For sufficiently large electric fields, the three-dimensional ion velocity distribution displays toroidal and bean-shaped characteristics, depending on the collision-to-cyclotron frequency ratio.

The confirmation of the Monte Carlo simulations that toroidal and bean-shaped characteristics occur for realistic collision models has important implications for space physics, particularly with regard to the stability of the terrestrial F-region plasma at high latitudes. Although the non-Maxwellian characteristics obtained with the polarization and hard sphere collision models are similar to those obtained with the relaxation model, the deviations from a Maxwellian are much smaller for the realistic collision models for given electric and magnetic field strengths. Also, for given field strengths, the distribution functions obtained with the hard sphere model are closer to Maxwellian than those obtained with the polarization model. For both collision models, the deviations from a Maxwellian 'saturate' as the electric field is increased. For the relaxation model, on the other hand, the non-Maxwellian deviations increase without limit as

the electric field is increased.

The basic conclusions that we presented in chapter (IV) about the adequacy of a given series expansion were confirmed for the more realistic collision models considered in chapter (V). In particular, the bi-Maxwellian-based 16-moment expansion for the distribution function is generally better suited to describing anisotropic plasmas than the Maxwellian-based 20-moment expansion. However, for the more realistic collision models considered in chapter (V), the deviations from a Maxwellian are not very large, and consequently, both series expansions are good approximations for the plasma flow problem considered.

As mentioned earlier, although the results obtained in chapters (IV) and (V) are not directly applicable to most of space physics problems, it should provide clues to the adequacy of different approximations for solving these problems. For example, in the high latitude F-region, where the  $O-O^+$  resonant charge exchange interaction dominates, accuracies similar to those found for the relaxation model are expected. For the polar wind, results similar to those of the polarization model are more probable. The Coulomb collision, which is dominant in the case of the solar wind, was not discussed in this work. However, it should give results somewhere between the relaxation model and the polarization model.

## REFERENCES

- Bowers E and Hains M G 1962 Phys. Fluids 11 2695
- Brandt J C 1970 Introduction to the Solar Wind (San Francisco: Freeman)
- Burgers J M 1969 Flow Equations for Composite Gases (New York: Academic Press)
- Chapman S and Cowling T G 1970 The Mathematical Theory of Non-Uniform Gases (Cambridge: Cambridge University Press)
- Chew G F, Goldberger M L and Low F E 1956 Proc. R. Soc. A236 112-118
- Chodura R and Pohl F 1971 Plasma Phys. 13 645
- Crooker N U, Eastman T E and Stiles G W 1979 J. Geophys. Res. 84 869-874
- Demars H G and Schunk R W 1979 J. Phys. D: Appl. Phys. 12 1051-1077
- Espedal M S 1969 Proc. 9th Int. Conf. on Phenomena in Ionized Gases (Bucharest: Ek. Acad. Rep. Soc. Rom.)
- Frieman E, Davidson R and Langdon B 1966 Phys. Fluids 9 1475
- Grad H 1958 Handb. Phys. XII 205-294
- Grad H 1949 Comm. Pure Appl. Math. 2 331-407
- Gradshteyn I S and Ryzhik I W 1973 Tables of Integrals, Series and Products (New York: Academic Press)
- Holzer T E, Fedder J A and Banks P M 1971 J. Geophys. Res. 76 2453-2468
- Hundhausen A J 1972 Coronal Expansion and Solar Wind (New York: Springer)
- Kennel C F and Green J M 1966 Ann. Phys. N.Y. 38 63
- Lin S L and Bardsley J N 1977 J. Chem. Phys. 66 435-445
- MacMahon A 1965 Phys. Fluids 8 1840
- Mikhailovskii A B and Tsypin V S 1971 Plasma Phys. 13 785
- Graevskii V, Chodura R and Feneberg W 1968 Plasma Phys. 10 819
- Schunk R W 1977 Rev. Geophys. Space Phys. 15 429

- Schunk R W and St-Maurice J P 1981 J. Geophys. Res. 86 4823-4827
- Schunk R W and Watkins D S 1979 Planet. Space Sci. 27 433
- Schunk R W and Watkins D S 1981 J. Geophys. Res. 86 91
- Schunk R W and Watkins D S 1982 J. Geophys. Res. 87 171-180
- Skullerud H R 1973 J. Phys. B: Atom. Molec. Phys. 6 728-742
- Srivastava M P and Bhatnagar P L 1975 Beitr. Plasma Phys. (Germany) 14 79
- St-Maurice J P 1975, Ion Velocity Distribution in the Auroral Ionosphere  
Ph.D. dissertation, Yale University
- St-Maurice J P and Schunk R W 1973 Planet. Space Sci. 21 1115-1130
- St-Maurice J P and Schunk R W 1974 Planet. Space Sci. 22 1-18
- St-Maurice J P and Schunk R W 1979 Rev. Geophys. Space Phys. 17 99-134
- Tanenbaum B S 1967 Plasma Physics (New York: McGraw-Hill)
- Wannier G H 1953 Bell Syst. Tech. J. 49 170-254
- Whang Y C 1971 J. Geophys. Res. 76 7503
- Whealton J H and Woo S B 1971 Physical Rev. A 6 2319-2325

APPENDIX

Here, I discuss in more detail the Monte Carlo simulation technique used in chapter (V). In general, the Monte Carlo method is a way of gaining statistical information about a system by following an individual member through a large number of random processes. The result of such a procedure is knowledge about one member of the assembly for a long period of time. Time averages of various kinds can be obtained from such data; these time averages are then set equal to instantaneous averages over the assembly, in accordance with ergodic theory. In the following paragraphs, I explain the procedures used to implement this method for the different collision models presented in chapter (V).

For the case of hard sphere collision model, the following steps are followed;

1. The probe ion starts with zero initial velocity.
2. The time interval between collisions is randomly generated such that it has an exponential probability density function [ $pr(x) \sim \exp(-kx)$ ]. The subroutine GGEXN, from the International Mathematical and Statistical Library (IMSL), is used for this purpose. Then, the ion final velocity is computed.
3. A neutral particle is randomly picked from a Maxwellian distribution (of temperature  $T_n$ ) using the subroutine GGNQF from the IMSL.
4. The relative speed between the colliding particles ( $g$ ) is computed and used to decide if the collision is 'real' or 'null' as explained by Lin and Bardsley (1977). If the collision is null we return to step 2, otherwise, we proceed to the next step.
5. The time spent in each velocity bin is registered using an array corresponding to the proper grid (see chapter (V)).



6. The scattering angle (in the center-of-mass frame of reference) is randomly generated such that it corresponds to isotropic scattering (i.e.  $\text{pr}(\chi, \phi) = \text{const.}$ ). The subroutine GGUBFS (from the IMSL) is used to generate such angles.

7. The ion velocity after collision is computed and steps 2-7 are repeated using this velocity as the initial ion velocity.

For the case of the polarization model, similar steps are followed except that all collisions are real. As a matter of fact, the same code was used and the parameter (VMAX) was set to zero. Moreover, the procedure used for the relaxation model is similar to that used for the polarization model, except that the ion velocity after collision is taken to be the neutral velocity before collision.

The codes used to implement these procedures is listed in the following pages. However, dimensionless normalized variables are used in these codes for convenience.

```

*****
* THIS PROGRAM IMPLEMENTS THE MONTE CARLO SIMULATION FOR PARALLEL ELECTRIC *
* AND HASKETIC FIELDS AND FOR RELAXATION COLLISION MODEL. *
*****

```

```

      REAL GGNOF,R(1)
      DOUBLE PRECISION DVPL,DVPER,DTIME
      DIMENSION Z(0:9,-9:15)
      TYPE*,* GIVE DVPL,DVPER,DTIME,D*
      ACCEPT*,DVPL,DVPER,DTIME,D
      C=3*D
1     TYPE*,* GIVE NR*
      ACCEPT*,NR
      IF(NR.EQ.-100)STOP
      DO 10 N=1,NR
      VPLI=2.12132*GGNOF(DVPL)
      CALL GGENX(DVPER,1.,1,R)
      VPER=3*SQRT(R(1))
      CALL GGENX(DTIME,C,1,R)
      VPLF=VPLI*R(1)
      N=ININD(9,INT(VPER))
      NMIN=INIXD(-9,ININD(15,INT(VPLI)))
      NMAX=IXAXD(-9,ININD(15,INT(VPLF)))
      DO 20 I=NMIN,NMAX
20     Z(N,I)=Z(N,I)+1
      CONTINUE
      Z(N,NMIN)=Z(N,NMIN)-(VPLI-NMIN*0.5)
      Z(N,NMAX)=Z(N,NMAX)-(NMAX*0.5-VPLF)
      S1=S1+R(1)
      VPER2=VPER*VPER
      S12=S12+R(1)*VPER2
      T1=VPLI/VPLI
      T2=VPLF/VPLF
      T3=T2-T1

```

```

S2=S2+T3
S22=S22+T3*WPER2
T1=T1*WPL1
T2=T2*WPLF
S3=S3+T2-T1
T1=T1*WPL1
T2=T2*WPLF
S4=S4+T2-T1
10 CONTINUE
T1=1./3.
U=T1*S2/S1/2.
PPL=T1*T1*S3/S1/3.
PPER=T1*T1*S12/S1/2.
QPL=T1*T1*T1*S4/S1/4.
OPER=T1*T1*T1*S22/S1/4.
QPL=QPL-S.*PPL*WJ+2*U*U*U
OPER=OPER-U*PPER
PPL=PPL-U*U
TYPE*, 'U=', U
TYPE*, 'PPL=', PPL, ' PPER=', PPER
TYPE*, 'QPL=', QPL, ' OPER=', OPER
OPEN(UNIT=7, NAME='FILE.DAT', TYPE='NEW')
WRITE(7, 100) ((2(I, J), I=0, 99), J=-9, 15)
100 FORMAT(25(10(2X, E10.3), /))
CLOSE(UNIT=7)
GO TO 1
END

```

```

*****
* THIS PROGRAM IMPLEMENTS THE MONTE CARLO SIMULATION FOR PARALLEL ELECTRIC *
* AND MAGNETIC FIELDS AND FOR HARD SPHERE COLLISION MODEL. IT CAN BE USED FOR *
* THE CASE OF POLARIZATION MODEL IF WE TAKE (VMAX=0). *
*****

```

```

REAL GGUBFS,GGNQF
DOUBLE PRECISION DT1,DT2,DT3,DSCAT1,DSCAT2,DCOL,DHUL
CHARACTER TLE*15
DIMENSION R(1),VI(3),VF(3),VT(3),DIR(3),
> Z(0:9,-9:15),VR(3),VCG(3)
TYPE*, 'ENTER THE SEED FILE NAME'
ACCEPT*, (A), TLE
OPEN(UNIT=3, NAME=TLE, TYPE='OLD')
READ(3, *) DT1, DT2, DT3, DSCAT1, DSCAT2, DCOL, DHUL
CLOSE(UNIT=3)
TYPE*, 'ENTER D, SCV, VMAX'
ACCEPT*, D, SCV, VMAX
TYPE*, 'ENTER M/NIT'
ACCEPT*, L, RN
RM2=1./.(1.+RM)
TWOP1=6.283
1 TYPE*, 'ENTER # OF COLLISIONS'
ACCEPT*, H
IF(H.EQ.-100) STOP
DO 20 I=1, H
2 CALL GBEXH(DCOL, D, 1, R)
DELV=DELV*VR(1)
VF(3)=VI(3)+DELV
VT(1)=0.7071*GGNQF(DT1)
VT(2)=0.7071*GGNQF(DT2)
VT(3)=0.7071*GGNQF(DT3)
DO 30 J=1, 3
VR(J)=VF(J)-VT(J)
30 CONTINUE
VRMAG=SQRT(VR(1)*VR(1)+VR(2)*VR(2)+VR(3)*VR(3))
IF(VRMAG.LT.GGUBFS(DHUL)*VMAX) GO TO 2
VPER2=VI(1)*VI(1)+VI(2)*VI(2)
VPER=SQRT(VPER2)
VPERP=SCV*VPER

```

```

NVPERP=IINT(VPERP)
IF (NVPERP.LT.10) THEN
  VPLIP=AMAX1(-9.,AMINI(15.,SCV*VI(3)))
  VPLFP=AMAX1(-9.,AMINI(15.,SCV*VF(3)))
  NVPLIP=IINT(VPLIP)
  NVPLFP=IINT(VPLFP)
  DO 70 J=NVPLIP,NVPLFP
    Z(NVPERP,J)=Z(NVPERP,J)+1
    CONTINUE
70  Z(NVPERP,NVPLIP)=Z(NVPERP,NVPLIP)-(VPLIP-NVPLIP+0.5)
  Z(NVPERP,NVPLFP)=Z(NVPERP,NVPLFP)-(NVPLFP+0.5-VPLFP)
  END IF
S1=S1+DELV
S12=S12+DELV*VPER2
T1=VI(3)*VI(3)
T2=VF(3)*VF(3)
T3=T2-T1
S2=S2+T3
S22=S22+T3*VPER2
T1=T1*VI(3)
T2=T2*VF(3)
S3=S3+T2-T1
T1=T1*VI(3)
T2=T2*VF(3)
S4=S4+T2-T1
DIR(3)=1.-2.*GGUSFS(DSCAT1)
T1=SQRT(1.-DIR(3)*DIR(3))
FI=TWOP1*GGUSFS(DSCAT2)
DIR(2)=T1*COB(FI)
DIR(1)=T1*SIN(FI)
  DO 40 J=1,3
    VCG(J)=RM*VF(J)+VT(J)
    VI(J)=RM2*(VCG(J)+VRHAG*DIR(J))
40  CONTINUE
DELV=0.0
VF(1)=VI(1)
VF(2)=VI(2)
20  CONTINUE

```

```

U=0.5*S2/S1
PPL=S3/S1/3.
PPER=0.5*S12/S1
QPL=0.25*S4/S1
QPER=0.25*S22/S1
QPER=QPER-U*PPER
QPL=QPL-3.*U*PPL+2.*U*U*U
PPL=PPL-U*U
TYPE*, 'U=' ,U
TYPE*, 'PPL=' ,PPL , ' PPER=' ,PPER
TYPE*, 'QPL=' ,QPL , ' QPER=' ,QPER
TYPE*, 'ENTER MOMENT FILE NAME'
ACCEPT '(A)' , TLE
OPEN (UNIT=5 , NAME=TLE , TYPE='NEW')
WRITE (6 , *) U , PPL , PPER , QPL , QPER
CLOSE (UNIT=5)
TYPE*, 'ENTER OUTPUT FILE NAME'
ACCEPT '(A)' , TLE
OPEN (UNIT=7 , NAME=TLE , TYPE='NEW')
WRITE (7 , 1000) ((Z (I , J) , I=0 , 9) , J=-9 , 15)
CLOSE (UNIT=7)
GO TO 1
1000  FORMAT (25 (10 (2X , E10.3) , /))
END

```

```

* THIS PROGRAM IMPLEMENTS THE MONTE CARLO SIMULATION FOR THE CASE OF
* PERPENDICULAR ELECTRIC AND MAGNETIC FIELDS AND FOR HARD SPHERE COLLISION
* MODEL. IT CAN BE USED FOR THE CASE OF POLARIZATION MODEL IF WE SET
* (VMAX=0).

```

```

REAL GGNOF,GSUBFS
CHARACTER TLE*10
DOUBLE PRECISION DT1,DT2,DT3,DSCAT1,DSCAT2,DCOL,DMAX
DIMENSION RR(1),VT(3),VCG(3),VR(3),VI(3),VF(3),DIR(3),
> Z(0:8,0:8,0:23)
DATA VI(3)/0.0/,THETA1/0.0/,DELTH/0.0/,SN/0.0/,
> STHETA/0.0/,Z/1944*0.0/,TWOP1/6.203/
TYPE*, 'ENTER THE FILE OF SEEDS'
ACCEPT*, 'ENTER (A)', TLE
OPEN(UNIT=3, NAME=TLE, TYPE='OLD')
READ(3, *) DT1, DT2, DT3, DSCAT1, DSCAT2, DCOL, DMAX
CLOSE(UNIT=3)
TYPE*, 'ENTER M/MT, VD, ALFA'
ACCEPT*, RH, VD, ALFA
RH2=1./ (1.+RH)
TWLOPI=24./TWOP1
ROH=VD
TYPE*, 'ENTER SCV, VMAX'
ACCEPT*, SCV, VMAX
1 TYPE*, 'ENTER # OF COLLISIONS'
ACCEPT*, N
IF (N.EQ.-100) STOP
DO 40 I=1,N
2 CALL GSEXII(DCOL, ALFA, 1, RR)
DELTH=DELTH+RR(1)
THETAF=THETA1+DELTH
VF(1)=ROH*COS(THETAF)
VF(2)=ROH* SIN(THETAF)
VF(3)=VI(3)
VT(1)=VD+9.7071*GGNOF(DT1)
VT(2)=0.7071*GGNOF(DT2)
VT(3)=0.7071*GGNOF(DT3)

```

20

```

DO 20 J=1,3
  VR(J)=VF(J)-VT(J)
  CONTINUE
VRMAG=SQRT(VR(1)*VR(1)+VR(2)*VR(2)+VR(3)*VR(3))
IF (VRMAG.LT.VMAX*GGUDPS(DMAX)) GO TO 2
VF3S=VF(3)*VF(3)
S0=S0+DELTH
ROH2=ROH*ROH
T3=VF(2)-VI(2)
S010=S010+T3
SS010=SS010+T3*VF3S
S012=S012+T3*ROH2
S002=S002+ROH2*DELTH
T3=VF(1)-VI(1)
S100=S100+T3
SS100=SS100+T3*VF3S
S102=S102+T3*ROH2
T2=VF(1)*VF(1)
T1=VI(1)*VI(1)
S200=S200+T2-T1
S300=S300+T2*VF(1)-T1*VI(1)
S210=S210+T2*VF(2)-T1*VI(2)
S110=S110+VF(1)*VF(2)-VI(1)*VI(2)
S2=S2+VF3S*DELTH
NV3=I INT (ABS (VF (3)) *SCV)
NROH=I INT (ROH*SCV)
IF ((NV3.LT.9).AND.(NROH.LT.9)) THEN
  THETIP=THETA1*TLUOPI
  THETFP=THETA2*TLUOPI
  ITHIP=I INT (THETIP)
  ITHFP=I INT (THETFP)
DO 70 J=ITHIP, ITHFP
  MODJ=IMOD(J,24)
  Z(NV3,NROH,MODJ)=Z(NV3,NROH,MODJ)+1.
  CONTINUE
Z(NV3,NROH,ITHIP)=Z(NV3,NROH,ITHIP)-(THETIP-ITHIP)
Z(NV3,NROH,MODJ)=Z(NV3,NROH,MODJ)-(ITHFP+1,-THETFP)
END IF

```

70



```

DIR(3)=1.-2.*GGUBFS(DSCAT1)
T1=SQRT(1.-DIR(3)*DIR(3))
F1=TWOP1*GGUBFS(DSCAT2)
DIR(2)=T1*CCOS(F1)
DIR(1)=T1*SSIN(F1)
DO 30 J=1,3
  VCG(J)=RMM*VF(J)+VT(J)
  VI(J)=RM2*(VCG(J)+VRHAG*DIR(J))
30  CONTINUE
  RGH=SQRT(VI(1)*VI(1)+VI(2)*VI(2))
  THETA1=ACOS(VI(1)/RGH)
  IF(VI(2).LT.0.0)THETA1=TWOP1-THETA1
  STHETA=STHETA+DELTH
40  DELTH=0.0
  CONTINUE
  SN=SN+1
  TYPE*, 'AVERAGE ALFA=',STHETA/SN
  TYPE*, 'ENTER OUTPUT FILE NAME'
  ACCEPT '(A)',TLE
  OPEN (UNIT=7, NAME=TLE, TYPE='NEW')
1000 WRITE (7, 1000) (((2(I,J,K), J=0.0), K=0, 23), I=0, 8)
  FORMAT (9G(/), 24(/), 9(2X, E11.4))
  CLOSE (UNIT=7)
  DIR(3)=1.-2.*GGUBFS(DSCAT1)
  U1=5010/50
  U2=-5100/50
  P11=0.5*(S002+S110)/50
  P22=0.5*(S002-S110)/50
  P33=S2/50
  P12=-0.5*S200/50
  Q111=(2*S012+S210)/3./50
  Q222=(-S102+S300/3.)/50
  Q112=-S300/3./50
  Q122=(S012-S210)/3./50
  Q133=S0010/50
  Q233=-S5100/50
  Q133=-Q133+U1*P33
  Q233=Q233-U2*P33

```

```

Q111=-Q111+3.*U1*P11-2*U1*U1*U1
Q222=Q222-3.*U2*P22+2*U2*U2*U2
Q112=Q112-U2*P11-2.*U1*P12+2*U1*U1*U2
Q122=-Q122+U1*P22+2.*U2*P12-2.*U1*U2*U2
P11=P11-U1*U1
P22=P22-U2*U2
P12=-P12+U1*U2
U1=VD-U1
TYPE*, 'U1=', U1, ' U2=', U2
TYPE*, 'P11=', P11, ' P22=', P22
TYPE*, 'P33=', P33, ' P12=', P12
TYPE*, 'Q111=', Q111, ' Q222=', Q222
TYPE*, 'Q112=', Q112, ' Q122=', Q122
TYPE*, 'Q133=', Q133, ' Q233=', Q233
TYPE*(A)*, 'CENTER KON. FILE : '
ACCEPT*(A)*, TLE
OPEN(UNIT=4, NAME=TLE, TYPE='NEW')
WRITE(4, #) U2, U1, P22, P11, P33, P12, (P11+P22+P33)/3.
WRITE(4, #) Q222, Q112, Q233, Q122, Q111, Q133
CLOSE(UNIT=4)
GO TO 1
END

```

## VITA

Abdallah R. Barakat

Candidate for the Degree of

Doctor of Philosophy

Dissertation: On the Transport Equations for Anisotropic Plasmas

Major Field: Physics

Biographical Information:

Personal Data: Born at Behera, Egypt, February 14, 1950; married Wedad Abdelrazek in 1980; children -- Merate.

Education: Recieved the B. Sc. degree in electrical engineering from Alex. University in 1972, and the M. Sc. degree in electrical engineering from Cairo University in 1978.

Professional Experience: 1973 - 1976, research engineer at The Atomic Energy Establishment, Cairo, Egypt; 1976 - 1978, teaching assistant at Alex. University.